Aus dem

Institut für Physiologie der Universität Tübingen

Modification of Eryptosis, the Suicidal Erythrocyte Death, by Afatinib, Ceritinib, and Volasertib

Inaugural-Dissertation
zur Erlangung des Doktorgrades
der Humanwissenschaften

der Medizinischen Fakultät
der Eberhard Karls Universität
zu Tübingen

vorgelegt von

Bhuyan, Abdulla Al-Mamun

2021

Dekan: Professor Dr. B. Pichler

1. Berichterstatter Professor Dr. Dr. F. Lang
2. Berichterstatter: Professor Dr. Dr. B. Nürnberg
3. Berichterstatter: Professor Dr. A. Nordheim

Tag der Disputation: 30.03.2021

Contents

Abbreviations:

AA	Arachidonic acid
ADP	Adenosine diphosphate
AE1	Anion exchanger 1
AEs	Adverse effects
ALK	Anaplastic lymphoma kinase
ALT	Alanine aminotransferase
AM	Acetoxymethyl
AML	Acute myeloid leukaemia
AMPK	AMP-activated kinase
ANOVA	Analysis of variance
ASCEND	Activity and safety of ceritinib in patients with ALK-rearranged non-small-cell lung cancer
AST	Aspartate aminotransferase
ATP	Adenosine triphosphate
AWB	Annexin wash buffer
BC	Breast cancer
BSA	Bovine serum albumin
$CaCl_2$	Calcium chloride
Ca^{++}	Calcium ion
Casp	Caspase
CD36	Cluster of differentiation 36
CDK4	Cyclin-dependent kinase 4
Cer	Ceramide
Cl^-	Chloride ion
cGMP	Cyclic guanosine monophosphate
cGK1	cGMP-dependent protein kinase 1
CK1α	Casein kinase 1α
CO_2	Carbon dioxide
COX	Cyclooxygenase
CR	Complete response
CXCL16	Chemokine ligand 16
DCF	Dichlorofluorescein
DCFDA	Dichlorodihydrofluorescein diacetate
DMSO	Dimethyl sulfoxide
EGFR	Epidermal growth factor receptor
ERK	Extracellular signal-regulated kinase
EPO	Erythropoietin
FBS	Foetal bovine serum
FDA	Food and drug administration
FL	Fluorescence
Fluo-3	{[2-(2-{2-[Bis(carboxymethyl)amino]-5-(2,7-dichloro-6-hydroxy-3-oxo-3H-xanthen-9-yl)phenoxy}ethoxy)-4-methylphenyl](carboxymethyl)amino}acetic acid
FACS	Fluorescence-activated cell sorting
FS	Forward scatter
FSC	Forward scatter channel

g	Gravity
G	Gram
GM	Geometric mean
GERD	Gastroesophageal reflux disease
$G\alpha_{i2}$	G protein α i2 isoform
H^+	Hydrogen ion
Hb	Haemoglobin
HBA	Haemoglobin alpha
HBB	Haemoglobin beta
HCO_3^-	Bicarbonate ion
HEPES	N-2-hydroxyethylpiperazine-n-2-ethanesulfonic acid
HER1	Human epidermal growth factor receptor 1
HER2	Human epidermal growth factor receptor 2
HER3	Human epidermal growth factor receptor 3
HER4	Human epidermal growth factor receptor 4
HNSCC	Head and neck squamous cell cancer
hrs	Hours
HS	Hyperosmotic shock
IC_{50}	Half maximal inhibitory concentration
JAK3	Janus activated kinase 3
K^+	Potassium ion
KCl	Potassium chloride
KCNN4	Potassium calcium-activated channel subfamily N member 4
K-Ras	Kirsten rat sarcoma viral oncogene homolog
l	Litre
LASERS	Light amplification by stimulated emission of radiation
M	Marker
MAPK	Mitogen-activated protein kinase
Mg	Milligram
$MgSO_4$	Magnesium sulphate
Min	Minute
ml	Millilitre
mM	Millimolar
MSK	Mitogen-and stress-activated kinase
MTD	Maximum tolerated dose
mTOR	Mammalian target of rapamycin/ Mechanistic target of rapamycin
n	Number
NaCl	Sodium chloride
Na^+	Sodium ion
NaOH	Sodium hydroxide
nm	Nanometre
nM	Nanomolar
NO	Nitric oxide
NSCC	Non-selective cation channel
NSCLC	Non-small-cell lung cancer
OS	Oxidative stress
ORR	Overall response rate
P38 MAPK	p38 mitogen-activated protein kinase

PAF	Platelet activating factor
PAK2	p21-activated kinase 2
PR	Partial response
PBS	Phosphate-buffered saline
PFS	Progression-free survival
PGE_2	Prostaglandin E_2
pH	Potential of hydrogen
Pi	Inorganic phosphate
PI3K	Phosphoinositide 3-kinase
PKB	Protein kinase B
PKC	Protein kinase C
PLA	Phospholipase A
PLA_2	Phospholipase A_2
PLK1	Polo-like kinase 1
PLK2	Polo-like kinase 2
PLK3	Polo-like kinase 3
PMT	Photomultiplying tube
PS	Phosphatidylserine
RBC	Red blood cell
RPMI	Roswell Park Memorial Institute
ROS	Reactive oxygen species
SAC	Spindle assembly checkpoint
Scr	Scramblase
sCr	Serum creatinine
SD	Standard deviation
SM	Sphingomyelinase
SNP	Sodium nitroprusside
SS	Side scatter
SSC	Side scatter channel
STAT	Signal transducer and activator of transcription protein
TBILI	Total bilirubin
TCA	Tricarboxylic acid
TGF-α	Transforming growth factor alpha
TK	Tyrosine kinase
TKI	Tyrosine kinase inhibitor
TRPC6	Transient receptor potential cation channel subfamily C member 6
z-VAD-FMK	Carbobenzoxy-valyl-alanyl-aspartyl-[O-methyl]- fluoromethylketone
°C	Degree Celsius
µg	Microgram
µl	Microliter
µM	Micromolar

List of Figures:

List of Tables:

1. Introduction

1. 1. Erythrocytes and their physiological importance

Erythrocytes (red blood cells (RBCs), red cells, red blood corpuscles, haematids, erythroids) are one of the most abundant and unique cells of the body considering their architecture and functional features. On average, 20-30 trillion ($2–3 \times 10^{13}$) red blood cells circulate within the human body; this is considered 25% of the total body cells or 50% of the total blood volume (Qadri et al., 2017; Föller et al., 2008c). Adult men and women possess approximately 5-6 million or 4-5 million erythrocytes per µl of blood, respectively (Hillman et al., 2005). However, people who live at high altitudes or regularly dive in deep seas have a higher number of red cells than normal because of increased oxygen demand (Pierige et al., 2008). Erythrocytes are comparatively smaller in size than most other cells with a diameter of 6-8 µm. They are about 2 µm thick, which allows them to pass easily through tiny capillaries (Mohandas and Gallagher, 2008; Mukherjee et al., 2015). In contrast to nucleated cells, erythrocytes do not possess important cellular organelles such as nuclei, mitochondria, or ribosomes (Berg et al., 2001). These characteristics allow them to hold more oxygen-binding protein haemoglobin (Hb) (Qadri et al., 2017). Moreover, the biconcave shape of the erythrocytes' surface permits them to have an enlarged surface area (Mohandas and Gallagher, 2008; Goodman et al., 2007). Finally, through this large surface, increased amounts of oxygen, carbon dioxide, and other gases can permeate (Goodman et al., 2007) and bind to haemoglobin (Bessis and Delpech, 1981). Furthermore, haemoglobin protein has the capability of binding to or releasing nitric oxide (NO), which leads to vasodilation of the arterioles (Bessis and Delpech, 1981).

1. 1. 1. Ionic exchange in erythrocytes

There are various transport proteins such as Ca^{++}-ATPase, Na^+/K^+-ATPase, Gardos channels, Na^+/Cl^- co-transporters, K^+/Cl^- co-transporters, $Na^+/K^+/2Cl^-$ co-transporters, Na^+/H^+ exchangers, Band 3 anion exchanger 1 (AE1) proteins, Glucose transporter 1 (Glut1) proteins, Kidd antigen proteins, and Aquaporins, which are engaged in transport across the red blood cell membrane (Mohandas and Gallagher, 2008; Maher and Kuchel, 2003). Figure 1 demonstrates the different transporters found in erythrocytes.

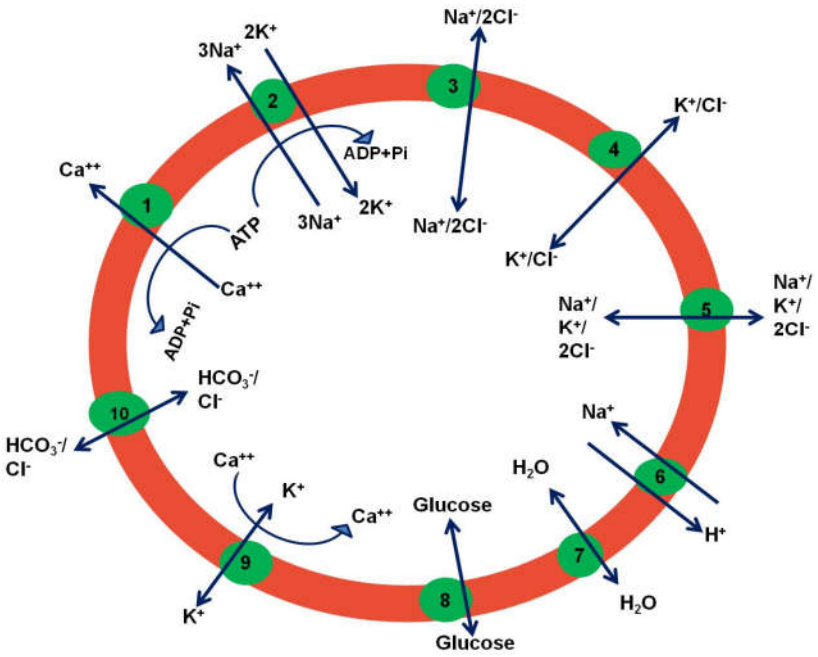

Figure 1: Transporters in erythrocytes [modified from (Maher and Kuchel, 2003)]. The figure represents the different channels in the erythrocyte membrane, which transport ions (Na^+, K^+, Cl^-, Ca^{++}, HCO_3^-) and other molecules such as water and glucose. 1: Ca^{++}-ATPase; 2: Na^+/K^+-ATPase; 3: $Na^+/2Cl^-$ co-transporter; 4: K^+/Cl^- co-transporter; 5: $Na^+/K^+/2Cl^-$ co-transporter; 6: Na^+/H^+ exchanger; 7: Aquaporin; 8: Glucose Transporter 1 (Glut1); 9: Gardos channel; 10: Band 3 anion exchanger 1 (AE1). Ca^{++}: calcium ion; Na^+: sodium ion; K^+: potassium ion; Cl^-: chloride ion; ATP: adenosine triphosphate; ADP: adenosine diphosphate; Pi: inorganic phosphate.

The transmembrane protein Ca^{++}-ATPase is responsible for the transport of Ca^{++} to the extracellular space from the intracellular space (Lang et al., 2007a). The inhibition or defect of this protein results in a rise of the cytosolic calcium concentration, which further triggers the apoptotic pathway of erythrocytes known as eryptosis (Lang et al., 2007a). The Na^+/K^+-ATPase membrane protein takes part in the maintenance of the Na^+ and K^+ ionic balance within the erythrocyte by permitting the influx of two K^+ ions and efflux of three Na^+ ions (Lew and Bookchin, 2005). Energy is required for the proper function of the Na^+/K^+-ATPase and energy depletion can impair the function of this pump and may initiate eryptosis (Lang and Lang, 2015). The progenitor cells of erythrocytes are rich in the active form of the K^+/Cl^- co-transporters and the Band 3 anion exchanger 1 (AE1) protein. In reticulocytes, the K^+/Cl^- co-transporter is responsible for the passive movement of K^+ (Hall and Ellory, 1986). Assembly of the

membrane skeleton for the development of the erythroblast is largely dependent on the Band 3 anion exchanger 1 (AE1) protein (Peters et al., 1996).

The calcium-sensitive K^+ channels in erythrocytes are known as Gardos channels (KCNN4) and approximately 100-200 Gardos channels have been reported in the erythrocyte plasma membrane (Lew et al., 1982; Alvarez and Garcia-Sancho, 1987). At an intracellular calcium concentration of 20-50 nM, the Gardos channel remains silent. However, with increasing cytosolic calcium (150 nM - 2 μM) the channel becomes active (Lew and Bookchin, 2005), which plays an important role in the stimulation of eryptosis or suicidal erythrocyte death (Lang et al., 2003b; Ghashghaeinia et al., 2012). The opening of the channels causes the exit of K^+, hyperpolarisation, the exit of Cl^-, and parallel loss of water resulting in shrinkage of erythrocytes (Föller et al., 2008b).

1. 2. Eryptosis

The term eryptosis indicates the suicidal death of red blood cells, which is initiated upon injury before their biological demise (Berg et al., 2001; Bratosin et al., 2001; Daugas et al., 2001; Lang and Qadri, 2012). It is a strongly regulated and balanced cell death programme without destruction of the cell membrane or release of cytoplasmic content to the extracellular space (Lang et al., 2012b). Eryptotic erythrocytes are characterised by the formation of cell membrane blebbing, cell shrinkage, and scrambling of the cell membrane, which leads to the externalisation of phosphatidylserine (PS) from the cell interior to the outer surface of erythrocytes (Mohandas and Gallagher, 2008; Mukherjee et al., 2015; Goodman et al., 2007). In contrast to apoptosis of nucleated cells, the eryptosis is devoid of mitochondrial depolarisation, nuclear condensation, or DNA fragmentation (Suzuki-Karasaki et al., 2014; Tone et al., 2007). Erythrocytes exposing phosphatidylserine on their surface are rapidly engulfed by macrophages and cleared from the bloodstream which, thus, prevents haemolysis (de Back et al., 2014; Kurosaka et al., 2003; Lang et al., 2012a). Haemoglobin which is released during haemolysis would otherwise pass through the kidney, subsequently blocking the tubules of nephrons by precipitating in their acidic lumen and damaging the kidney functions (Lang and Lang, 2015; Harrison et al., 1947). Thus, eryptosis is considered to be a soft and unique approach to avoid haemolysis (Lang et al., 2012a).

1. 2. 1. Signalling pathways involved in eryptosis

The enhanced intracellular calcium concentration of erythrocytes, resulting from activation of calcium-permeable non-selective cation channels (NSCC) (Lang et al., 2003a; Berg et al., 2001; Bratosin et al., 2001; Daugas et al., 2001) and calcium-sensitive K^+ channels (Gardos channels), plays the main role in executing eryptosis (Maher and Kuchel, 2003; Lang et al., 2007a). The enzyme scramblase of the cell membrane becomes activated as a result of increased cytosolic calcium which, in turn, leads to the breakdown of the plasma membrane phospholipid asymmetry resulting in membrane scrambling and, finally, externalisation of PS from the inner membrane to the outer membrane of erythrocytes (Connor et al., 1994). Besides inducing the translocation of PS, increased calcium further triggers the formation of vesicles within the erythrocytes (Allan and Michell, 1977) and activates an enzyme called cysteine endopeptidase calpain, which is responsible for the degradation of the cytoskeleton, resulting in cell membrane blebbing (Pompeo et al., 2010).

The Gardos channels that are calcium-sensitive K^+ channels further become active because of an increased cytosolic calcium concentration with the subsequent efflux of K^+. The efflux of K^+ causes hyperpolarisation of the plasma membrane and allows for the exit of chloride. Besides, water from the cytoplasm also passively flows along the concentration gradient (Lang et al., 2003b; Lang et al., 2007a; Maher and Kuchel, 2003). The cellular loss of KCl and water leads to shrinkage of the cell, which is the second most important feature of eryptosis (Lang et al., 2003b). Furthermore, activation of caspases by oxidative stress, leukotrienes, or by α-lipoic acid plays a vital role in stimulating erythrocyte death (Duranton et al., 2002; Lang et al., 2014; Pretorius et al., 2016b; Lang and Lang, 2015). Caspase activation as a result of increased oxidative stress causes cleavage of the anion exchanger AE1 resulting in an inadequate exchange of Cl^- and HCO_3^- followed by increased eryptosis (Mandal et al., 2002). Eryptosis mediated by caspases does not depend on the entry of cytosolic calcium (Lang et al., 2004). Moreover, Cl^- channels are stimulated by oxidative stress resulting in an efflux of Cl^- from the erythrocytes (Huber et al., 2002) and shrinkage of the cells (Lang et al., 2004).

The channel proteins of the NSCC have not been identified at the molecular level but it is assumed that the transient receptor potential cation channel subfamily C member

6 (TRPC6) is involved (Föller et al., 2008c). It is reported that in erythrocytes lacking TRPC6, cytosolic calcium is significantly blunted (Föller et al., 2008c). Again, the NSCC could be activated by oxidative stress (Duranton et al., 2002; Lang et al., 2003a), hyperosmotic shock (Lang et al., 2003a; Huber et al., 2001), removal of extracellular chloride (Huber et al., 2001; Duranton et al., 2002), or by the formation of prostaglandin E_2 (PGE_2) (Lang et al., 2005a), followed by an increase of cytosolic calcium and enhanced erythrocyte death. In addition, energy depletion (Klarl et al., 2006), impaired antioxidant function (Bilmen et al., 2001; Mavelli et al., 1984; Damonte et al., 1992), and different endogenous substances, as well as various xenobiotics (Lang and Qadri, 2012) may cause erythrocytes' suicidal death.

Ceramide also plays a vital role in initiating eryptosis (Lang et al., 2004; Lang et al., 2010). Ceramide formation occurs through the breakdown of the membrane phospholipid sphingomyelin by the enzyme sphingomyelinase (SM) (Lang et al., 2010; Lang et al., 2004). Ceramide activates the scramblase of the membrane, resulting in the scrambling of the erythrocyte membrane and translocation of PS (Lang et al., 2012a). Activation of SM depends on the formation of the platelet-activating factor (PAF), which is produced by the breakdown of membrane phospholipids by the phospholipase A_2 (PLA_2) enzyme following hyperosmotic shock (Lang et al., 2005a). Hence, ceramide or PAF-mediated eryptosis does not depend on a rise of cytosolic calcium (Lang et al., 2005a; Lang et al., 2005b) although both have a synergistic action on eryptosis.

Furthermore, many kinases trigger signalling pathways involved in suicidal erythrocyte death. The most remarkable kinases involved are protein kinase C (PKC) (Klarl et al., 2006), Janus-activated kinase 3 (JAK3) (Bhavsar et al., 2011), p38 MAPK (Gatidis et al., 2011), casein kinase 1α (CK1α) (Zelenak et al., 2012), and cyclin-dependent kinase 4 (CDK4) (Lang et al., 2015c). In contrast, eryptosis may be blunted by sunitinib-sensitive tyrosine-kinases (Shaik et al., 2012) and sorafenib-sensitive tyrosine-kinases (Lupescu et al., 2012), AMP-activated kinase (AMPK) (Zelenak et al., 2011), mitogen-and stress-activated kinases MSK1 and MSK2 (Lang et al., 2015a), cGMP dependent protein kinase (Föller et al., 2008a), and p21-activated kinase 2 (PAK2) (Zelenak et al., 2011). Figure 2 illustrates the underlying signalling pathways involved in eryptosis.

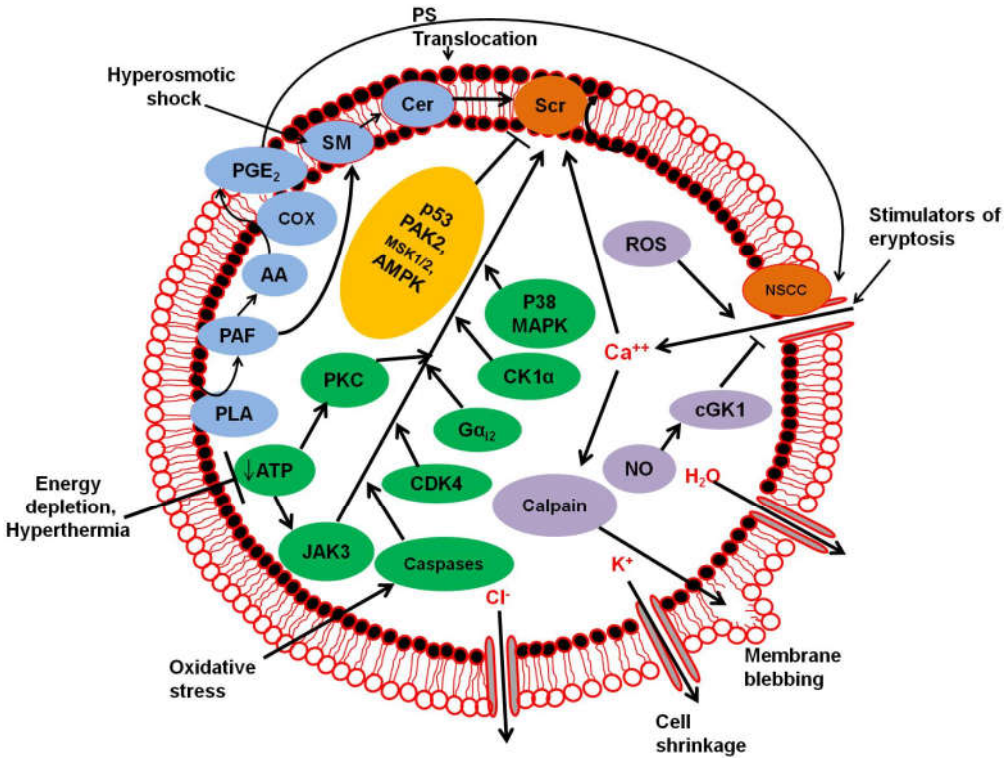

Figure 2: Signalling associated with suicidal erythrocyte death [modified from (Lang et al., 2017)]. The figure depicts the modulation of apoptotic pathways in erythrocytes. Hyperosmotic shock, oxidative stress, energy depletion, hyperthermia, and other xenobiotics stimulate kinases, activate caspases, increase cytosolic calcium concentration resulting in activation of scramblase, Gardos channel, and calpain, followed by translocation of phosphatidylserine, cell shrinkage, and membrane blebbing. AMPK, MSK1/2, PAK2, p53 inhibit the scramblase, and cGK1 inhibit the NSCC resulting in inhibition of eryptosis. SM: sphingomyelinase; Cer: Ceramide; SCR: Scramblase; PS: Phosphatidylserine; NSCC: Non selective cation channel; Ca^{++}: Calcium ion; PKC: Protein kinase C; p38 MAPK: p38 Mitogen-activated protein kinase; CK1: Casein kinase 1; JAK3: Janus activated kinase 3; CDK4: Cyclin-dependent kinase 4; $G\alpha_{i2}$: G protein Galpha$_{i2}$; PLA: Phospholipase A; PAF: Platelet-activating factor; AA: arachidonic acid; COX: Cycloxygenase; PGE_2: Prostaglandin E_2; ATP: Adenosine triphosphate; ROS: Reactive oxygen species; MSK1/2: Mitogen and stress-activated kinase 1/2; PAK2: p21-activated kinase 2; AMPK: AMP-activated kinase; cGK1: cGMP-dependent protein kinase 1; NO: Nitric oxide.

1. 2. 2. Diseases and clinical conditions associated with eryptosis

Increased eryptosis has been observed in diverse diseases or in clinical conditions (Table 1).

Table 1: Diseases or clinical conditions with enhanced eryptosis

No	Diseases or clinical conditions
01	Diabetes (Awasthi et al., 2015; Viskupicova et al., 2015).
02	Sickle cell anaemia (Chakrabarti et al., 2016).
03	Thalassemia (Chakrabarti et al., 2016).
04	Glucose 6-phosphate dehydrogenase deficiency (Ghashghaeinia et al., 2016).
05	Hepatic injury (Lang et al., 2007b).
06	Cardiac failure (Attanasio et al., 2015).
07	Chronic kidney disease (Bissinger et al., 2016b; Bonan et al., 2016).
08	Haemolytic uremic syndrome (Lang and Qadri, 2012).
09	Dehydration (Abed et al., 2013a).
10	Phosphate depletion (Lang and Lang, 2015).
11	Calcitriol excess (Lang et al., 2015b).
12	Inflammation (Bester and Pretorius, 2016).
13	Arteritis (Bissinger et al., 2016c).
14	Fever (Crisp et al., 2016).
15	Sepsis (Kempe et al., 2007).
16	Systemic lupus erythematosus (Jiang et al., 2016).
17	Mycoplasma infection (Lang and Qadri, 2012).
18	Malaria (Gaudreault et al., 2015; Tagami et al., 2016).
19	Iron deficiency (Pretorius et al., 2016a).
20	Hereditary spherocytosis (Crisp et al., 2016).
21	Paroxysmal nocturnal haemoglobinuria (Lang and Qadri, 2012).
22	Wilson's disease (Lang and Qadri, 2012).
23	Parkinson's disease (Pretorius et al., 2014).
24	Malignancy (Bissinger et al., 2016e; Qadri et al., 2012).

Stimulated eryptosis has also been observed in several gene-targeted mouse models, indicating the involvement of the respective gene for erythrocyte survival (Table 2).

Table 2: Mouse models with accelerated eryptosis

No	Name of the mouse models
01	Sickle cell anaemia (HBB deficiency) (Lang and Qadri, 2012).
02	Thalassemia (HBA/HBB deficiency) (Lang and Qadri, 2012).
03	Annexin A7 deficiency (Lang et al., 2012b).
04	MSK1/2 deficiency (Lang et al., 2015a).
05	cGKI deficiency (Föller et al., 2008a).
06	AMPK deficiency (Föller et al., 2009b).
07	Endothelin B receptor deficiency (Föller et al., 2010).
08	Klotho deficiency (Abed et al., 2013b).
09	AE1 deficiency (Akel et al., 2007).
10	APC deficiency (Qadri et al., 2012).
11	EPO excess (Föller et al., 2007).

Table 3 represents mouse models associated with reduced eryptosis.

Table 3: Mouse models with decreased eryptosis

No	Name of the mouse models
01	PDK1 deficiency (Föller et al., 2008d).
02	TRPC6 deficiency (Föller et al., 2008c).
03	PAF receptor deficiency (Lang and Lang, 2015).
04	Heterotrimeric G-protein subunit $G\alpha_{i2}$ deficiency mice (Bissinger et al., 2016d).
05	JAK3 deficiency (Bhavsar et al., 2011).

1. 2. 3. Consequences of eryptosis

Although eryptosis is a physiological phenomenon, excessive erythrocyte demise as a result of diseases, toxicity, stress, or inadequate compensatory mechanisms may result in anaemia (Lang and Lang, 2015). As long as the rate of eryptosis and erythropoiesis is balanced, the number of circulating erythrocytes remains unchanged. If the erythropoiesis rate or the production of new erythrocytes is, however, lower, anaemia ensues (Lang and Qadri, 2012; Lang et al., 2012a; Bilmen et al., 2001).

Phosphatidylserine-exposing erythrocytes are recognised by specific receptors of macrophages (Lang and Qadri, 2012). Thereafter, erythrocytes are engulfed and degraded by macrophages averting haemolysis and thus preventing the detrimental consequences of increased haemoglobin levels in the blood. Haemoglobin may be filtered in the kidney, possibly leading to precipitation in the acidic lumen of nephrons and resulting in the occlusion of renal tubules (Lang and Qadri, 2012; Lang et al., 2012b; Foller et al., 2013).

Erythrocytes harbouring the Plasmodium parasite seem to undergo increased oxidative stress resulting in activation of different ion channels in the plasma membrane of erythrocytes, which is eventually needed for the pathogen to survive within the cells (Duranton et al., 2002; Huber et al., 2002). When the NSCC channels are activated, intracellular calcium levels increase and promote eryptosis. Eryptotic erythrocytes with the pathogen are engulfed by macrophages (Föller et al., 2009a).

The chemokine CXCL16 is a small soluble cytokine that can express as a receptor on endothelial cells (Borst et al., 2012) and platelets (Walker et al., 2014; Ashraf and Gupta, 2011) responsible for capturing PS-exposing erythrocytes resulting in microcirculation impairment. In addition to CXCL16, endothelial CD36 (McCormick et al., 1997) and thrombospondin (Wandersee et al., 2004) and CD36 of platelets (Ashraf and Gupta, 2011) may be involved in the adhesion of eryptotic erythrocytes to the vascular endothelial cells and promote the development of thrombosis in different clinical conditions such as chronic kidney disease (Yang et al., 2017; Gao et al., 2015) and hepatic failure (Wu et al., 2016).

1. 3. Cytostatic compounds and eryptosis

Cytostatic molecules are substances that inhibit the growth or stimulate the death of cells (Rixe and Fojo, 2007). Treatment with cytostatic compounds not only stimulates apoptotic cell death but also triggers eryptosis (Lang et al., 2012b). Excessive eryptosis has been reported in lung cancer patients receiving cytostatic molecules (Bissinger et al., 2016e). Excessive eryptosis stimulates the development of anaemia (Lang et al., 2012a; Lang et al., 2012b; Lang and Qadri, 2012). Anaemia has been reported as a side effect of afatinib (Mukai et al., 2015; Chu et al., 2014), ceritinib (Khozin et al., 2015; Shaw et al., 2014), and volasertib (Awada et al., 2015; Stadler et al., 2014). Earlier *in*

vitro studies demonstrate that administering cytostatic molecules like sorafenib (Lupescu et al., 2012), sunitinib (Shaik et al., 2012), gefitinib (Al Mamun Bhuyan et al., 2017b), dasatinib (Chan et al., 2018), lapatinib (Zierle et al., 2015), and pazopanib (Signoretto et al., 2016) lead to eryptosis. However, till date, there is no information available about the role of cytostatic compounds like afatinib/ceritinib/volasertib in modulating eryptosis *in vitro* or *in vivo*.

1. 3. 1. Afatinib

Afatinib or BIBW 2992 (Giotrif®), chemically known as (N-[4-[(3-chloro-4-fluorophenyl) amino]-7-[[(3S)-tetra-hydro-3-furanyl]oxy]-6-quinazolinyl]-4-(di-methyl-amino)-2-butenamide (Figure 3), is a second-generation, inflexible tyrosine kinase inhibitor (Li et al., 2008). It is approved as targeted monotherapy and is used as a first-line treatment for metastatic non-small cell lung cancer (NSCLC) associated with epidermal growth factor receptor (EGFR) mutations. Afatinib is recommended for oral administration at 40 mg once daily (Liao et al., 2013; Nelson et al., 2013).

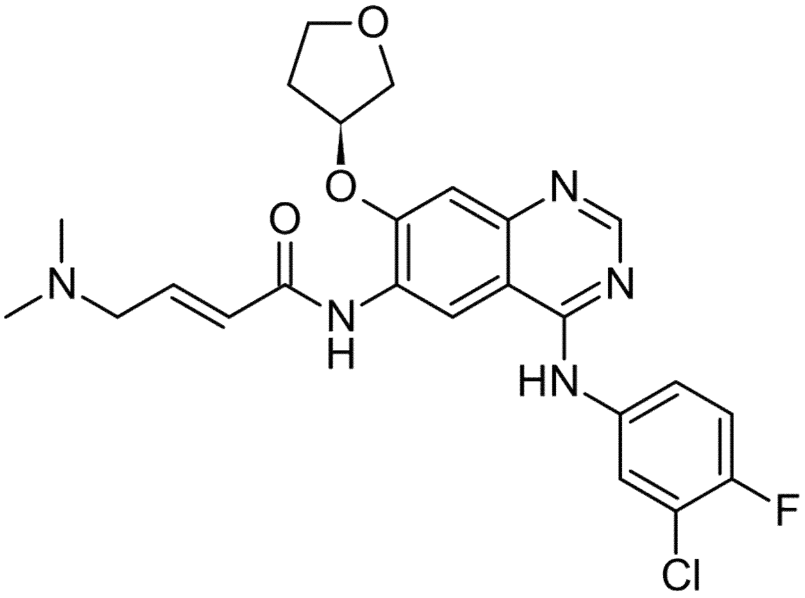

Figure 3: The chemical structure of afatinib (Wind et al., 2017; Wikipedia, 2019a).

Afatinib is a derivative of anilinoquinazoline possessing a highly reactive acrylamide group that covalently binds to the tyrosine kinase domains of EGFR/ human epidermal growth factor receptor 1 (HER1), human epidermal growth factor receptor 2 (HER2),

and to human epidermal growth factor receptor 4 (HER4) resulting in inhibiting tyrosine kinase autophosphorylation or the transphosphorylation of human epidermal growth factor receptor 3 (HER3) (Solca et al., 2012; Li et al., 2008) which, in turn, results in the downregulation of ErbB signalling as a result of inhibiting the Ras/ERK, PI3K/Akt, and STAT pathways (Modjtahedi et al., 2014). Afatinib not only inhibits the autophosphorylation of EGFR but also TGF-α induced phosphorylation (Lee et al., 2013).

To evaluate the functional potential of afatinib, cell-free assays were conducted. These assays demonstrated that afatinib is a powerful inhibitor of HER1, HER2, and HER4 with an IC_{50} of 10, 14, and 1 nM, respectively (Li et al., 2008). The efficacy of afatinib was almost similar to or greater than other tyrosine kinase inhibitors (TKIs) such as gefitinib, canertinib, erlotinib, and lapatinib (Solca et al., 2012; Li et al., 2008).

Many *in vitro* studies have also been conducted with different cell lines to check the potential of afatinib to inhibit the growth and proliferation of the cells (Li et al., 2008; Solca et al., 2012; Modjtahedi et al., 2014; Lee et al., 2013; Cha et al., 2012). Among them, the NSCLC has been studied most frequently followed by breast cancer (BC) and head and neck squamous cell cancer (HNSCC) (Modjtahedi et al., 2014). Moreover, afatinib showed its strong inhibitory action on the growth and proliferation of gastric cancer cells (Cha et al., 2012; Tanaka et al., 2012), biliary tract cells (Nam et al., 2012b), colorectal cancer cell lines, pancreatic cancer cell lines (Ioannou et al., 2011), bladder cancer (Greulich et al., 2012; Quesnelle and Grandis, 2011), endometrial cancer (Schwab et al., 2014), basal cell carcinoma (Eberl et al., 2012), and epidermal cell carcinoma (Cha et al., 2012).

Phase-I clinical trials were carried out in patients with advanced solid tumours focused on various afatinib schedules and dosages selection (Eskens et al., 2008; Marshall et al., 2013; Yap et al., 2010) resulting in 50 mg afatinib once daily recommended for the phase-II clinical trials (Yap et al., 2010). Afatinib's therapeutic efficacy in advanced NSCLC was determined from the phase-II and phase-III clinical trials (LUX-Lung trials) (Metro and Crino, 2011). The initial afatinib dose was reduced from 50 mg to 40 mg in the phase-II LUX-Lung-2 (Yang et al., 2012), phase-III LUX-Lung-3 (Keating, 2014), and the phase-III LUX-Lung-6 (Keating, 2014) clinical trials, which provided a

higher therapeutic index (Yang et al., 2012). The LUX-lung-3 clinical trials compared the efficacy of oral afatinib treatment with intravenous cisplatin plus pemetrexed in NSCLC patients with EGFR mutation (Sequist et al., 2013). The progression-free survival (PFS) rate significantly increased following afatinib treatment compared to cisplatin plus pemetrexed administration (Sequist et al., 2013). Oral afatinib as first-line therapy was compared with intravenous cisplatin plus gemcitabine treatment in the LUX-lung-6 clinical trials (Keating, 2014) in patients with advanced adenocarcinoma and active EGFR mutation. Afatinib alone results in a significantly longer PFS than cisplatin plus gemcitabine treatment (Keating, 2014). LUX-lung-7 and LUX-lung-8 clinical studies also revealed the higher survival rate of NSCLC patients with an EGFR mutation subsequent to afatinib treatment in comparison to gefitinib or erlotinib treatment (Sharma and Graziano, 2018).

Afatinib treatment was not only positively associated with the patient's survival rate but also triggered many adverse effects. The most commonly observed side effects related to tyrosine kinase inhibitor (TKI) afatinib treatment are diarrhoea (Aw et al., 2017; Mukai et al., 2015), skin xerosis (Aw et al., 2017), rash (Aw et al., 2017), stomatitis (Aw et al., 2017; Mukai et al., 2015), paronychia (Aw et al., 2017), heart failure (Patras de Campaigno et al., 2017), leukopenia (Mukai et al., 2015), neutropenia (Mukai et al., 2015), and anaemia (Mukai et al., 2015; Chu et al., 2014). Less commonly observed adverse effects are dry skin, pruritus, cheilitis, conjunctivitis, and dry eyes (Yang et al., 2013).

1. 3. 2. Ceritinib

Ceritinib, chemically known as 5-chloro-N4-[2-[(1-methylethyl)sulfonyl] phenyl]-N2-[5-methyl–2-(1-methylethoxy)-4-(4-piperidinyl)phenyl]-2,4-pyrimidinediamine (Figure 4), is a second-generation, anaplastic lymphoma kinase (ALK) inhibitor, which is selected for the regimen of advanced or metastasized ALK-positive NSCLC and is permitted for oral administration (Dhillon and Clark, 2014; Nishio et al., 2015; Khozin et al., 2015; Cooper et al., 2015; El-Osta and Shackelford, 2015). Clinical studies demonstrated approximately 2-7% of NSCLC is anaplastic lymphoma kinase positive (ALK+) (Friboulet et al., 2014; Chia et al., 2014).

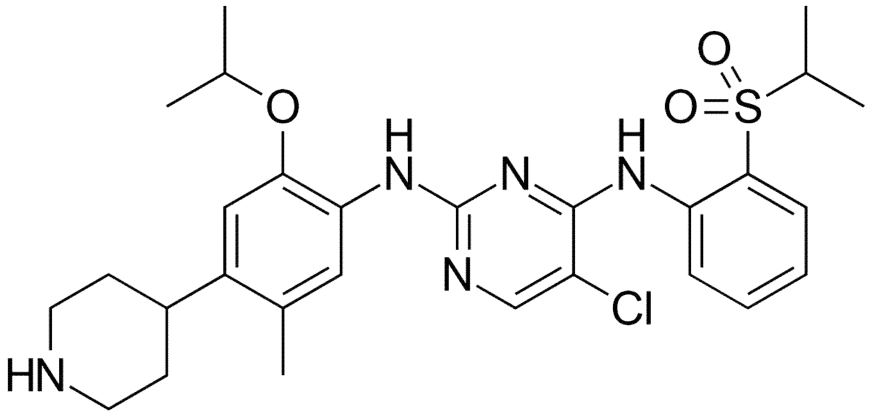

Figure 4: The chemical structure of ceritinib (El-Osta and Shackelford, 2015).

Ceritinib not only inhibits the phosphorylation of ALK but also the phosphorylation of the protein STAT3 (Novartis, 2015), ERK, ribosomal S6, and AKT, resulting in the suppression of the following signalling pathways: JAK-STAT3, MEK-ERK, mTOR, and PI3K-AKT, which ultimately decrease cell proliferation (Friboulet et al., 2014).

The potential of ceritinib is almost 20 times higher than that of crizotinib (Friboulet et al., 2014). NSCLC ALK+ cell lines were insensitive to alectinib treatment but were highly sensitive to ceritinib treatment (Katayama et al., 2014). However, ceritinib does not inhibit the growth of the cancer cells generated by mutation of EGFR, HER2, K-Ras, or PI3K (Friboulet et al., 2014).

Clinical trials with ceritinib have been conducted in two phases: Phase-I (ASCEND-1) (Shaw et al., 2014; Kim et al., 2016) and Phase-II (ASCEND-2) (Crino et al., 2016). The ASCEND-1 clinical trial enrolled ALK+ patients where 94% had NSCLC and underwent prior treatment with ALK inhibitors like crizotinib or alectinib (Kim et al., 2016). The maximum tolerated dose (MTD) of ceritinib was determined as 750 mg once daily from a phase-I clinical study (Shaw et al., 2014). Treatment of ALK+ NSCLC patients with ≥400 mg ceritinib daily yielded 2% complete response (CR), 55% partial response (PR), 22% no change, and 11% disease progression (Shaw et al., 2014). The overall response rate (ORR) was 56%, the disease progression-free survival (PFS) was seven months, and the overall survival was 17 months (Cooper et al., 2015). The ASCEND-2 clinical trial was carried out on ALK+ NSCLC patients who had prior 1-3 targeted-therapies with crizotinib or other standard therapies (Crino et al., 2016).

Results showed that the CR, PR, and ORR were 3%, 36%, and 39%, respectively (Deeks, 2016). The PFS was 7.2 months and the median overall survival was up to 15 months (Deeks, 2016).

The most common side effects of ceritinib are fatigue, anorexia, nausea, vomiting, diarrhoea, abdominal pain, constipation, hyperglycaemia, dyspepsia, dysphagia, rash, bradycardia, vision abnormalities, increased alanine aminotransferase (ALT), increased serum creatinine (sCr), increased aspartate aminotransferase (AST), decreased phosphate, increased lipase, gastroesophageal reflux disease (GERD), increased total bilirubin (TBILI) (Shaw et al., 2014), and anaemia (Khozin et al., 2015).

1. 3. 3. Volasertib

Volasertib or BI 6727 is a second novel dihydropteridinone derivative (Figure 5) that inhibits the polo-like kinase 1 (PLK1) followed by inhibiting mitotic spindle assembly, mitotic arrest, and apoptosis (Rudolph et al., 2009; Schoffski, 2009).

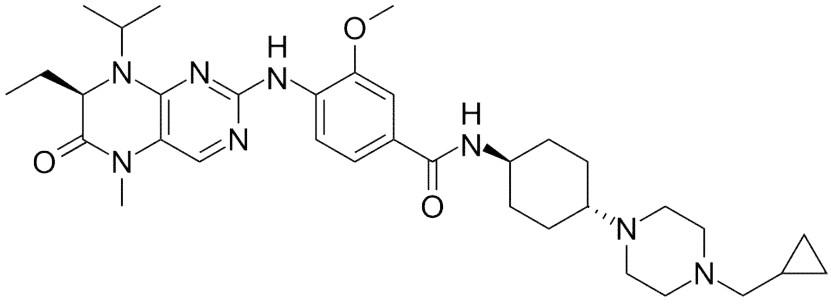

Figure 5: The chemical structure of volasertib (Gjertsen and Schoffski, 2015; Wikipedia, 2019b).

Preclinical studies showed cell lines such as AML, lung, colon, prostate, melanoma, hematopoietic malignancies, hepatocellular carcinoma, urothelial and multiple paediatric tumours treated with volasertib (IC_{50} = 11 – 37 nmol/l) significantly induce mitotic arrest and programmed cell death (Rudolph et al., 2009; Wissing et al., 2010; Cholewa et al., 2014; Sparta et al., 2014).

Different clinical trials have been performed with volasertib on various advanced solid tumours including metastasized urothelial cancer, advanced NSCLC, advanced ovarian

cancer, and in AML (Gjertsen and Schoffski, 2015). In clinical trials, volasertib was effective for treating acute myeloid leukaemia (AML) (Goroshchuk et al., 2019) but its monotherapy did not show a complete response (CR) of the patients. Again, volasertib with cytarabine showed a higher fatality rate (Adachi et al., 2017). Therefore, suitable combination therapy with volasertib and other agents is required. Volasertib is permitted to be applied orally or intravenously (Rudolph et al., 2009).

The maximum tolerated dose of volasertib was determined as 400 mg from the phase-I clinical trial (65 patients) with a single hour infusion every three weeks. The phase-I study showed complete response (CR) in 17% of patients, partial response (PRs) in 5% of patients with ovarian cancer, urothelial cancer, or melanoma, and the disease was stable among 40% of patients (Schoffski et al., 2012). Besides this, patients who received chemotherapy previously showed an 89% response to volasertib (Schoffski et al., 2012). In the phase-II clinical trials involving urothelial cancer, 14% of patients achieved PRs and 26% of patients were stable in the disease condition when receiving 300 mg of volasertib intravenously every 3 weeks (Gjertsen and Schoffski, 2015). The efficacy of volasertib with low dose cytarabine (LDAC) in AML was investigated in a phase-III clinical trial. However, the results did not show a significant difference in comparison to controls (Ingelheim, 2020).

Volasertib-related adverse effects (AEs) reported are anaemia (22%), neutropenia (15%), febrile neutropenia (8%), fatigue (15%), thrombocytopenia (14%), nausea (9%), and alopecia (9%). Grade 3/4 AEs (24%) that were observed were mostly haematological disorders (18%) like neutropenia (28%) and thrombocytopenia (20%) (Schoffski et al., 2012; Stadler et al., 2014).

1. 4. Aims of the study

The present investigation was carried out with the following objectives:

1. To explore the influence of afatinib on eryptosis.
2. To explore the influence of ceritinib on eryptosis.
3. To explore the effect of volasertib on eryptosis.

2. Materials and Methods

2. 1. Materials

2. 1. 1. Equipments

Name of the Equipment	Manufacturer
Autoclave	HICLAVE-50 HMC Labor systemtechnik, Germany.
Laboratory centrifuge machine	Eppendorf AG, Hamburg, Germany.
Eppendorf centrifuge machine	Hinz GmbH. Hamburg. Germany.
Magnetic stirrer	IKA-Werke GmbH & Co. KG, Germany.
pH meter 646	Carl Zeiss, Oberkochen. Germany.
Votex VX-100	Labned, Langenfeld, Germany.
FACS-Calibur	BD Biosciences, Heidelberg, Germany.
Incubator	Thermo Electron Corporation, Dreieich, Germany.
Water bath	Julabo GmbH, Seelbach, Germany.

2. 1. 2. Instruments

Name of the Instrument	Manufacturer
Pipettes 0.1-2 µl , 0.5-10 µl, 1-20 µl, 10-100 µl, 10-200 µl, and 10-1000 µl	Eppendorf AG, Hamburg, Germany.
Multichannel pipette 0.5-300 µl	Eppendorf AG, Hamburg, Germany.

2. 1. 3. Consumable materials

Name of the material	Manufacturer
SteriCup-GP (0,22µm) Millipore	Merck Millipore, Germany.
Eppendorf cups, 1.5 ml, 2 ml	Eppendorf, Hamburg, Germany.
Falcon tubes (15, 50 ml)	Greiner bio-one, Frickenhausen, Germany.
Tips 10 µl, 200 µl, 1000 µl	Biozym Scientific, Hess. Oldendorf, Germany.
Corning® Costar® 12 well plates	Sigma, Taufkirchen, Germany.
Corning® 24 well plates	Sigma, Taufkirchen, Germany.
Corning® 96 well plates	Sigma, Taufkirchen, Germany.

2. 1. 4. Chemicals

Name of the Chemical	Manufacturer
Afatinib	MedChemExpress, 1 Deer Park Dr, Suite Q, Monmouth Junction, NJ 08852, USA.
Ceritinib	Selleckchem, Karl-Schmid-Str. 14, 81829 Munich, Germany.
Volasertib	MedChemExpress, 1 Deer Park Dr, Suite Q, Monmouth Junction, NJ 08852, USA.
Dimethyl sulfoxide	Sigma, Taufkirchen, Germany.
Phosphate Buffer Saline (PBS)	Sigma, Taufkirchen, Germany.
Bovine Serum Albumin (BSA)	Sigma, Taufkirchen, Germany.
Sodium Chloride (NaCl)	Sigma, Taufkirchen, Germany.
Potassium Chloride (KCl)	Sigma, Taufkirchen, Germany.
Magnesium Sulphate ($MgSO_4$)	Sigma, Taufkirchen, Germany.
Calcium Chloride ($CaCl_2$)	Sigma, Taufkirchen, Germany.
N-2-hydroxyethylpiperazine-N-2-ethanesulfonic acid (HEPES)	Sigma, Taufkirchen, Germany.
Sodium nitroprusside (SNP)	Sigma, Taufkirchen, Germany.
Sodium Hydroxide (NaOH)	Sigma, Taufkirchen, Germany.
2',7'-dichlorodihydrofluorescein diacetate (DCFDA)	Sigma Aldrich, Hamburg, Germany.
A6730	Sigma, Taufkirchen, Germany.
Glucose	Carl Roth, Karlsruhe, Germany.
Annexin-V FITC-conjugated	ImmunoTools, Friesoythe, Germany.
Fluo3-AM ester	Biotium, Hayward, USA.
FITC Goat Anti-Mouse IgG/IgM	BD Pharmingen, Hamburg, Germany.
RPMI-1640 medium	Biochrom GmbH, Berlin, Germany.
Penicillin-Streptomycin	Invitrogen, Karlsruhe, Germany.
SB 203580	Tocris bioscience, Bristol, UK.
D4476	Tocris bioscience, Bristol, UK.

Staurosporine	Enzo Life Sciences, Lörrach, Germany.
Chelerythrine	Enzo Life Sciences, Lörrach, Germany.
Zvad	Enzo Life Sciences, Lörrach, Germany.
Ceramide monoclonal antibody (MID 15B4)	Enzo Life Sciences, Lörrach, Germany.

2. 1. 5. Cell line

Name of the cell line	**Manufacturer**
K562	Sigma Aldrich, Hamburg, Germany.

2. 1. 6. Software

Name of the software	**Manufacturer**
GraphPad Prism, version 6.0	GraphPad, La Jolla California USA.

2. 1. 7. Solutions

2. 1. 7. 1. Ringer's solution

As erythrocytes are devoid of cell organelles like mitochondria or nuclei, they cannot produce energy from the tricarboxylic acid (TCA) cycle. They rather generate energy through glycolysis (van Wijk and van Solinge, 2005). Hence, the erythrocyte concentrates can be preserved in the medium holding glucose as a source of energy. The Ringer's solution used in this study was adequate to maintain the ionic balance and homeostasis of water within the stored erythrocytes. The Ringer's solution contained the following components (Table 4):

Table 4: Constituents of Ringer's solution

Components	**Concentration in mM**	**Manufacturer**
Sodium Chloride (NaCl)	125	Sigma, Taufkirchen, Germany.
Potassium Chloride (KCl)	5	Sigma, Taufkirchen, Germany.
Magnesium Sulphate ($MgSO_4$)	1	Sigma, Taufkirchen, Germany.
Calcium Chloride ($CaCl_2$)	1	Sigma, Taufkirchen, Germany.
N-2-hydroxyethylpiperazine-N-2-	32.2	Sigma, Taufkirchen, Germany.

ethanesulfonic acid (HEPES)		
Glucose	5	Carl Roth, Karlsruhe Germany.
Sodium Hydroxide (NaOH)	13	Sigma, Taufkirchen, Germany.

After weighing the chemicals mentioned in Table 4, 982.798 ml of distilled water was added and mixed properly with a stirrer for thirty minutes or more until the substances were dissolved. The pH of the Ringer's solution was checked and adjusted to 7.4 with the help of NaOH or HEPES to obtain a physiological environment. Finally, the Ringer's solution was filtered to remove the unwanted particles and stored at 4˚C for further use. Before using the solution, it was warmed in the water bath at 37˚C to achieve body temperature (Jemaa et al., 2017).

2. 1. 7. 2. Annexin wash buffer (AWB)

The binding of the PS exposing erythrocytes to annexin-V is solely calcium-dependent. Hence, the concentration of calcium chloride used in the AWB (5 mM) was much higher than the one used in the Ringer's solution (1 mM). The components of the AWB are listed in Table 5.

Table 5: Components of the annexin wash buffer

Substances	**Concentration in mM**	**Manufacturer**
Sodium Chloride (NaCl)	125	Sigma, Taufkirchen, Germany.
HEPES	10	Sigma, Taufkirchen, Germany.
Calcium Chloride ($CaCl_2$)	5	Sigma, Taufkirchen, Germany.
Sodium Hydroxide (NaOH)	4	Sigma, Taufkirchen, Germany.

Deionized water (989.588 ml) was added to the above constituents. All substances were mixed properly with a magnetic stirrer for thirty minutes or more until the substances were completely dissolved. The pH of the annexin wash buffer was balanced to 7.4 using HEPES or NaOH. Later, the solution was filtered and preserved in a cool room. Before the AWB was used, it was heated to 37°C (body temperature) in a water bath (Jemaa et al., 2017).

2. 2. Methods

2. 2. 1. Isolation and treatment of the erythrocytes

Fresh whole blood samples were received from healthy donors regardless of sex and age. The specimens were collected from the blood bank of the University of Tubingen. The blood was drawn in vials containing lithium and heparin to prevent coagulation. For this study, ethical permission was taken from the university ethics committee and the permission number was 184/2003 V.

To obtain pure erythrocyte concentrates, three ml of Ringer's solution were taken into a five ml sterilized test tube and subsequently, one ml of whole blood was added. Afterwards, the tube was centrifuged with 120 × *g* at 21˚C for twenty minutes. The thrombocytes and leukocytes containing supernatant were removed and pure erythrocytes were collected from the bottom of the tubes and stored in 1.5 ml sterile Eppendorf tubes (Bissinger et al., 2016a). *In vitro* treatments were performed with fresh erythrocytes using 0.4% haematocrit in the Ringer's solution with different pre-decided concentrations of the assigned cytostatic compounds, i.e., afatinib, ceritinib, and/or volasertib. Finally, the samples were incubated for 48 hours at 37˚C.

2. 2. 2. Fluorescence-activated cell sorting (FACS)/ Flow cytometry

Fluorescence-activated cell sorting or flow cytometry is a modern technique used in analysing extracellular or intracellular molecules, which describes and identifies the cells from a heterogeneous population and determines the purity of isolated cells or even the size, volume, and granularity of the cells. It is also possible to assess the multi parameters of a single cell using flow cytometry. The basic principles of FACS are the measurement of the fluorescence intensity generated by fluorochrome-labelled antibodies to detect protein or ligands or any cell-associated molecules besides forward scatter (FS) or side scatter (SS) of the cells (Baumgarth and Roederer, 2000).

In the current study, FACS-Calibur (BD Biosciences, Heidelberg, Germany) was used for FACS analysis, which consists of two LASERs. One was a 488 nm argon LASER and the other was a 635 nm diode LASER. This FACS machine consisted of four LASER channels (FL-1, FL-2, FL-3, and FL-4). Each of the channels was wavelength-specific. For example, the FL-1, FL-2, FL-3, and FL-4 channels could detect the emitted light with 533/530 nm, 585/540 nm, 670 nm, and 675/625 nm, respectively, when

excited by a 488 nm wavelength. In our study, an argon LASER was used for exciting the fluorescence dye and the FL-1 channel was employed to identify the signals. For each parameter, 50,000 erythrocytes were evaluated.

2. 2. 3. Measurement of annexin-V-binding erythrocytes

Following 48 hours of incubation, the cytostatic-compound-treated erythrocytes, as well as control cells were vortexed for a few seconds to make a homogenous suspension. Afterwards, a 150 µl cell suspension was taken into a microwell plate and centrifugation was performed at 287 × *g* for three minutes at 21˚C. The supernatant was removed to obtain the cell pellet. To stain the erythrocytes, a master mix with the annexin-V antibody (ImmunoTools, Friesoythe, Germany) and annexin wash buffer (AWB) at a dilution of 1:200 was made. It is indicated that the annexin-V antibody was conjugated with fluorescein isothiocyanate (FITC) and the excitation wavelength and the emission wavelength of the FITC are 488 nm, and 530 nm, respectively. Subsequently, 150 µl AWB with annexin-V antibody was loaded to each probe and incubated in the dark for twenty minutes. Finally, the probes were transferred to FACS and the annexin-V fluorescence was measured in the FL-1 channel. An arbitrary marker (M1) was fixed to differentiate the phosphatidylserine externalised erythrocytes from the control cells. The measurement was done on a logarithmic scale (Jemaa et al., 2017; Al Mamun Bhuyan et al., 2017b).

2. 2. 4. Measurement of forward scatter (FSC) of erythrocytes

The volume or size of erythrocytes was measured from the forward scatter (FSC). For this purpose, subsequent to respective treatment and incubation, a 150 µl cell suspension was transferred into a multiwell plate. This suspension was then shifted from the plates to small FACS tubes using a multichannel pipette and measured without any staining. A dot plot was made for FSC vs SCC on a linear scale. The geometric mean (GM) of the respective probe was analysed to measure the volume of cells. For the control cells, the geometric mean was fixed around 500 (arbitrary unit) by changing the amplifier for understanding the shifting of the cells. The movement of the pulses to the right side of the scales from the control indicated the swelling of cells and the shift of the pulses towards the left side of the scale from the control indicated shrunken cells (Jemaa et al., 2017).

2. 2. 5. Assessment of cytosolic calcium of erythrocytes

Cytosolic calcium is a second messenger within live cells and increased intracellular calcium is one of the most important catalysts of eryptosis. Fluo3-AM-dependent fluorescence (Biotium, Hayward, USA) was used to quantify the cytosolic calcium. In a normal state, Fluo3 is a nonfluorescent substance that cannot enter cells through the plasma membrane. However, when Fluo3 is tagged with an acetoxymethyl (AM) group, it gains the strength to enter cells. The acetoxymethyl (AM) group binds with Fluo3 *via* an ester bond. Hence, Fluo3-AM is the modified form of the dye Fluo3. As soon as the Fluo3-AM reaches inside the cells, the cytosolic esterases break the ester bond between Fluo3 and the acetoxymethyl (AM) group. The free Fluo3 then binds to the cytosolic calcium ions and forms a chelate. The excitation wavelength of normal Fluo3 is 488 nm but when Fluo3 binds to cellular calcium ions, a marked increase of the fluorescence with an emission wavelength of 530 nm is observed.

To measure the cytosolic calcium, 150 µl cell suspension aliquots were transferred to microtiter plates and centrifuged at 287 × *g* for three minutes at 21˚C to obtain a cell pellet. Thereafter, the cells were stained with Fluo3-AM (10 µM) using AWB and incubated in the dark for thirty minutes at 37˚C. Finally, intracellular calcium was measured from the FL-1 channel of the FACS machine (Bissinger et al., 2014).

2. 2. 6. Assessment of cytosolic reactive oxygen species (ROS)

To assume the abundance of ROS or to measure the redox form within the erythrocyte, 2',7'-dichlorofluorescein diacetate (DCFDA) (Sigma Aldrich, Hamburg, Germany) was used. In general, DCFDA has inherent fluorescent properties and can easily cross the cell membrane. Using DCFDA, it is possible to determine the hydroxyl, superoxide, peroxyl or other cytosolic ROS. When DCFDA enters the cells, the intracellular esterases deacetylate the fluorogenic DCFDA into a non-fluorogenic compound. Subsequently, this compound is oxidized by cytosolic ROS to 2´7´-dichlorofluorescein (DCF), which possesses fluorescent properties and is captured by flow cytometry (Amer et al., 2003). Finally, 150 µl of erythrocyte suspension was taken from each sample into a microwell plate after predefined treatment and 48-hour incubation at 37˚C. The supernatant was thrashed out after centrifugation (287 × *g*, 3 minutes at 21˚C) to isolate the erythrocytes. Subsequently, the erythrocytes were stained with DCFDA (10 µM) in

Ringer's solution and incubated for thirty minutes under light protection. After the respective incubation, the erythrocyte suspension washed twice with Ringer's solution (150 µl in each probe). The DCFDA-dependent fluorescence intensity was measured using the FL-1 channel where the excitation wavelength was 488 nm and the emission wavelength was 530 nm (Bissinger et al., 2014).

2. 2. 7. Determination of ceramide

Earlier research showed inhibition of the cation channel with amiloride or removal of extracellular calcium, still stimulate the PS externalisation (Lang et al., 2003a) indicating involvement of other mechanism in inducing eryptosis. Afterwards, it was found that ceramide can induce eryptosis beyond involving the cation channel or cytosolic calcium upsurge. The sphingomyelinase (SM) enzyme causes the generation of ceramide from membrane sphingomyelin and, subsequently, stimulates the scramblase, leading to PS externalisation (Lang et al., 2004).

To measure the ceramide abundance, 100 µl erythrocyte suspension was transferred into a multiwell plate and centrifuged at 287 × *g* for three minutes at 21˚C for pelleting of the erythrocytes. Subsequently, the erythrocyte pellets were stained with anti-ceramide antibody at 1 µg/ml (Enzo Life Sciences, Lörrach, Germany) at a dilution of 1:10 in phosphate-buffered saline (PBS) containing 0.1% bovine serum albumin (BSA) and incubated at 37˚C for one hour. After the incubation, the cells were washed twice with 100 µl PBS-BSA buffer and stained with FITC-tagged goat anti-mouse IgG and IgM precise antibody at a dilution 1:50 (BD Pharmingen, Hamburg, Germany) in the same buffer. After thirty minutes of incubation, the cell pellet was washed twice again to get rid of the unbound secondary antibody. Finally, the cells were reloaded with 200 µl PBS-BSA and transferred to flow cytometry. The fluorescence measured at an excitation wavelength of 488 nm and an emission wavelength of 530 nm in the FL-1 channel (Bissinger et al., 2015).

2. 2. 8. Determination of haemolysis

For this purpose, erythrocytes were exposed to the respective cytostatic compound, as well as with their vehicles and incubated for 48 hours at 37˚C. As a positive control, erythrocytes exposed to distilled water. After the respective treatment and incubation, a homogenous erythrocyte suspension was made by gentle vortex and centrifugation at

287 × *g* for five minutes at 21˚C. Subsequently, 100 µl of supernatant was shifted to a microtiter plate. To obtain the background data, 100 µl distilled water was taken into a separate column of the microtiter plate. Finally, the absorption of haemoglobin (Hb) in the supernatant was assessed photometrically at a wavelength of 405 nm (Al Mamun Bhuyan et al., 2016a).

2. 2. 9. Culture and treatment of K562 cell

Human leukemic K562 cells (Sigma Aldrich, Hamburg, Germany) were cultured with an RPMI-1640 medium (Biochrom GmbH, Berlin, Germany) enriched with 2.0 g/l $NaHCO_3$ with the absence of L-glutamine. The medium was prepared by incorporating 10% foetal bovine serum (FBS) and 1% antibiotics (Penicillin and Streptomycin). Finally, the cells were cultured in 12 well-plates in a moistened incubator by maintaining 37°C with 5% CO_2. Where indicated, the volasertib (0.8 – 2.4 µM) was added directly to the cell culture medium.

2. 3. Statistical analysis

Statistical results are shown as means ± SD. An ANOVA test was used to find out the statistical difference between the multi-parameter of the samples with a Tukey test as a post-test. Otherwise, the unpaired t-test was employed for the analysis. Graph Pad Prism was used for all analysis (Version: 6.00, GraphPad, La Jolla California USA). $P<0.05$ was accepted as the lowest level of significance. The number of the respective erythrocyte samples was denoted by n. Every donor has a physiological difference that may affect the susceptibility of the erythrocytes to eryptosis. To avert bias, the same erythrocyte concentrates were used for the same experimental and control conditions.

3. Results

3. 1. The effect of afatinib on eryptosis

The present investigation explored whether afatinib stimulates suicidal erythrocyte death or eryptosis. The phospholipid asymmetry in erythrocytes along with translocation of phosphatidylserine from the inner cell surface to the outer cell surface is one of the most important hallmarks of eryptosis. To test the dose-dependent effect of afatinib on cell membrane scrambling, erythrocytes from healthy donors were exposed to different concentrations of afatinib (Figure 6) in Ringer's solution and incubated for 48 hours at 37˚C. In the control group, erythrocytes were exposed to Ringer's solution only under the same experimental conditions. Afterwards, the phosphatidylserine exposing erythrocytes were quantified from the annexin-V antibody docked with FITC. The FITC emitted fluorescence was captured by the FL-1 channel in a flow cytometer. Figure 7 demonstrates that after the respective incubation period, afatinib augments the phosphatidylserine exposing erythrocytes and the effect reaches statistical significance at 8.2 µM afatinib.

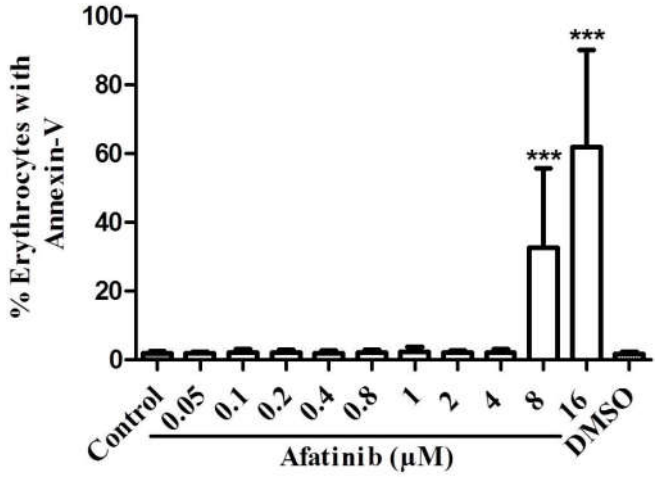

Figure 6: Dose-dependent sensitivity of afatinib on the phosphatidylserine (PS) externalisation. The bar chart indicates PS-externalised erythrocytes (data represented as arithmetic means ± SD, n = 10) following 48 hours of incubation in Ringer's solution. The grey bar indicates the control group and the white bars indicate the afatinib-treated (0.05 – 16 µM) erythrocytes whereas the striped bar represents the effect of the solvent (DMSO). ***($p<0.001$) points out the statistical distinction arising from the absence of afatinib (ANOVA).

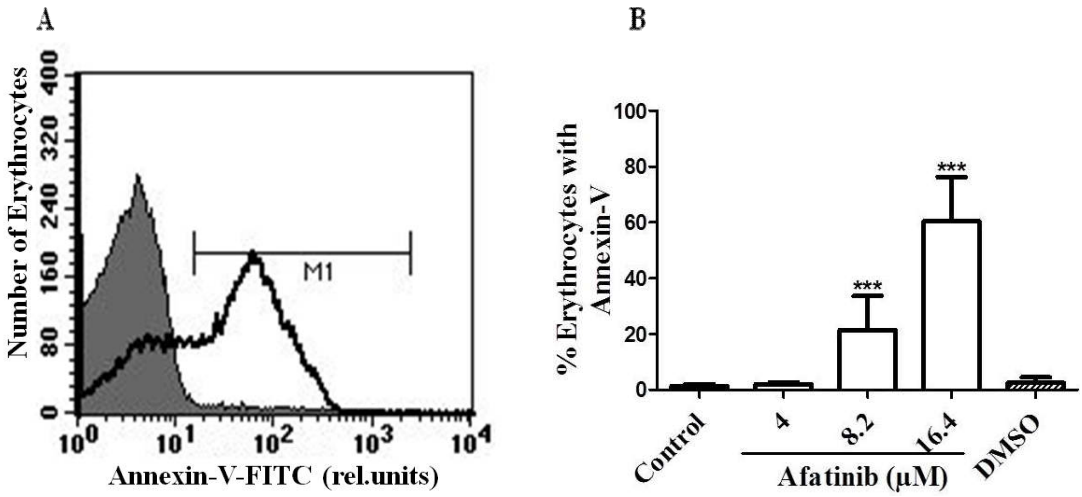

Figure 7: The sensitivity of afatinib on the externalisation of phosphatidylserine. **(A)** The histogram represents the erythrocytes with annexin-V following 48 hours of treatment. The grey plot indicates the control group and the black line indicates afatinib-treated (16.4 µM) erythrocytes. **(B)** A bar chart showing PS translocated erythrocytes (data represented as arithmetic means ± SD, n = 15) following 48 hours of incubation in Ringer's solution. The grey bar indicates the control group and the white bars indicate the afatinib-treated (4 – 16.4 µM) erythrocytes whereas the striped bar represents the effect of the solvent (DMSO). ***($p<0.001$) points out the statistical distinction arising from the absence of afatinib (ANOVA) [from (Al Mamun Bhuyan and Lang, 2018)].

An elevated intracellular calcium concentration is a fundamental catalyst of eryptosis. Hence, the cytosolic calcium was measured from Fluo3-emitted fluorescence employing flow cytometry after treating the healthy erythrocytes without and with afatinib (4 – 16.4 µM) in Ringer's solution with 48 hours of incubation. Figure 8 shows that afatinib increases the Fluo3 fluorescence and statistically significant fluorescence commences with a concentration of 8.2 µM afatinib.

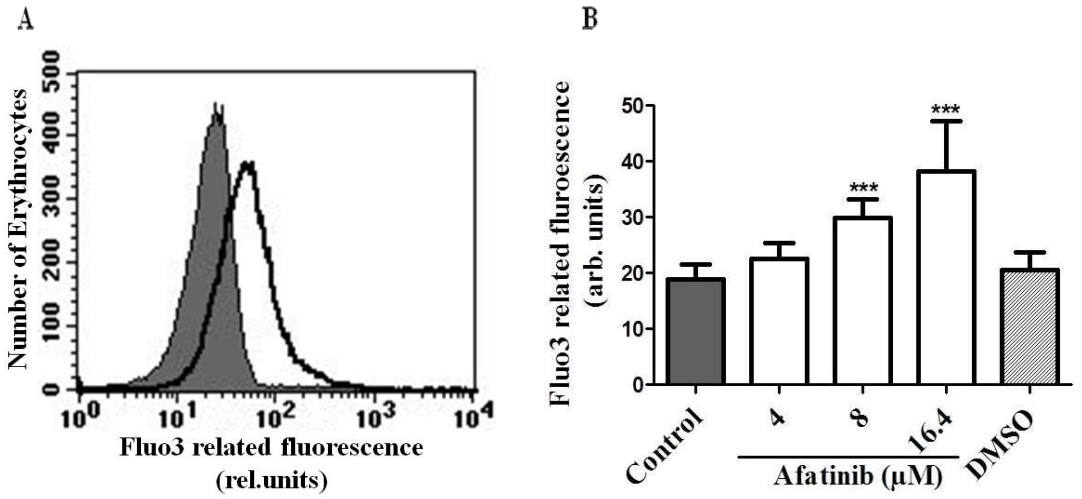

Figure 8: The sensitivity of afatinib on cytosolic calcium concentration. (A) A histogram showing Fluo3 fluorescence following exposure of erythrocytes to afatinib for 48 hours. The grey plot indicates the control group and the black line indicates afatinib-treated (16.4 µM) erythrocytes. **(B)** A bar chart showing Fluo3 fluorescence of erythrocytes (data represented on arithmetic means ± SD, n = 15) following 48 hours of incubation in Ringer's solution. The grey bar indicates the control group and the white bars indicate the afatinib-treated (4 – 16.4 µM) erythrocytes whereas the striped bar represents the effect of the solvent (DMSO). **($p<0.01$), ***($p<0.001$) points out the statistical distinction arising from the absence of afatinib (ANOVA) [from (Al Mamun Bhuyan and Lang, 2018)].

Another important feature of eryptosis is the shrinkage or decrease in the volume of erythrocytes. The shrunken erythrocytes were recognised from the decreased forward scatter (FSC). For this purpose, isolated healthy erythrocytes were incubated for 48 hours in Ringer's solution without or with afatinib using the concentration of 4 – 16.4 µM. As depicted in Figure 9, the volume of the cells decreases subsequent to afatinib exposure in all concentrations (4 – 16.4 µM) and statistically significant shrunken erythrocytes are noticed at 8.2 µM afatinib.

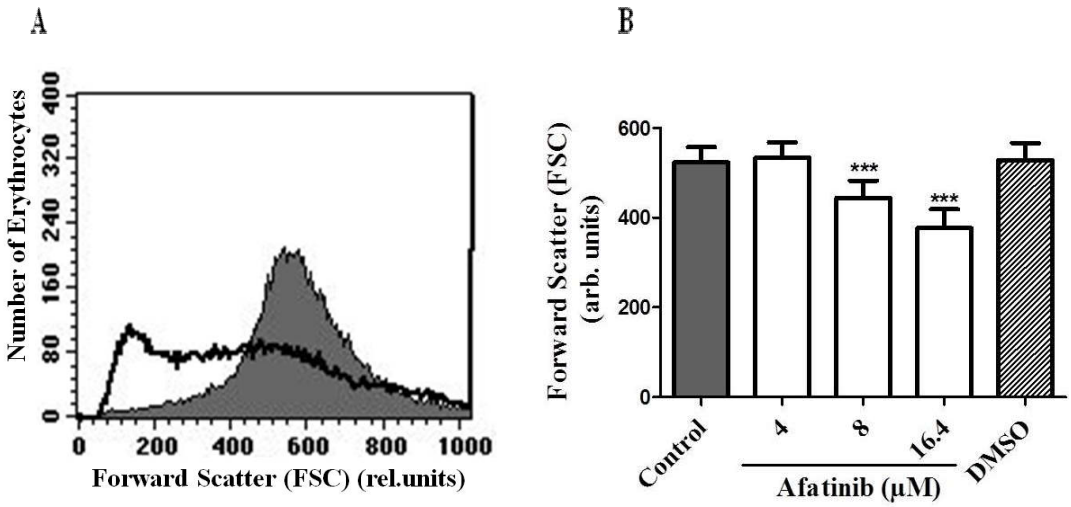

Figure 9: The sensitivity of afatinib on the erythrocyte size. (A) A histogram representing the volume of erythrocytes following 48 hours of treatment with afatinib. The grey plot indicates the untreated erythrocytes and the black line indicates afatinib-treated (16.4 µM) erythrocytes. **(B)** A bar chart showing the FSC of erythrocytes (data represented on arithmetic means ± SD, n = 15) following 48 hours of incubation in Ringer's solution. The grey bar indicates the control group and the white bars indicate the afatinib-treated (4 – 16.4 µM) erythrocytes whereas the striped bar represents the effect of the solvent (DMSO). ***($p<0.001$) points out the statistical distinction arising from the absence of afatinib (ANOVA) [from (Al Mamun Bhuyan and Lang, 2018)].

To explore the role of extracellular calcium in the afatinib-induced eryptosis, healthy erythrocytes were treated with and without 16.4 µM of afatinib in Ringer's solution for 48 hours at 37°C in the presence and absence of extracellular calcium. Then, the

annexin-V tagged erythrocytes were quantified. The result confirms the percentage of afatinib-induced annexin-V-binding cells decrease significantly without extracellular calcium (Figure 10). Nevertheless, afatinib increases the erythrocytes' membrane scrambling significantly even without extracellular calcium. Thus, afatinib-mediated phosphatidylserine translocation is partially induced by the influx of extracellular calcium.

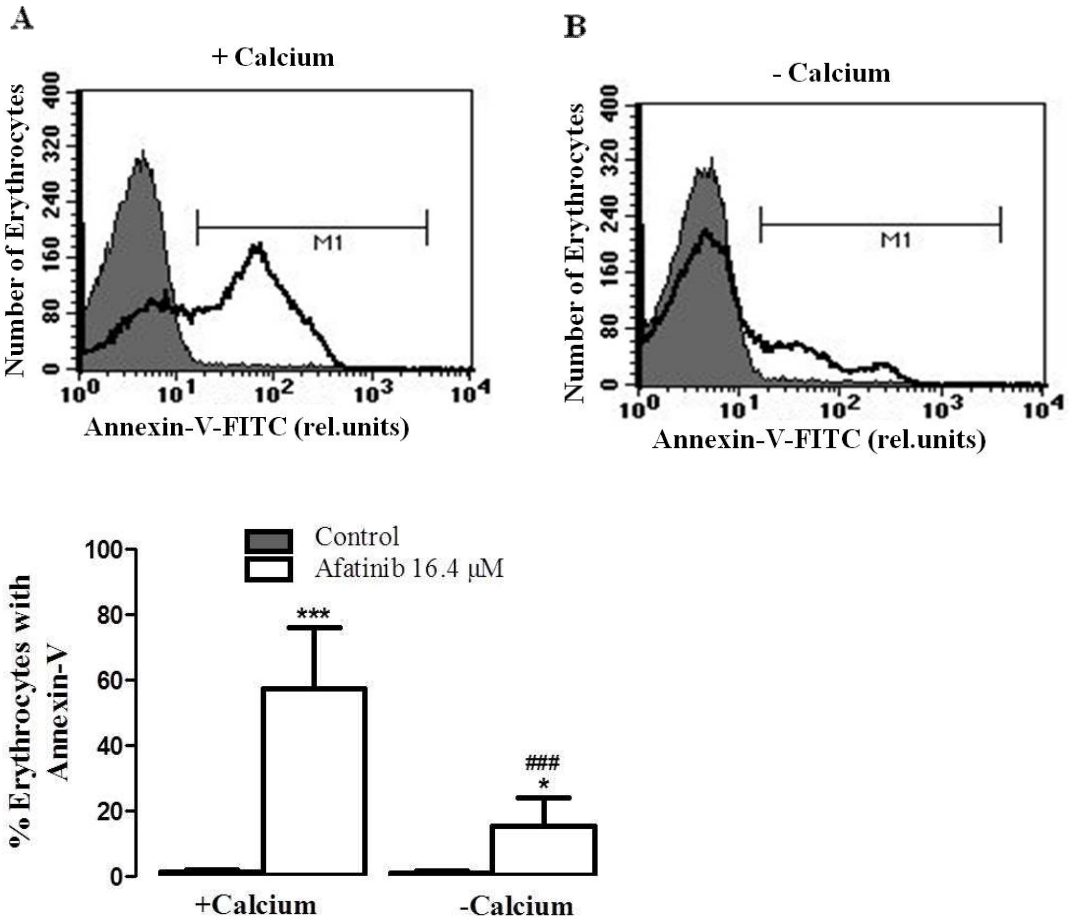

Figure 10: Calcium sensitivity on afatinib-induced PS externalisation. (A, B) Histograms of PS-exposing erythrocytes following 48 hours of afatinib treatment. The grey plots indicate the control group of erythrocytes and the black lines indicate afatinib-treated (16.4 µM) erythrocytes with **(A)** and without **(B)** extracellular calcium**. (C)** A bar chart showing PS-externalised erythrocytes (data represented on arithmetic means ± SD, n = 15) following exposure to afatinib for 48 hours of incubation in Ringer's solution. The grey bars represent the control group and the white bars indicate the afatinib-treated (16.4 µM) erythrocytes with (left bars) and without (right bars) extracellular calcium. *($p<0.05$), ***($p<0.001$) points out the statistical distinction arising from the absence of afatinib (ANOVA). ###($p<0.001$) points out the statistically significant difference arising from the presence of extracellular calcium (ANOVA) [from (Al Mamun Bhuyan and Lang, 2018)].

Again, to explore the effect of extracellular calcium on erythrocyte volume, the erythrocyte FSC was assessed following the removal of extracellular calcium. After exposure to afatinib, the volume of the erythrocytes decreased both in the presence and absence of extracellular calcium (Figure 11). Once more, the volume of shrunken erythrocytes was significantly enhanced in the group without extracellular calcium compared to the group with extracellular calcium. Therefore, it can be stated that the shrinkage of erythrocytes largely depends on the influx of extracellular calcium following afatinib treatment.

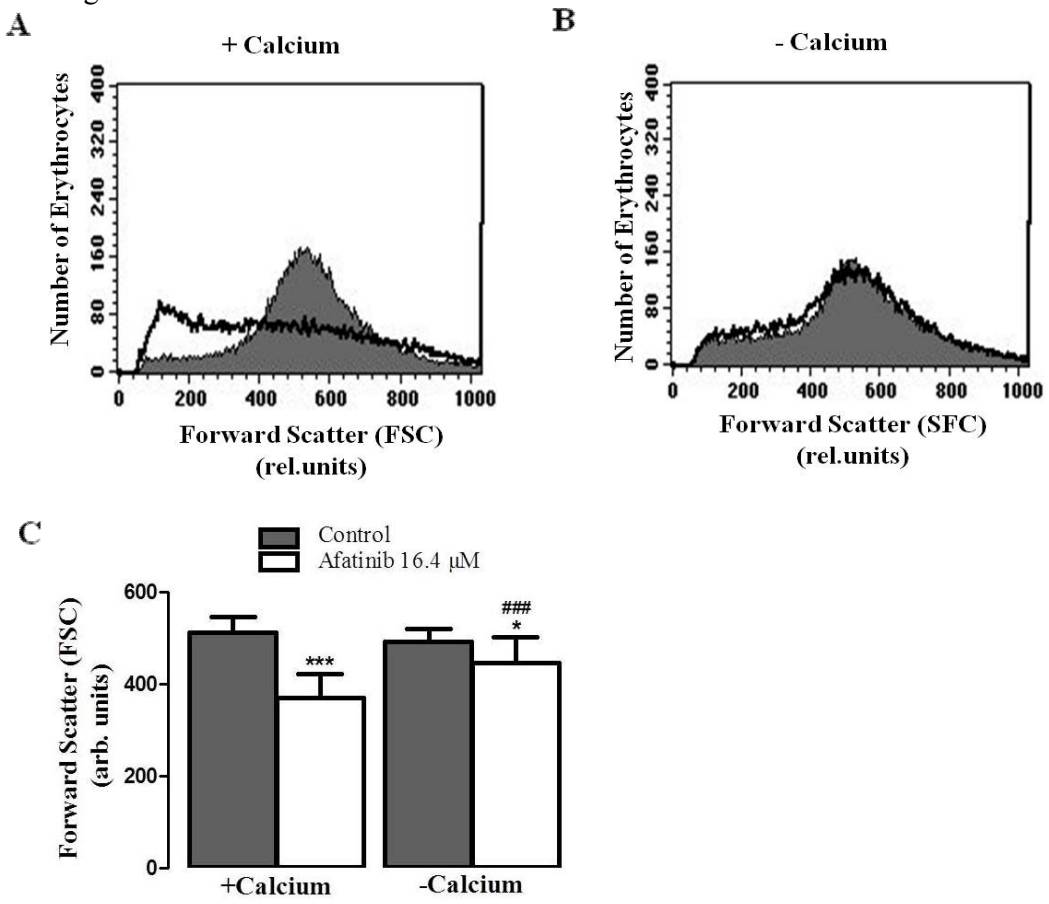

Figure 11: Calcium sensitivity on afatinib-induced cell shrinkage. (A, B) Histograms representing the erythrocyte volume after 48 hours of treatment. The grey plots indicate the control group and the black lines indicate afatinib-treated (16.4 µM) erythrocytes with **(A)** and without **(B)** extracellular calcium. **(C)** A bar chart showing the forward scatter of erythrocytes (data represented on arithmetic means ± SD, n = 15) following 48 hours of incubation in Ringer's solution. The grey bars represent the untreated erythrocytes and the white bars indicate the afatinib-treated (16.4 µM) erythrocytes with (left bars) and without (right bars) extracellular calcium. *($p<0.05$), ***($p<0.001$) points out the statistical distinction arising from the absence of afatinib (ANOVA). ###($p<0.001$) indicates a statistical difference arising from the group with extracellular calcium (ANOVA) [from (Al Mamun Bhuyan and Lang, 2018)].

AKT/PI3K along with PLCγ/PKC-dependent signalling pathways are upregulated by afatinib in nucleated cells (Modjtahedi et al., 2014). Considering this, an additional experiment was performed to explore the involvement of the AKT protein on afatinib-mediated eryptosis. To this end, erythrocytes were treated without and with AKT1/2 inhibitor A6730 (58 nM) in the presence of afatinib (16.4 µM) for 48 hours. The result depicts that the ratio of increased annexin-V-binding erythrocytes are almost same in the absence (from 2.46 ± 0.52 to 23.64 ± 2.19%, n = 5) and presence (from 4.07 ± 0.47 to 25.26 ± 6.41%, n = 5) of Akt1/2 inhibitor A6730 (58 nM). Thus, AKT1/2 protein has no significant role in afatinib-induced eryptosis.

Oxidative stress is an important stimulator of eryptosis (Lang et al., 2014). DCFDA-dependent fluorescence was assessed to quantify ROS generation in the erythrocytes. Figure 12 demonstrates DCFDA fluorescence was significantly enhanced in erythrocytes incubated with afatinib (16.4 µM) for 48 hours. Thus, afatinib-induced eryptosis partially correlates with oxidative stress.

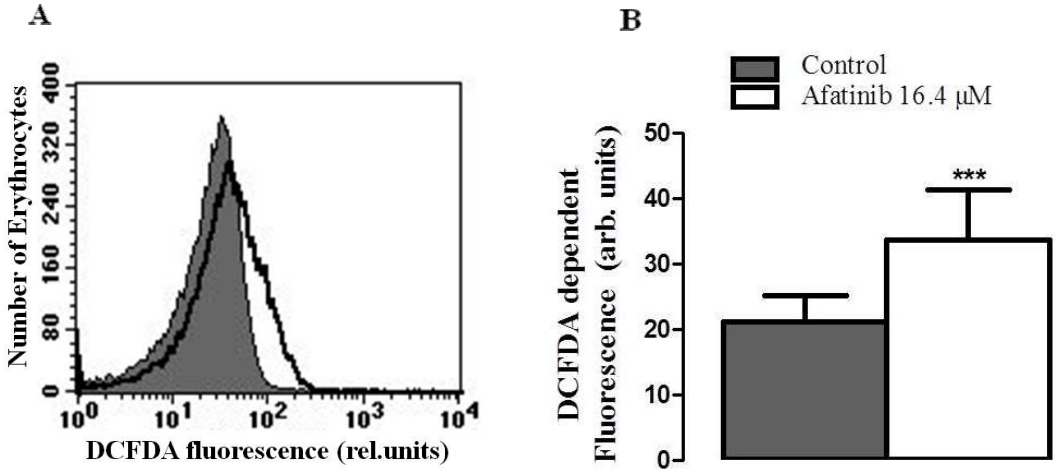

Figure 12: The significance of afatinib treatment on ROS formation. (A) The histogram represents DCFDA fluorescence within erythrocytes following exposure to afatinib for 48 hours. The grey plot and black line indicate the unexposed and afatinib-exposed (16.4 µM) erythrocytes, respectively. **(B)** A bar chart with DCFDA fluorescence of erythrocytes (data represented on arithmetic means ± SD, n = 13) following 48 hours of incubation in Ringer's solution. The grey column represents the control group and the white bar represents the afatinib-treated (16.4 µM) erythrocytes. ***($p<0.01$) indicates a significant difference when there was an absence of afatinib (unpaired t-test) [from (Al Mamun Bhuyan and Lang, 2018)].

Further, ceramide is a well-established eryptosis stimulator (Lang et al., 2004; Lang et al., 2010). The enzyme sphingomyelinase is the key regulator for generating ceramide by splitting sphingomyelin (Lang et al., 2004; Lang et al., 2010). The abundance of ceramide on the erythrocyte surface was measured using ceramide-specific antibodies. As shown in Figure 13, erythrocytes exposed to afatinib (16.4 µM) showed a higher ceramide generation in comparison to the control group. This result points to ceramide production playing an important role in afatinib-mediated eryptosis.

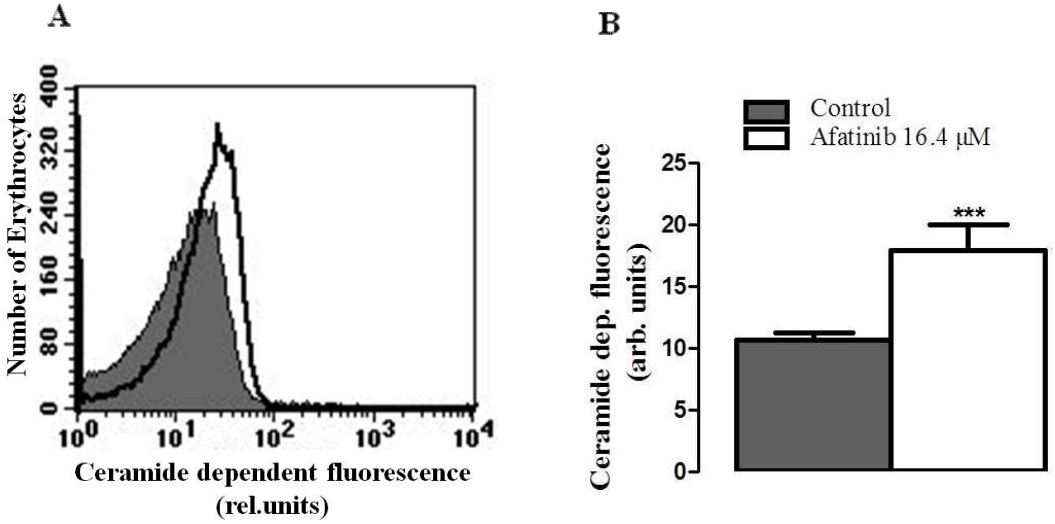

Figure 13: The significance of afatinib treatment on ceramide generation. (A) The histogram represents ceramide abundance on the surface of erythrocytes following exposure to afatinib for 48 hrs. The grey plot represents the untreated erythrocytes and the black line represents the afatinib-treated (16.4 µM) erythrocytes. **(B)** A bar chart representing ceramide-generated erythrocytes (data represented on arithmetic means ± SD, n = 5) following 48 hours of incubation in Ringer's solution. The grey bar points to the control group and the white bar points to the afatinib-treated (16.4 µM) erythrocytes. ***($p<0.01$) points out the statistical distinction arising from the absence of afatinib (unpaired t-test) [from (Al Mamun Bhuyan and Lang, 2018)].

The next experiments were performed to elucidate the role of kinases and caspases in afatinib-induced phosphatidylserine externalisation. For this purpose, healthy erythrocytes were exposed to afatinib with and without a PKC inhibitor, i.e., chelerythrine (1 µM). The results demonstrate the percentage of PS-translocated erythrocytes subsequent to afatinib (16.4 µM) treatment are almost identical in the absence (from 1.17 ± 0.33% to 22.63 ± 14.04%, n = 5) and in the presence (from 2.47 ± 0.83% to 29.65 ± 12.34%, n = 5) of chelerythrine (1 µM). Hence, the result proves the negligence of PKC on afatinib-mediated eryptosis.

p38 kinase often participates in eryptosis regulation (Gatidis et al., 2011). Therefore, an additional experiment with afatinib (16.4 μM) was conducted in the absence and presence of p38 kinase inhibitor SB203580 with a concentration of 2 μM for 48 hours. Thereafter, annexin-V antibody-tagged erythrocytes were quantified by FACS. The data show no statistically significant distinction in the proportion of phosphatidylserine-exposing erythrocytes without (from 1.19 ± 0.45% to 27.72 ± 20.71%, n = 5) and with (from 1.22 ± 0.41% to 40.28 ± 11.71%, n = 5) SB203580 (2 μM) treatment. Thus, afatinib-triggered erythrocyte demise is not affected by p38 kinase.

Previous studies suggested the participation of casein kinase 1α (CK1α) in eryptosis stimulation (Zelenak et al., 2012). Therefore, the following experiment was performed to test the influence of CK1α on afatinib-induced membrane scrambling. Erythrocytes were exposed to afatinib (16.4 μM) in the absence and presence of CK1α inhibitor D4476 (10 μM). The results demonstrate that afatinib increased the phosphatidylserine-exposing erythrocytes to the same extent following incubation without (from 1.17 ± 0.33% to 22.63 ± 14.04%, n = 5) and with (from 1.07 ± 0.45% to 19.62 ± 10.65%, n = 5) D4476 (10 μM). Thus, CK1α has no stimulating effect on afatinib-induced eryptosis.

Another experiment was done without and with Janus kinase 3 (JAK3) inhibitor WHI-P154 (56 μM) to explore the impact of JAK3 on afatinib-targeted (16.4 μM) erythrocyte death. The results indicate the increase of the percentage of PS-translocated erythrocytes is similar in the absence (from 1.22 ± 0.21% to 15.74 ± 8.75%, n = 5) and presence (from 1.39 ± 0.43% to 16.49 ± 6.83%, n = 5) of JAK3 inhibitor WHI-P154 (11.2 μM). These findings explain that JAK3 does not influence afatinib-triggered eryptosis.

Moreover, caspases are often reported to play a role in the externalisation of the protein phosphatidylserine from the inner to the outer surface of the erythrocyte membrane (Mandal et al., 2005; Mandal et al., 2002). To determine the response of caspases on afatinib-induced (16.4 μM) eryptosis, an experiment was performed in the absence and presence of pan-caspase inhibitor zVAD (10 μM). The experimental findings illustrate the percentage of eryptotic erythrocytes increased to the same extent in the absence (from 1.51 ± 0.28% to 45.96 ± 24.89%, n = 5) and in the presence (from 8.71 ± 3.59% to 61.88 ± 24.63%, n = 5) of zVAD (10 μM), which points to caspase-independent eryptosis triggered by afatinib.

Xenobiotics often cause haemolysis (Signoretto et al., 2016; Shaik et al., 2012; Lupescu et al., 2012). Hence, an experiment was conducted to investigate the sensitivity of afatinib on haemolysis. For this reason, haemoglobin concentration in the supernatant was quantified subsequent to 48 hours of incubation with afatinib. Figure 14 shows that afatinib stimulates haemolysis in all concentrations (4 – 16.4 µM) but increased haemolysis with statistical significance is observed at a concentration of 16.4 µM.

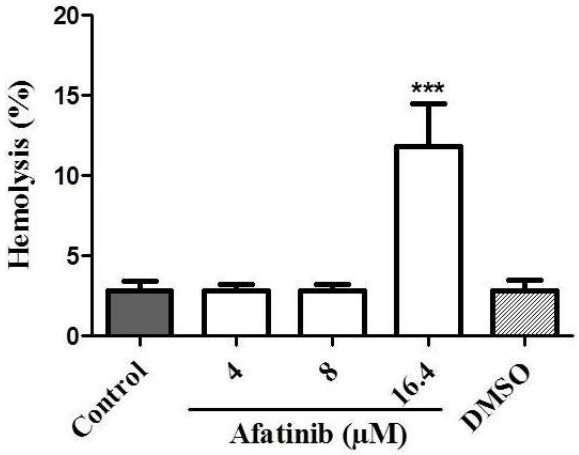

Figure 14: The effect of afatinib on haemolysis. A bar chart representing haemolytic erythrocytes (data represented on arithmetic means ± SD, n = 5) following incubation for 48 hours in Ringer's solution. The grey bar indicates the control group and the white bars indicate the afatinib-treated (4 – 16.4 µM) groups. The striped bar points out the effect of the solvent (DMSO).***($p<0.001$) points out the statistical distinction arising from the absence of afatinib (ANOVA) [from (Al Mamun Bhuyan and Lang, 2018)].

Taken together, the cytostatic molecule afatinib stimulates suicidal erythrocyte death and causes an elevated cytosolic calcium concentration and enhanced production of ceramide and ROS, which are crucial in orchestrating afatinib-triggered eryptosis.

3. 2. The effect of ceritinib on eryptosis

The present investigation addressed the effect of ceritinib on eryptosis. The main feature of eryptosis is the translocation of PS from the inner to the outer surface of the erythrocyte plasma membrane. For this experimental purpose, erythrocytes from healthy donors were exposed to different concentrations of ceritinib in Ringer's solution with a haematocrit of 0.4% and stored in the incubator for 48 hours maintaining 37°C to check its effect (Figure 15). For the control group, the erythrocytes were exposed to isotonic Ringer's solution without ceritinib.

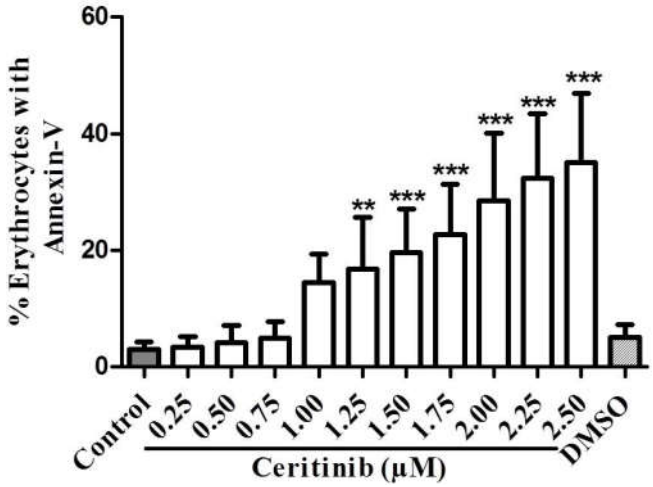

Figure 15: Dose-dependent sensitivity of ceritinib on PS externalisation. A bar chart showing PS-translocated erythrocytes (data represented on arithmetic means ± SD, n = 10) following 48 hours of incubation in Ringer's solution. The grey bar indicates the control group and the white bars indicate the ceritinib-treated (0.25 – 2.5 µM) erythrocytes whereas the striped bar shows the impact of the solvent. ** ($p<0.01$), ***($p<0.001$) points out the statistical distinction arising from the absence of ceritinib (ANOVA).

As the exposure of phosphatidylserine is the main indicator of eryptosis, after respective treatment and incubation time, the erythrocytes were stained with FITC-conjugated annexin-V antibody. Subsequently, the erythrocytes were subjected to flow cytometry to quantify the number of PS-exposing cells. Figure 16 shows that ceritinib increases the apoptotic erythrocytes in all concentrations and a statistically significant number of dead erythrocytes are noticed at a concentration of 1.34 µM ceritinib.

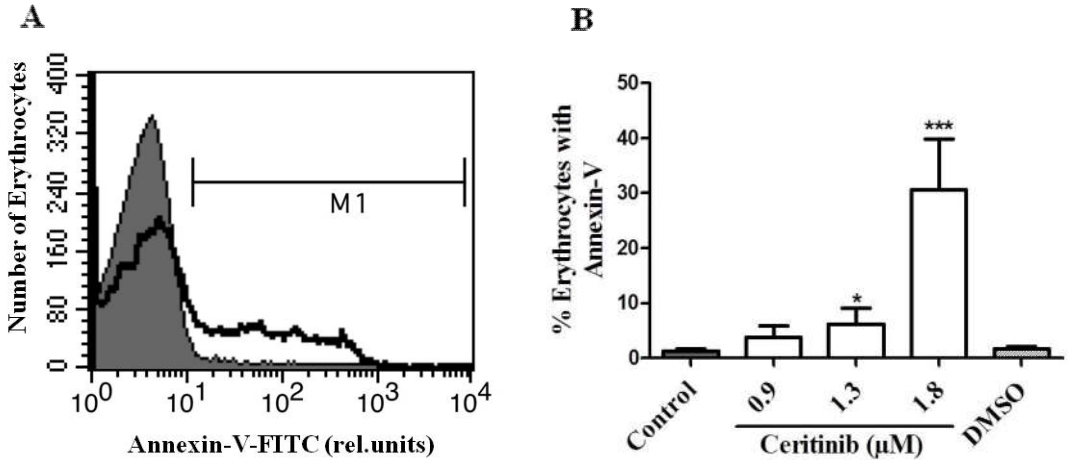

Figure 16: The sensitivity of ceritinib on phosphatidylserine translocation. (A) The histogram represents annexin-V-binding erythrocytes following 48 hours of treatment. The grey plot indicates the erythrocytes without treatment and the black line indicates ceritinib-treated (1.8 µM) erythrocytes. **(B)** A bar chart showing PS-translocated erythrocytes (data represented on arithmetic means ± SD, n = 17) following 48 hours of incubation in Ringer's solution. The grey bar represents the control group and the white bars represent the ceritinib-treated (0.9 – 1.8 µM) erythrocytes whereas the striped bar designates the impact of the solvent. *($p<0.05$), ***($p<0.001$) points out the statistical distinction arising from the absence of ceritinib (ANOVA) [from (Al Mamun Bhuyan et al., 2016b)].

The shrinkage of erythrocytes is another important characteristic of eryptosis (Lang and Qadri, 2012) and the shrunken erythrocytes were evaluated from the FSC. To perform this experiment, erythrocytes were incubated in Ringer's solution for 48 hours without and with different concentrations (0.9 – 1.8 µM) of ceritinib. Afterwards, the volume or size of the erythrocytes was quantified by employing flow cytometry. Figure 17 demonstrates the volume of erythrocytes decreases as a result of ceritinib exposure but 1.8 µM concentration of ceritinib causes significant shrinkage in the erythrocytes.

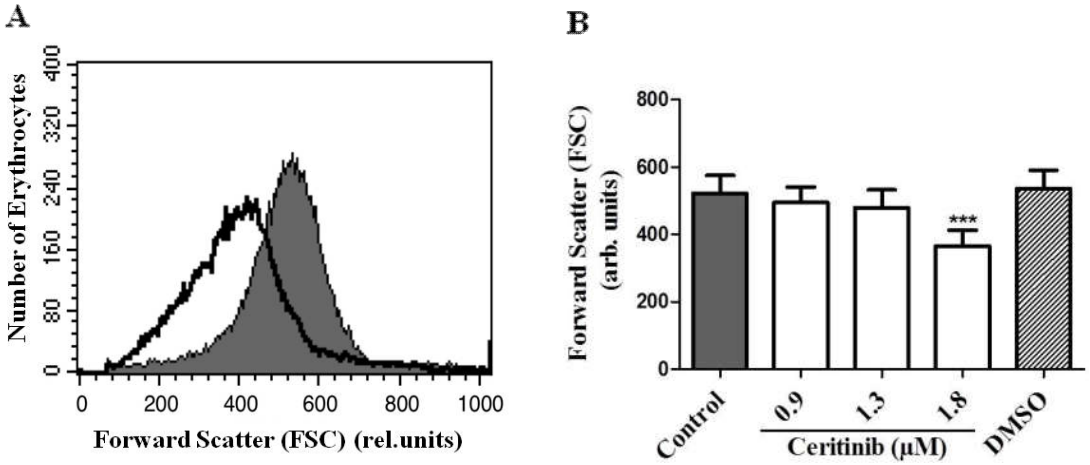

Figure 17: The influence of ceritinib on the size of erythrocytes. (A) The histogram represents the erythrocyte volume following 48 hours of treatment with ceritinib. The grey plot indicates the control group and the black line indicates ceritinib-treated (1.8 µM) erythrocytes. **(B)** A bar chart with FSC of erythrocytes (data represented on arithmetic means ± SD, n = 17) following 48 hours of incubation in Ringer's solution. The grey bar indicates the untreated and the white bars indicate the ceritinib-treated (0.9 – 1.8 µM) erythrocytes whereas the striped bar points out the significance of the solvent (DMSO). ***($p<0.001$) points out the statistical distinction arising from the control group (ANOVA) [from (Al Mamun Bhuyan et al., 2016b)].

The increased level of intracellular calcium is the chief regulator of eryptosis (Pretorius et al., 2016b) and was quantified from the Fluo3 fluorescence. For this experimental purpose, healthy, fresh erythrocytes were incubated with and without ceritinib (0.9 – 1.8 µM) and incubated for 48 hours. After the respective incubation time, the erythrocytes were stained with Fluo3-AM (10 µM) and incubated in the dark for 30 minutes. Subsequently, the Fluo3-emitted fluorescence was captured by the FL-1 channel of the flow cytometer. Figure 18 exhibits Fluo3 fluorescence increases as a result of ceritinib treatment and a statistically significant effect is observed at 1.8 µM concentration of ceritinib.

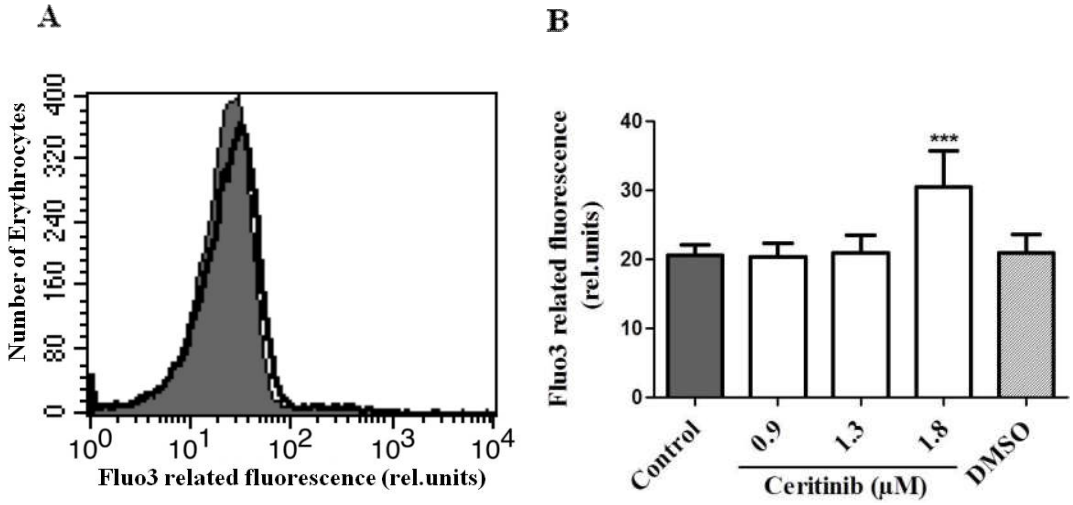

Figure 18: The effect of ceritinib on cytosolic calcium concentration. (A) A histogram on emitted Fluo3 fluorescence following ceritinib treatment on erythrocytes for 48 hours. The grey plot indicates the control group and the black line indicates 1.8 µM ceritinib-exposed erythrocytes. **(B)** A bar chart with Fluo3 fluorescence of erythrocytes (data represented on arithmetic means ± SD, n = 17) following 48 hours of incubation in Ringer's solution. The grey bar represents the control erythrocytes and the white bars represent the ceritinib-treated (0.9 – 1.8 µM) erythrocytes whereas the striped bar represents the effect of the solvent. ***($p<0.001$) points out the statistical distinction arising from the absence of ceritinib (ANOVA) [from (Al Mamun Bhuyan et al., 2016b)].

The next series of experiments was done to verify the requirement of extracellular calcium for ceritinib-triggered eryptosis. To conduct this experiment, erythrocytes were treated with and without ceritinib (1.8 µM) in the presence and absence of extracellular calcium. Figure 19 displays that the translocation of PS was significantly blunted following the withdrawal of extracellular calcium. Nevertheless, in the absence of extracellular calcium, ceritinib significantly translocated the phosphatidylserine to the outer surface of the cell membrane. These results highlight that ceritinib-induced erythrocyte membrane scrambling is partly dependent on the entry of interstitial calcium.

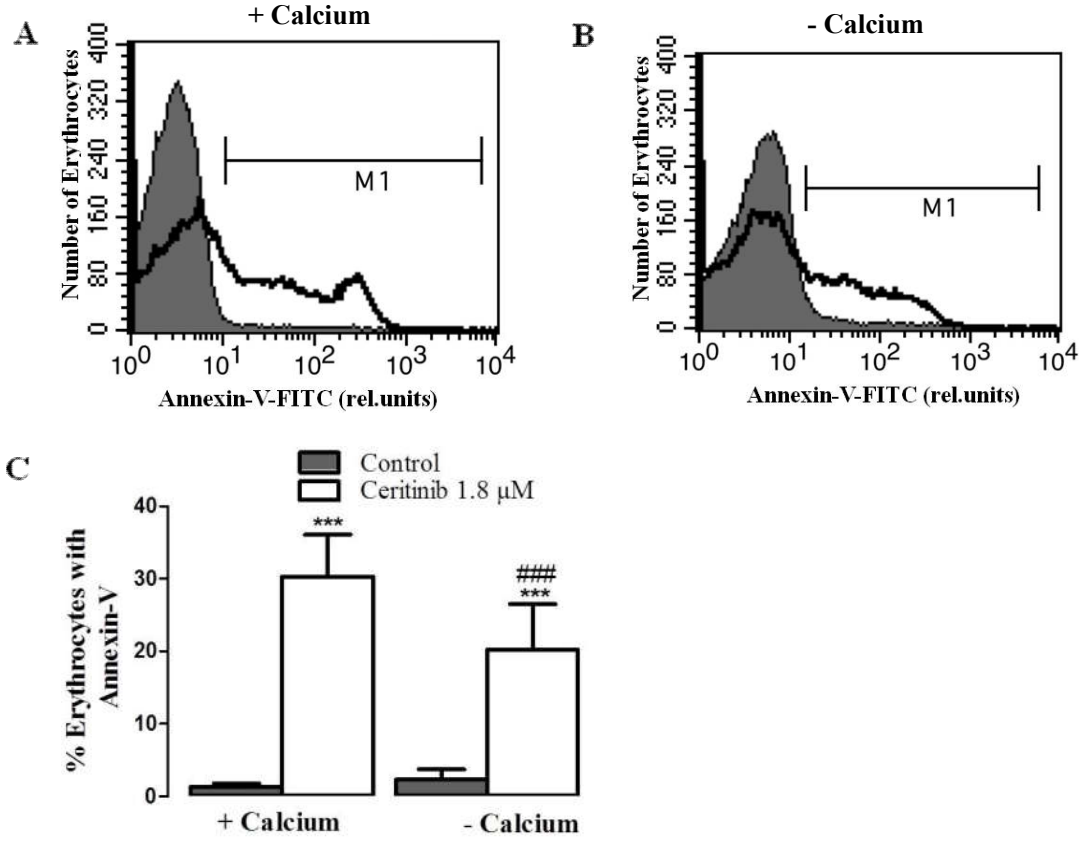

Figure 19: The influence of extracellular calcium on ceritinib-induced PS externalisation. (A, B) Histograms representing eryptotic erythrocytes following 48 hours of ceritinib treatment. The grey plots indicate the control group and the black lines indicate ceritinib-treated (1.8 µM) erythrocytes with (**A**) and without (**B**) extracellular calcium. **(C)** A bar chart of PS-externalized erythrocytes (data represented on arithmetic means ± SD, n = 17) following 48 hours of incubation in Ringer's solution. The grey bars indicate the control group and the white bars indicate the ceritinib-treated (1.8 µM) erythrocytes with (bars on the left side) and without (bars on the right side) extracellular calcium. ***($p<0.001$) designates the statistical distinction arising from the absence of ceritinib (ANOVA). ###($p<0.001$) indicates the statistical significant difference arising from the presence of extracellular calcium (ANOVA) [from (Al Mamun Bhuyan et al., 2016b)].

The non-selective cation channel (NSCC) is the main ion channel in erythrocytes to raise the cytosolic calcium concentration and, thus, promote eryptosis (Lang et al., 2003a). To check the functionality of NSCC subsequent to ceritinib (1.8 µM) exposure, the erythrocytes were incubated for 48 hours with and without the NSCC blocker amiloride (1 mM). Figure 20 shows that the number of annexin-V-binding erythrocytes significantly decreases in the amiloride-treated group, pointing at the stimulating role of NSCC for increasing the cytosolic calcium subsequent to ceritinib treatment and thus eryptosis. Nevertheless, even in the presence of amiloride, the ceritinib-mediated cell death increases significantly indicating the partial participation of NSCC in triggering apoptosis.

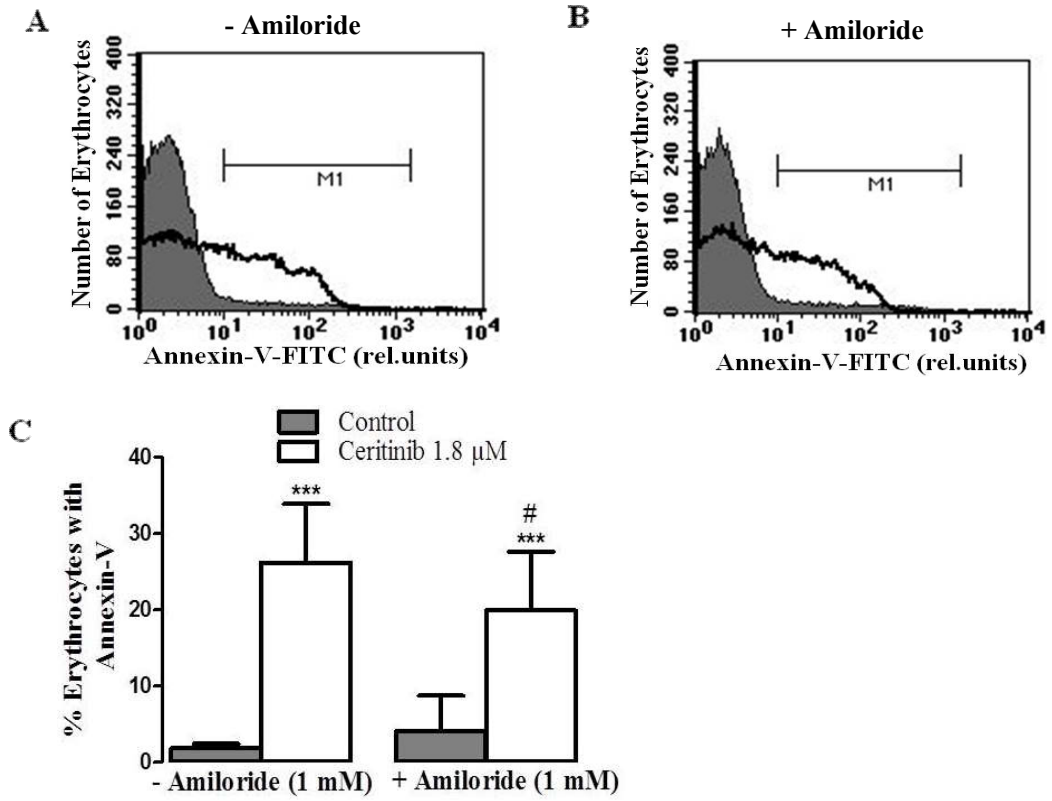

Figure 20: Amiloride sensitivity on ceritinib-mediated PS exposure. (A, B) Histograms representing PS-exposed erythrocytes after 48 hours of treatment. The grey plots indicate the untreated erythrocytes and the black lines indicate 1.8 µM ceritinib-treated erythrocytes without (**A**) and with (**B**) amiloride (1 mM). **(C)** A bar chart showing eryptotic erythrocytes (data represented on arithmetic means ± SD, n = 13) following 48 hours of incubation in Ringer's solution. The grey bars indicate the control group and white bars indicate the ceritinib-treated (1.8 µM) erythrocytes without (left bars) and with (right bars) amiloride. ***($p<0.001$) points out the statistical distinction arising from the absence of ceritinib (ANOVA). #($p<0.05$) indicates the statistical significant difference arising from the absence of amiloride (ANOVA) [from (Al Mamun Bhuyan et al., 2016b)].

Without an increased level of intracellular calcium, there are diverse triggers of eryptosis. Among them, ROS is a critical stimulator of eryptosis and indicates the redox state in a cell (Dong et al., 2016). To carry out this investigation, erythrocytes were incubated for 48 hours, with and without ceritinib (1.8 µM) and subsequently stained with DCFDA (10 µM) to quantify ROS within the cells. Figure 21 depicts there is no statistical difference between the DCFDA fluorescence within the control (20.56 ± 2.29 a.u., n = 10) and the ceritinib-treated group (19.34 ± 1.94 a.u., n = 10), indicating that ceritinib-mediated eryptosis is not associated with oxidative stress.

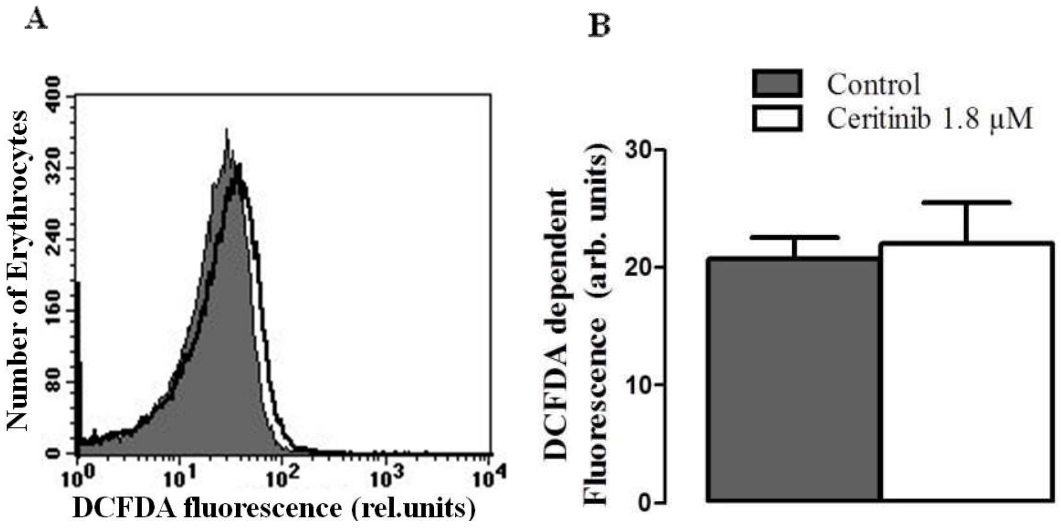

Figure 21: The effect of ceritinib treatment on ROS generation. (A) The histogram represents DCFDA fluorescence within erythrocytes following exposure to ceritinib for 48 hours. The grey plot represents the unexposed erythrocytes and the black line points at the ceritinib-exposed (1.8 µM) erythrocytes, respectively. **(B)** A bar chart with DCFDA fluorescence of erythrocytes (data represented on arithmetic means ± SD, n = 9) following 48 hours of incubation in Ringer's solution. The grey column indicates the control group and the white column indicates the ceritinib-treated (1.8 µM) group [from (Al Mamun Bhuyan et al., 2016b)].

Ceramide is a further mediator of eryptosis (Lang et al., 2004; Lang et al., 2010). Ceramide can stimulate the scrambling effect of calcium or can activate the scramblase enzyme by itself and translocate the PS to the erythrocyte's surface (Lang et al., 2004; Lang et al., 2010). Ceramide generation in the cells was evaluated using ceramide-specific antibodies. Hence, erythrocyte concentrates were exposed to Ringer's solution with and without ceritinib (1.8 µM) and stored in the incubator for 48 hours.

Subsequently, ceramide-associated fluorescence was assessed employing flow cytometry. According to Figure 22, the abundance of ceramide on the erythrocyte membrane is alike in the control (19.34 ± 1.95 a.u., n = 10) and ceritinib-treated (20.56 ± 2.29 a.u., n = 10) group. Thus, ceritinib-stimulated eryptosis is not dependent on ceramide formation.

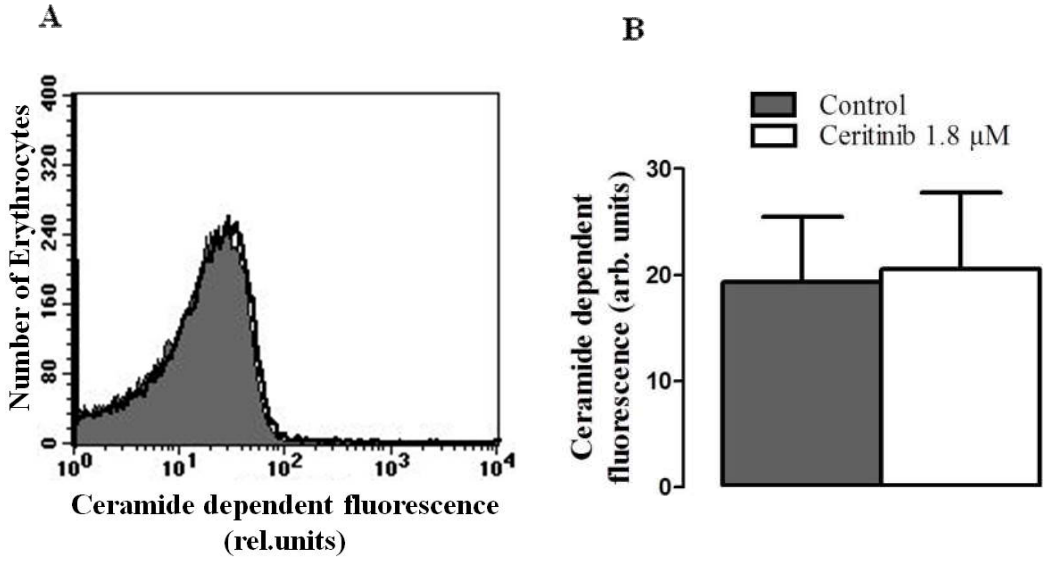

Figure 22: The effect of ceritinib treatment on ceramide generation. (A) The histogram represents the ceramide generation in erythrocytes following exposure to ceritinib for 48 hours. The grey plot represents the unexposed erythrocytes and the black line represents ceritinib-exposed erythrocytes. **(B)** A bar chart representing ceramide-generated erythrocytes (data represented on arithmetic means ± SD, n = 5) following 48 hours of incubation in Ringer's solution. The grey bar represents the control group and the white bar represents the ceritinib-treated (1.8 µM) group of erythrocytes [from (Al Mamun Bhuyan et al., 2016b)].

Another series of experiments was performed to determine the role of different kinases in ceritinib-induced eryptosis. For this objective, healthy erythrocytes were treated with ceritinib (1.8 µM) in the absence and presence of different kinases. To check the involvement of the AKT/PKB protein, erythrocytes were exposed to ceritinib (1.8 µM) in the absence and presence of AKT1/2 inhibitor A6730 (58 nM). Figure 23 depicts that A6730 significantly downregulates the percentage of annexin-V-binding erythrocytes. However, in the presence of the AKT/PKB inhibitor, ceritinib still significantly stimulated erythrocyte death. Thus, ceritinib-associated eryptosis is partially mediated through the AKT1/2 signalling pathway.

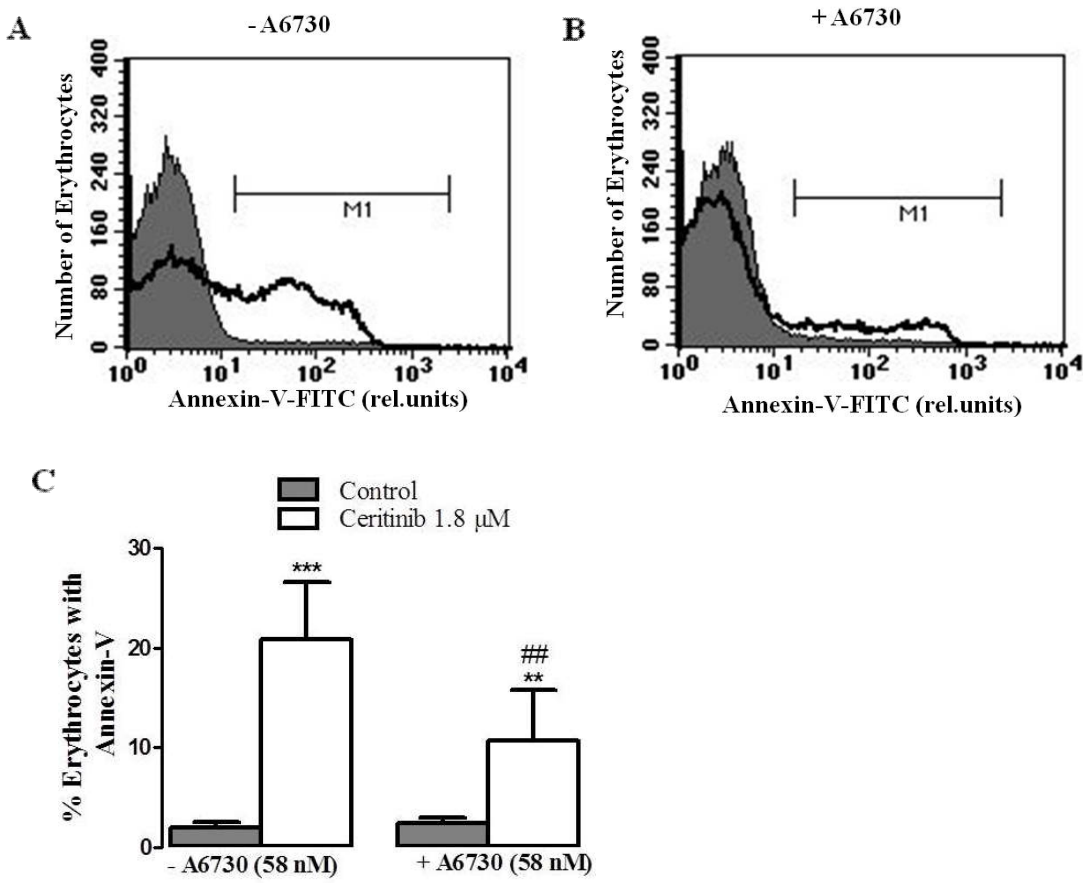

Figure 23: A6730 sensitivity on ceritinib-induced PS exposure. (A, B) The histograms represent the phosphatidylserine-externalised erythrocytes after 48 hours of treatment. The grey plots indicate the untreated erythrocytes and the black lines indicate 1.8 µM ceritinib-treated erythrocytes without **(A)** and with **(B)** A6730 (58 nM). **(C)** A bar chart showing annexin-V-binding erythrocytes (data represented on arithmetic means ± SD, n = 23) following 48 hours of incubation in Ringer's solution. The grey bars show the control group and white bars show the ceritinib-treated (1.8 µM) group without (left-sided bars) and with (right-sided bars) A6730 (58 nM). **($p<0.05$), ***($p<0.001$) points out the statistical distinction arising from the absence of ceritinib (ANOVA). ##($p<0.05$) points to the significant difference arising from the absence of A6730 (ANOVA) [from (Al Mamun Bhuyan et al., 2016b)].

To explore the influence of PKC on ceritinib-triggered eryptosis, erythrocytes were exposed to ceritinib (1.8 µM) in the absence and presence of PKC inhibitor staurosporine (1 µM). Figure 24 shows the addition of staurosporine significantly inhibits the effect of ceritinib on PS exposure. Nevertheless, even in the presence of staurosporine, ceritinib significantly upregulates the percentage of apoptotic erythrocytes. Thus, the staurosporine-sensitive PKC pathway is involved in the ceritinib-triggered erythrocyte death.

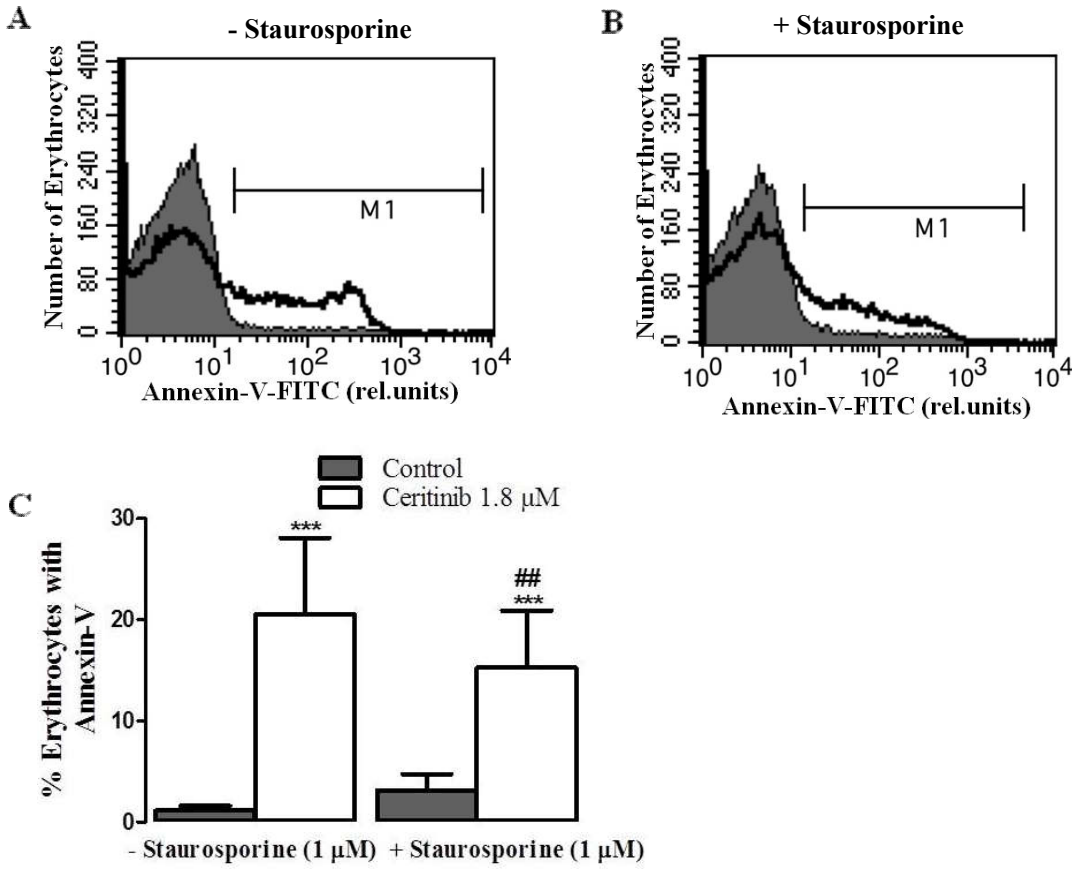

Figure 24: Staurosporine sensitivity on ceritinib-induced PS translocation. (A, B) The histograms represent the phosphatidylserine-externalised erythrocytes after 48 hours of treatment. The grey plots indicate the control group and the black lines indicate 1.8 µM ceritinib-treated erythrocytes without **(A)** and with **(B)** staurosporine (1 µM). **(C)** A bar chart showing annexin-V-binding erythrocytes (data represented on arithmetic means ± SD, n = 20) following 48 hours of incubation in Ringer's solution. The grey bars mark the control and the white bars mark the ceritinib-treated (1 µM) erythrocytes without (left-sided bars) and with (right-sided bars) staurosporine (1 µM). ***($p<0.001$) indicates the statistical distinction arising from the absence of ceritinib (ANOVA). #($p<0.05$) indicates a significant difference arising from the absence of staurosporine (ANOVA) [from (Al Mamun Bhuyan et al., 2016b)].

Moreover, erythrocytes were exposed to ceritinib (1.8 µM) without and with p38 kinase inhibitor SB203580 (2 µM) to assess the association between p38 kinase and ceritinib-stimulated erythrocyte death. Figure 25 demonstrates that SB203580 significantly blunts the action of ceritinib on phosphatidylserine exposure. Again, even in the presence of the p38 kinase inhibitor, ceritinib significantly upregulates the percentage of annexin-V-binding cells, which indicates ceritinib-induced eryptosis is partially dependent on p38 kinase.

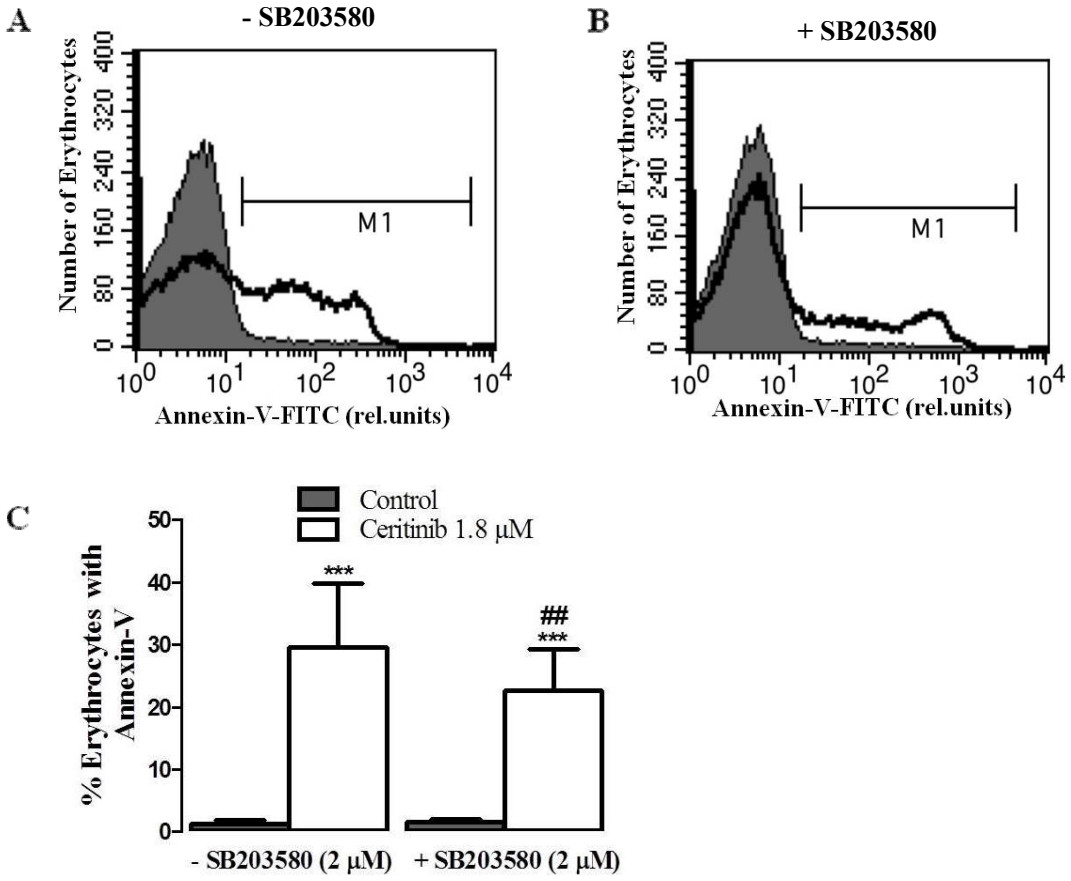

Figure 25: SB203580 sensitivity on ceritinib-stimulated PS externalisation. (A, B) The histograms represent the PS-externalised erythrocytes after 48 hours of treatment. The grey plots indicate the untreated erythrocytes and the black lines indicate 1.8 µM ceritinib-treated erythrocytes without **(A)** and with **(B)** SB203580 (2 µM). **(C)** A bar chart showing eryptotic erythrocytes (data represented on arithmetic means ± SD, n = 23) following 48 hours of incubation in Ringer's solution. The grey bars show the control group and white bars show the ceritinib-treated (1.8 µM) group without (left-sided bars) and with (right-sided bars) SB203580 (2 µM). ***($p<0.001$) points out the statistical distinction caused by the control group (ANOVA). ##($p<0.01$) points to the significant difference arising from the absence of SB203580 (ANOVA) [from (Al Mamun Bhuyan et al., 2016b)].

Further, to explore the involvement of CK1α in afatinib-triggered eryptosis, fresh erythrocytes were treated with afatinib with and without CK1α specific inhibitor D4476 (10 µM) for 48 hours. Subsequently, the percentage of annexin-V-binding erythrocytes was measured. The result shows that D4476 significantly declines the strength of ceritinib on cell membrane scrambling (Figure 26). However, ceritinib significantly

upregulates the number of PS-translocated erythrocytes, even in the presence of D4476, indicating that ceritinib-induced eryptosis is partly dependent on CK1α.

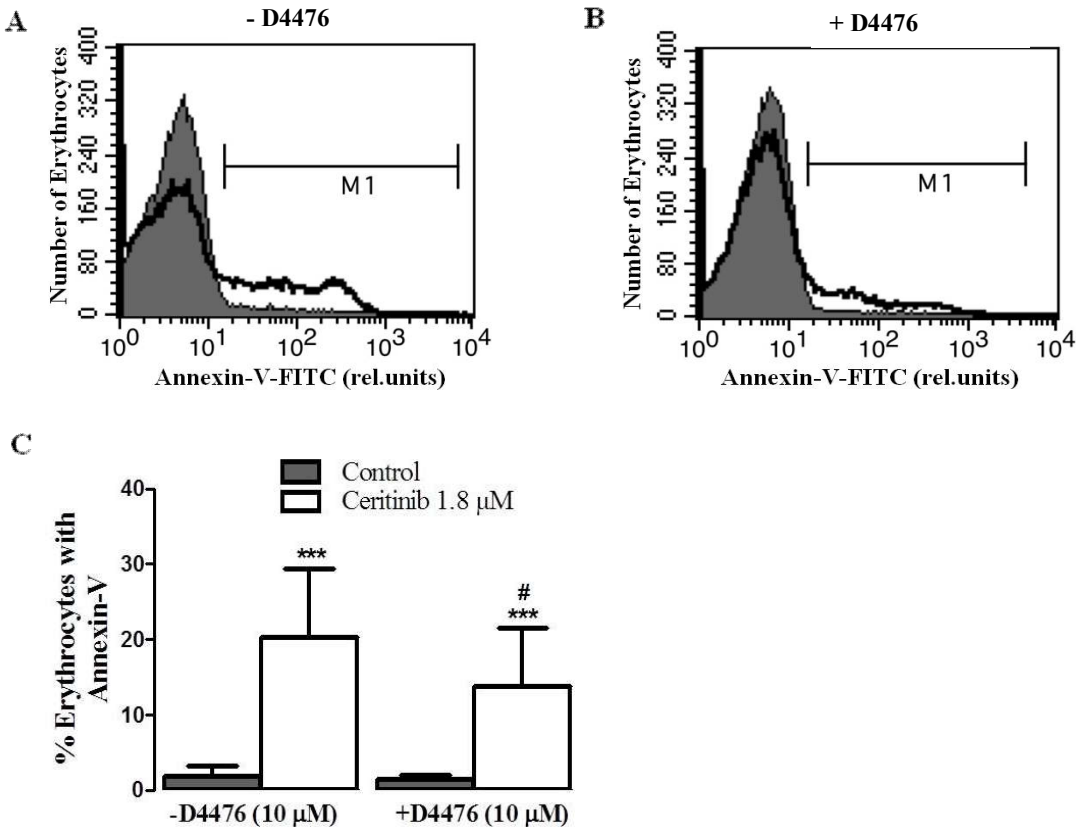

Figure 26: D4476 sensitivity on ceritinib-triggered PS externalisation. (A, B) The histograms represent the PS-translocated erythrocyte after 48 hours of treatment. The grey plots indicate the untreated erythrocytes and the black lines indicate 1.8 µM ceritinib-treated erythrocytes without **(A)** and with **(B)** D4476 (10 µM). **(C)** A bar chart representing PS-externalised erythrocytes (data represented on arithmetic means ± SD, n = 15) following 48 hours of incubation in Ringer's solution. The grey bars indicate the control group and the white bars indicate the ceritinib-treated (1.8 µM) group, without (left-sided bars) and with (right-sided bars) D4476 (10 µM). ***($p<0.001$) designates the statistical distinction arising from the absence of ceritinib (ANOVA). #($p<0.05$) designates the significant difference arising from the lack of D4476 (ANOVA) [from (Al Mamun Bhuyan et al., 2016b)].

Moreover, further investigations were performed to test the influence of caspases on ceritinib-induced (1.8 µM) eryptosis. Therefore, an experiment was conducted with and without pan-caspase inhibitor zVAD (10 µM). Figure 27 exhibits that zVAD significantly downregulates the ceritinib-triggered PS externalisation. Nevertheless, ceritinib significantly enhances the percentage of apoptotic erythrocytes even in the

presence of zVAD. In that aspect, ceritinib-induced eryptosis is not fully but partially dependent on the activation of caspases.

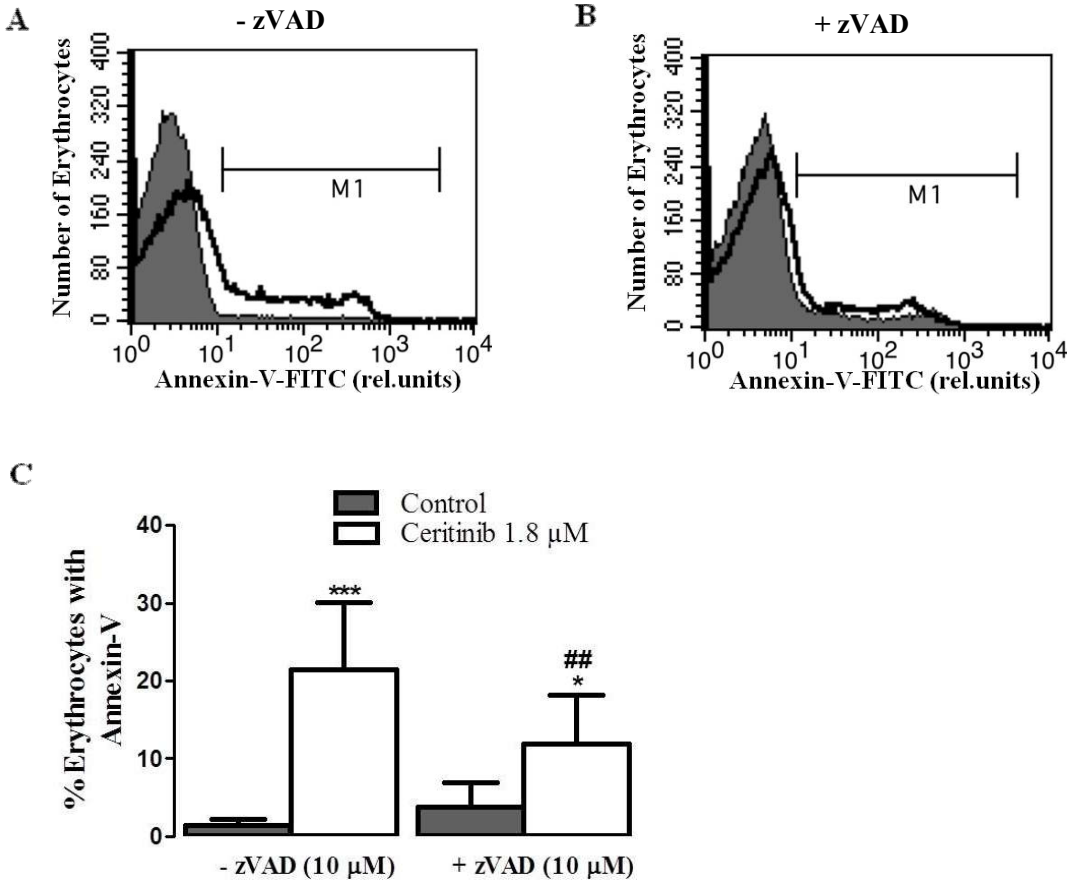

Figure 27: zVAD sensitivity on ceritinib-induced membrane scrambling. (A, B) The histograms represent the apoptotic erythrocytes after 48 hours of treatment. The grey areas indicate the control group and the black lines indicate 1 µM ceritinib-treated erythrocytes without **(A)** and with **(B)** zVAD (10 µM). **(C)** A bar chart representing apoptotic erythrocytes (data represented on arithmetic means ± SD, n = 9) following 48 hours of incubation in Ringer's solution. The grey bars indicate the control group and white bars indicate the ceritinib-treated (1 µM) erythrocytes without (left-sided bars) and with (right-sided bars) zVAD (10 µM). *($p<0.05$), ***($p<0.001$) indicates the statistical distinction arising from the control group (ANOVA). ##($p<0.01$) indicates the significant difference arising from the absence of zVAD (ANOVA) [from (Al Mamun Bhuyan et al., 2016b)].

Nitric oxide (NO) is the fundamental element for s-nitrosylation and the downregulation of S-nitrosylation leads to eryptosis (Ghashghaeinia et al., 2017; Nicolay et al., 2008). To test the influence of s-nitrosylation on ceritinib-induced eryptosis, healthy erythrocytes were treated with and without NO donor sodium nitroprusside (1 µM). Figure 28 demonstrates that the SNP significantly downregulates the percentage of

eryptotic cells. However, still in the presence of SNP, ceritinib significantly increases the number of eryptotic erythrocytes. Thus, an alteration in S-nitrosylation is also associated with ceritinib-triggered eryptosis.

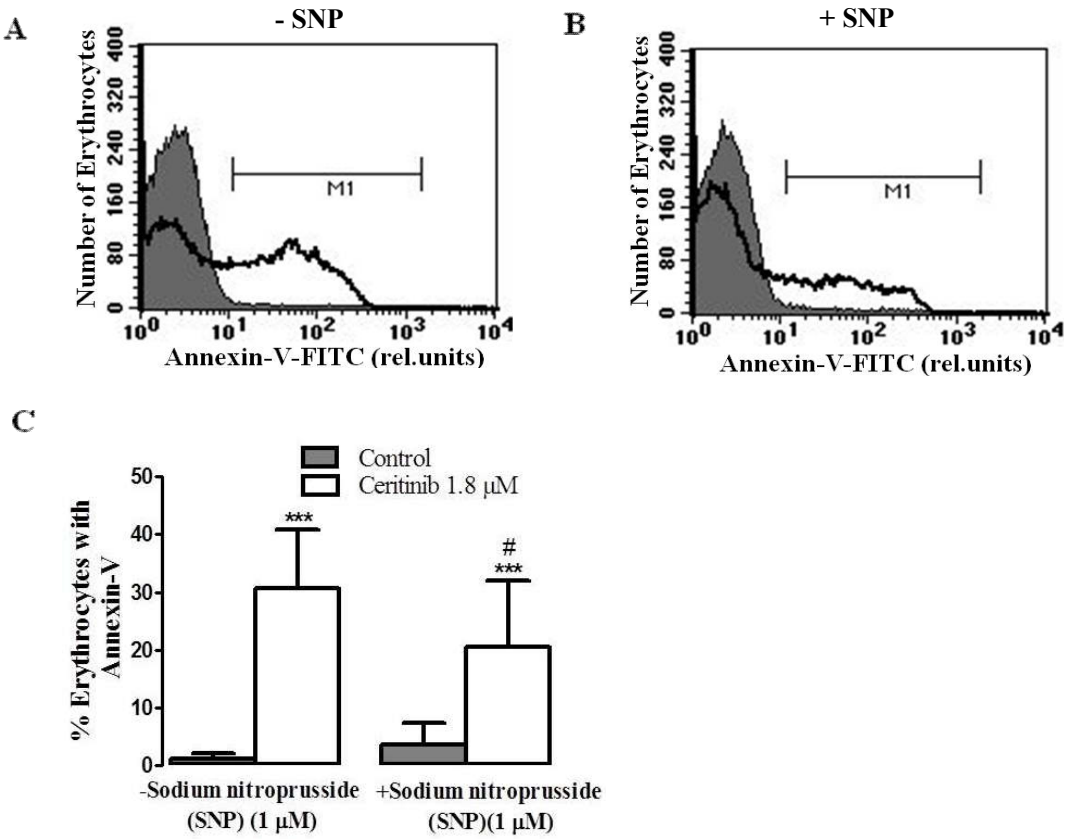

Figure 28: SNP sensitivity on ceritinib-stimulated PS translocation. (A, B) Histograms representing erythrocytes with phosphatidylserine exposure after 48 hours of treatment. The grey areas show the control group and the black lines indicate ceritinib-treated (1.8 µM) erythrocytes without **(A)** and with **(B)** SNP (1 µM). **(C)** A bar chart representing PS-externalised erythrocytes (data represented on arithmetic means ± SD, n = 13) following 48 hours of incubation in Ringer's solution. The grey bars show the control group and the white bars show the ceritinib-treated (1.8 µM) erythrocytes without (left bars) and with (right bars) SNP. ***($p<0.001$) indicates the statistical distinction arising from the absence of ceritinib (ANOVA). #($p<0.05$) indicates the statistical significant difference arising from the absence of SNP (ANOVA) [from (Al Mamun Bhuyan et al., 2016b)].

Excessive haemolysis is associated with the occurrence of anaemia (Haley, 2017) and cytostatic substances are often reported to induce haemolysis (Shaik et al., 2012; Signoretto et al., 2016). To assess the ceritinib-mediated (0.9 – 1.8 µM) haemolysis, Hb absorption was quantified from the supernatant of the samples using a spectrophotometer. As a positive control (100% haemolysis), erythrocytes were exposed

to water. According to Figure 29, ceritinib elevates the ratio of haemolytic cells and the effect reaches a statistically significant level at 1.8 μM ceritinib.

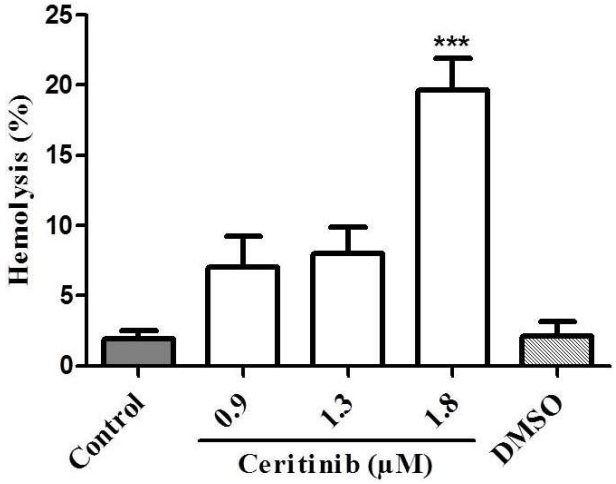

Figure 29: The effect of ceritinib on haemolysis. A bar chart representing haemolytic erythrocytes (data represented on arithmetic means ± SD, n = 5) following 48 hours of incubation. The grey bar shows the control group and white bars represent the ceritinib-treated (0.9 - 1.8 μM) erythrocytes. The striped bar designates the consequence of the solvent (DMSO) ***($p<0.001$) points out the statistical distinction arising from the absence of ceritinib [from (Al Mamun Bhuyan et al., 2016b)].

The second investigation discloses that ceritinib stimulates eryptosis, as well as haemolysis. Enhanced intracellular calcium concentration, AKT protein, p38 kinase, PKC, CK1α, caspase activation and downregulation of S-nitrosylation are possible underlying signalling mechanisms responsible for ceritinib-triggered eryptosis.

3. 3. The inhibition of suicidal erythrocyte death by volasertib

To explore the effects of volasertib on suicidal erythrocyte death, healthy erythrocytes were exposed to different concentrations of volasertib in glucose-depleted Ringer's solution, a well-known eryptosis stimulator (Figure 30). Erythrocytes were incubated for 48 hours at 37°C. Subsequently the percentages of PS-exposing erythrocytes and cell shrinkage were quantified by flow cytometry. The 0.8, 1.6, and 2.4 μM of volasertib were selected as working concentrations for further study.

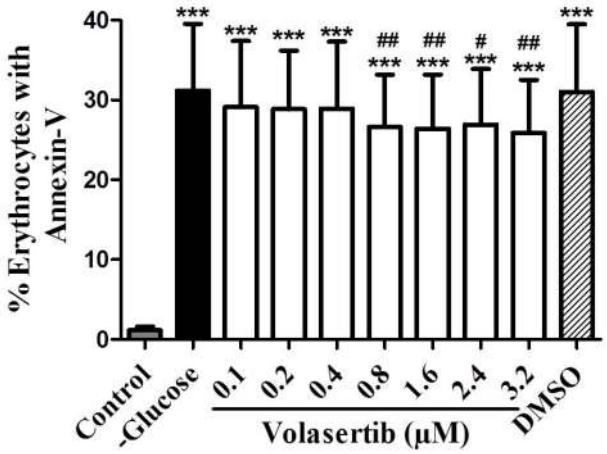

Figure 30: Dose-dependent sensitivity of volasertib in the inhibition of PS externalisation. A bar chart indicating the eryptotic erythrocytes (data represented on arithmetic means ± SD, n = 10) following 48 hours of treatment with Ringer's solution containing glucose (grey bar) or Ringer's solution without glucose (black bar) and in glucose-depleted Ringer's solution with (white bars) volasertib (0.1- 3.2 μM). The striped bar indicates the effect of the solvent (DMSO) with glucose-deprived Ringer's solution. ***($p<0.001$) indicates the significant distinction arising from the absence of glucose, #($p<0.05$), ##($p<0.01$), ###($p<0.001$) indicates the significant difference arising from the absence of volasertib (ANOVA).

As mentioned in Figure 31, there is a sharp increase in the percentage of eryptotic-erythrocytes in the glucose-depleted group. The percentage of eryptotic-erythrocytes decreases in the presence of volasertib (0.8 - 2.4 μM), the effect reaches a statistically significant level at 1.6 - 2.4 μM volasertib. However, even in the presence of volasertib, glucose deprivation significantly enhances the percentage of PS-exposing erythrocytes. Thus, volasertib shows a partially protective effect on eryptosis following glucose depletion.

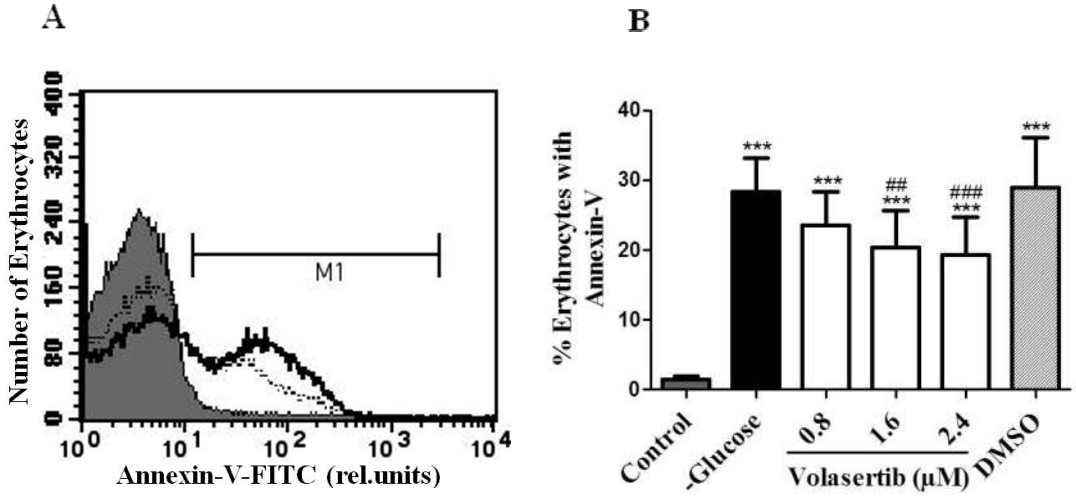

Figure 31: Volasertib sensitivity on PS translocation subsequent to energy depletion. (A) The histogram represents PS-translocated erythrocytes following 48 hours of exposure to glucose-containing Ringer's solution (grey area), glucose-deprived Ringer's solution (black line), and glucose-deprived Ringer's solution with volasertib (2.4 µM) (dashed line). **(B)** A bar chart representing eryptotic erythrocytes (data represented on arithmetic means ± SD, n = 14) following 48 hours of treatment with Ringer's solution containing glucose (grey bar), Ringer's solution without glucose (black bar), and in glucose-depleted Ringer's solution with (white bars) volasertib (0.8, 1.6 & 2.4 µM). The striped bar indicates the consequence of the solvent (DMSO) with glucose-deprived Ringer's solution. ***($p<0.001$) indicates the significant distinction arising from the absence of glucose, ##($p<0.01$), ###($p<0.001$) indicates the significant difference arising from the absence of volasertib (ANOVA) [from (Al Mamun Bhuyan et al., 2017a)].

The FSC of erythrocytes was also measured with and without energy depletion. The FSC of erythrocytes following 48 hours of incubation in the glucose containing Ringer's solution is similar in the absence (517 ± 6%, n = 14) and presence (522 ± 5.4%, n = 14) of volasertib (2.4 µM), indicating that volasertib does not influence cell shrinkage following energy repletion. Figure 32 demonstrates that incubation of erythrocytes in the Ringer's solution without glucose causes a significant decrease in the volume of the erythrocytes. Adding volasertib (0.8 - 2.4 µM) to the glucose-depleted Ringer's solution does not cause any changes in the erythrocyte forward scatter. Thus, volasertib does not influence erythrocyte volume following energy deprivation.

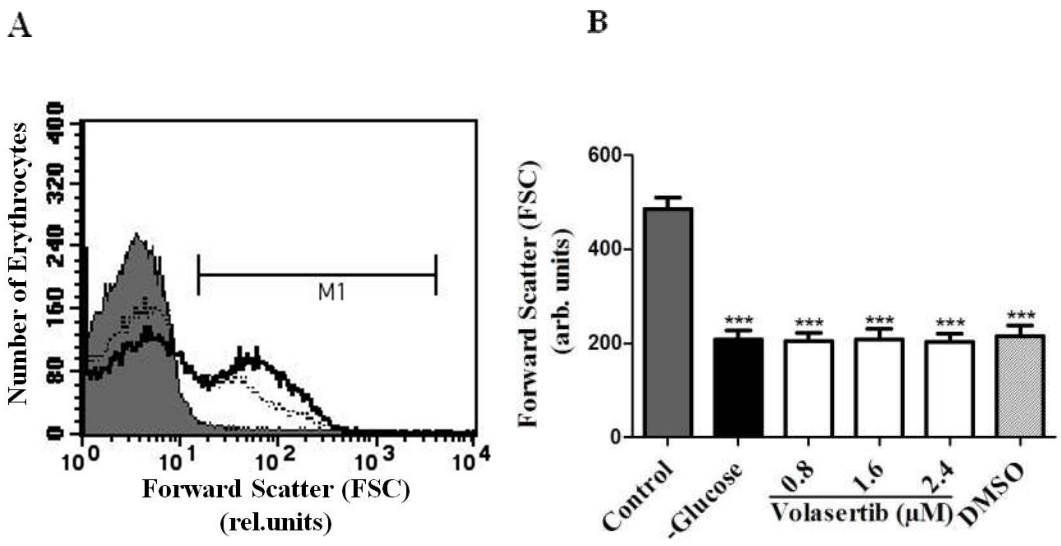

Figure 32: Volasertib sensitivity on cell volume following energy depletion. **(A)** The histogram represents the size of the erythrocytes following 48 hours of exposure to glucose-containing Ringer's solution (grey area), glucose-deprived Ringer's solution (black line), and with glucose-deprived Ringer's solution in the presence of volasertib (2.4 μM) (dashed line). **(B)** A bar chart showing the FSC of erythrocytes following 48 hours of treatment with Ringer's solution containing glucose (grey bar), and Ringer's solution deprived from glucose with the absence (black bar) and presence (white bars) of volasertib (0.8, 1.6 & 2.4 μM). The striped bar indicates the participatory effect of the solvent (DMSO) with glucose-deprived Ringer's solution. The data represented on arithmetic means ± SD, n = 14. ***($p<0.001$) indicates the statistical significance arising from the absence of glucose (ANOVA) [from (Al Mamun Bhuyan et al., 2017a)].

An important mechanistic tool for the induction of eryptosis is the increased level of intracellular calcium concentration (Lang et al., 2003a). Considering the inhibitory effect of volasertib on membrane scrambling following energy deprivation, this experiment was conducted to explore the impact of volasertib on intracellular calcium concentration following energy depletion. The cytosolic calcium was quantified from Fluo3-associated fluorescence using flow cytometry. Figure 33 depicts that removal of glucose significantly increases the cytosolic calcium level following 48 hours of incubation. However, Fluo3 fluorescence does not significantly modify after incubation with volasertib (0.8 - 2.4 μM) in the glucose-depleted Ringer's solution. Rather, the cytosolic calcium concentration is increased to the same extent with and without volasertib following energy depletion. Thus, the anti-eryptotic effect of volasertib may not be associated with changes in the intracellular calcium level.

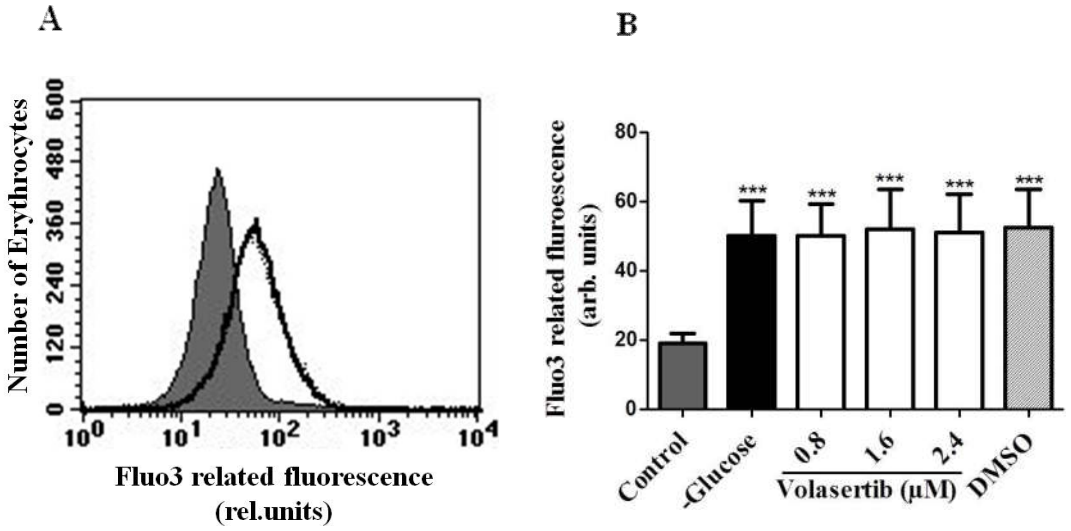

Figure 33: The effect of volasertib on cytosolic calcium concentration subsequent to energy depletion. (A) The histogram represents the cytosolic calcium concentration following 48 hours of exposure to glucose-containing Ringer's solution (grey area), glucose-deprived Ringer's solution (black line), and with glucose-deprived Ringer's solution in the presence of volasertib (2.4 µM) (dashed line). **(B)** The bar chart represents the intracellular calcium level of erythrocytes (data represented on arithmetic means ± SD, n = 14) following 48 hours of treatment with Ringer's solution containing glucose (grey bar) and Ringer's solution deprived from glucose without (black bar) and with (white bars) volasertib (0.8, 1.6 & 2.4 µM). The striped bar indicates the participatory effect of the solvent (DMSO) with glucose-deprived Ringer's solution. ***($p<0.001$) indicates the statistical significance arising from the absence of glucose (ANOVA) [from (Al Mamun Bhuyan et al., 2017a)].

ROS resulting from excessive oxidative stress may cause eryptosis (Bissinger et al., 2018). To test whether volasertib blunted eryptosis by a decline in ROS generation following glucose removal, erythrocyte concentrates were exposed to Ringer's solution and glucose-depleted Ringer's solution in the absence and presence of 2.4 µM of volasertib for 48 hours. DCFDA fluorescence was quantified to check the ROS generation. The result reveals that ROS formation was similar when cells were incubated with glucose containing Ringer's solution without (19.07 ± 0.64, n = 5) and with 2.4 µM volasertib (18.63 ± 0.46, n = 5). Figure 34 displays that in the glucose-depleted Ringer's solution, there was a significant upregulation of DCFDA fluorescence either in the absence or presence (2.4 µM) of volasertib. The presence of volasertib did not alter ROS generation in the erythrocytes following glucose removal. Thus, volasertib has no influence on ROS modification for protecting mature erythrocytes subsequent to energy depletion.

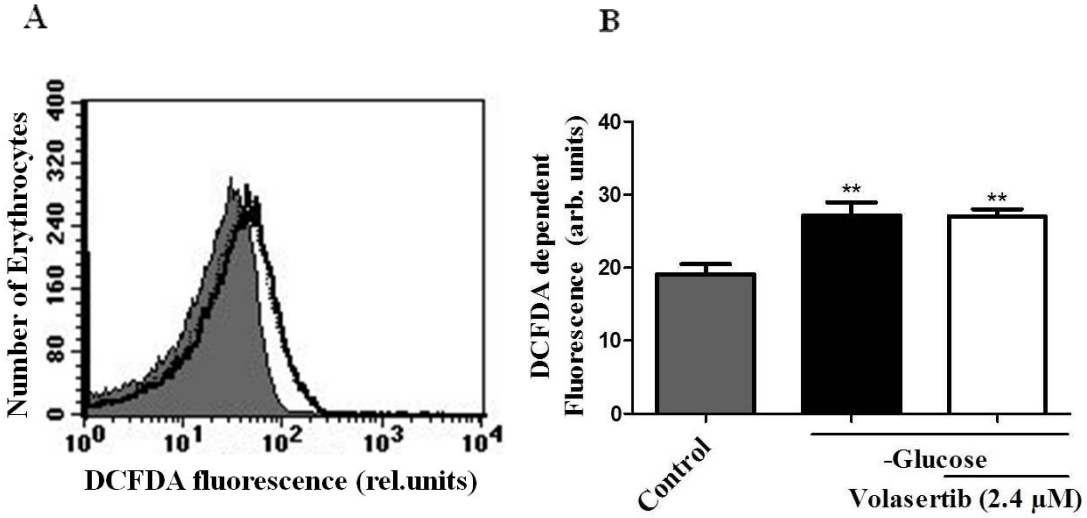

Figure 34: The effect of volasertib on ROS generation subsequent to energy depletion. (A) The histogram represents the DCFDA fluorescence in erythrocytes after 48 hours of exposure to Ringer's solution (grey area), glucose-depleted Ringer's solution (black line), and glucose-depleted Ringer's solution with volasertib (2.4 µM) (dashed line). **(B)** A bar chart showing the DCFDA-dependent fluorescence of erythrocytes (data represented on arithmetic means ± SD, n = 5) following 48 hours of treatment with Ringer's solution containing glucose (grey bar) and Ringer's solution deprived from glucose without (black bar) and with (white bar) volasertib (2.4 µM). **($p<0.01$) indicates the statistical significance arising from the absence of glucose (ANOVA) [from (Al Mamun Bhuyan et al., 2017a)].

Ceramide abundance on the erythrocyte surface was quantified to check whether volasertib inhibits eryptosis following energy depletion by decreasing ceramide generation. Ceramide was measured using ceramide-specific antibodies. The formation of ceramide in Ringer's solution is almost similar to the absence (9.84 ± 0.17, n = 5) and presence (10.11 ± 0.24, n = 5) of volasertib. Again, ceramide generation in glucose-depleted Ringer's solution increased in the same extent without (10.1 ± 0.2, n = 5) and with (9.8 ± 0.2, n = 5) 2.4 µM volasertib. Thus, the data reveal that volasertib has no inhibitory effect on ceramide formation following incubation in energy-repleted or energy-depleted Ringer's solution (Figure 35).

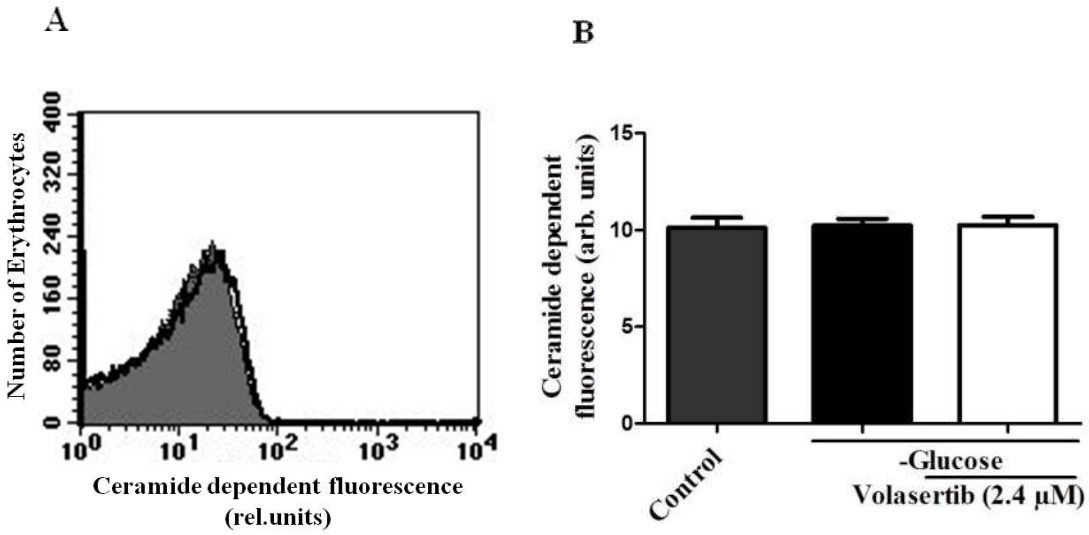

Figure 35: The effect of volasertib on ceramide generation subsequent to energy depletion. (A) The histogram represents the ceramide-dependent fluorescence in erythrocytes following 48 hours of exposure to Ringer's solution (grey area), glucose-deprived Ringer's solution (black line), and glucose-depleted Ringer's solution with volasertib (2.4 µM) (dashed line). **(B)** The bar chart indicates the ceramide-dependent fluorescence of erythrocytes (data represented on arithmetic means ± SD, n = 5) following 48 hours of treatment with Ringer's solution (grey bar) or glucose-deprived Ringer's solution in the absence (black bar) and presence (white bar) of volasertib (2.4 µM) [from (Al Mamun Bhuyan et al., 2017a)].

Data from previous research confirmed that volasertib has a stimulatory effect on the apoptosis of nucleated cells (Schoffski, 2009; Rudolph et al., 2009; Hugle et al., 2015). However, in anucleated erythrocytes, volasertib rather shows protective effects. Further experiments were performed in erythrocyte progenitor cells (K562) to explore whether volasertib induces programmed cell death. As demonstrated in Figure 36, exposure of K562 cells to volasertib (0.8 - 2.4 µM) for 48 hours significantly upregulates the rate of phosphatidylserine translocation. Again, as shown in Figure 37, volasertib (0.8 - 2.4 µM) leads to a significant decrease in the volume of K562 cells after 48 hours of incubation.

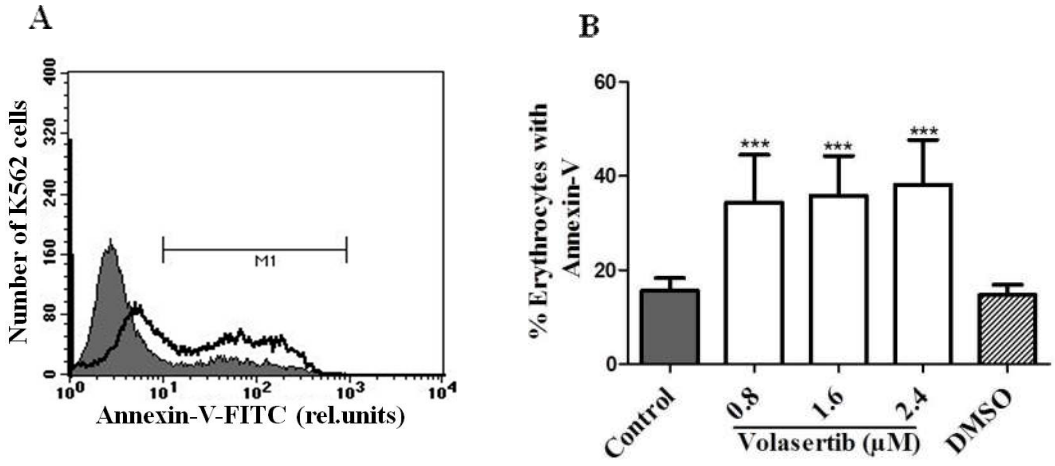

Figure 36: Volasertib sensitivity on PS translocation in K562 cells. (A) The histogram depicts the annexin-V bound K562 cells subsequent to volasertib treatment in RPMI 1640 cell culture medium for 48 hrs. The grey region designates the K562 cells without treatment and the black line indicates volasertib-treated (2.4 μM) K562 cells. **(B)** The bar chart represents apoptotic K562 cells (data represented on arithmetic means ± SD, n = 10) following 48 hours of incubation in an RPMI 1640 cell culture medium. The grey bar indicates the control group and white bars indicate the volasertib-treated (0.8 – 2.4 μM) K562 cells whereas the striped bar designates the influence of the solvent. ***($p<0.001$) points out the statistical distinction arising from the absence of volasertib (ANOVA) [from (Al Mamun Bhuyan et al., 2017a)].

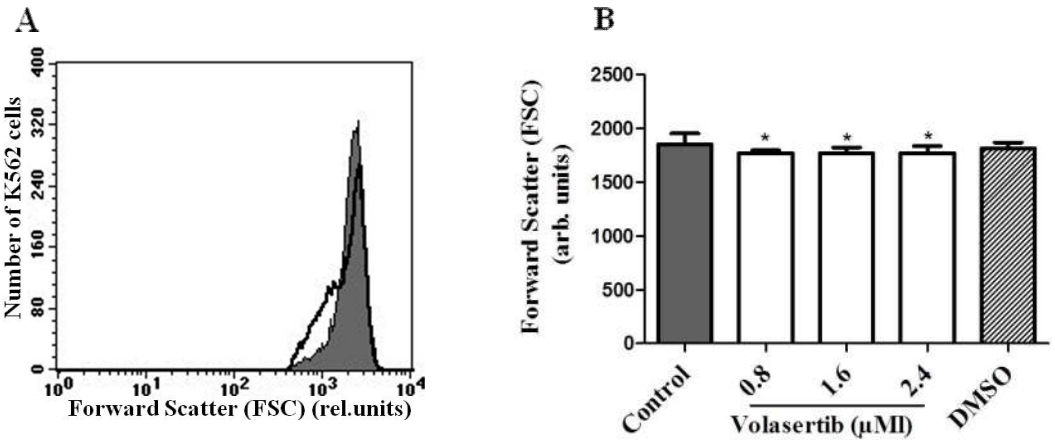

Figure 37: Volasertib sensitivity on the FSC of K562 cells. (A) The histogram represents the volume of K562 cells subsequent to volasertib treatment in an RPMI 1640 cell culture medium for 48 hours. The grey plot designates the K562 cells without treatment and the black line designates volasertib-treated (2.4 μM) K562 cells. **(B)** The bar chart represents shrunken K562 cells (data represented on arithmetic means ± SD, n = 10) following 48 hours of incubation in an RPMI 1640 cell culture medium. The grey bar represents the control cells and the white bars represent the volasertib-treated (0.8 – 2.4 μM) K562 cells. The striped bar designates the influence of the solvent. *($p<0.05$) points out the statistical distinction arising from the absence of volasertib (ANOVA) [from (Al Mamun Bhuyan et al., 2017a)].

Further experiments were conducted to check the inhibitory function of volasertib on eryptosis following hyperosmotic shock (HS). Sucrose (550 mM) was added in the Ringer's solution to make the hypertonic solution and erythrocytes were incubated for six hours to cause HS in the erythrocytes. As demonstrated in Figure 38, there is a sharp increase in the annexin-V-binding cells following HS whereas the percentage of eryptotic erythrocytes decreases in the presence of volasertib (0.8 - 2.4 µM)—an effect reaching statistical significance at 1.6 - 2.4 µM volasertib. However, also in the presence of volasertib, the percentage of PS-exposing erythrocytes increases significantly. Thus, volasertib shows a partial protective effect on PS externalisation after hyperosmotic shock.

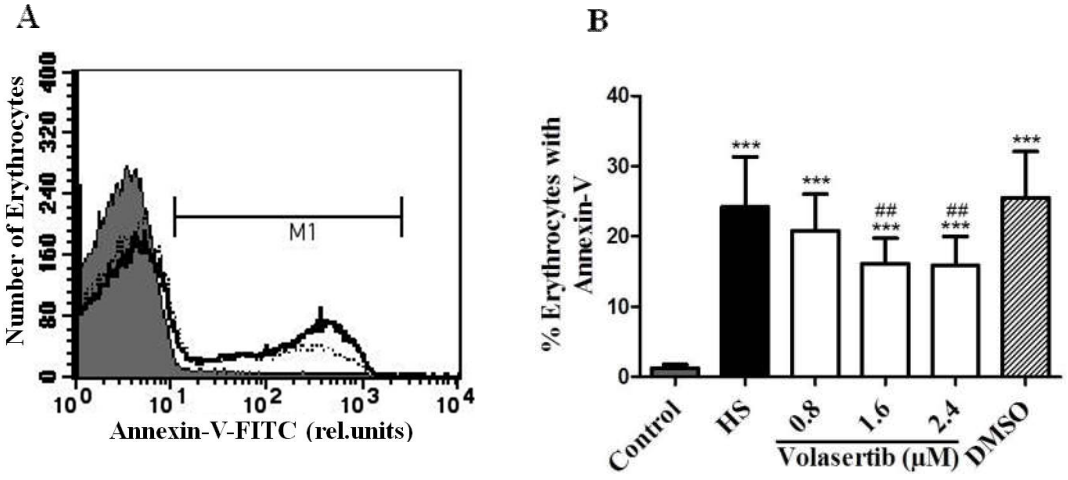

Figure 38: Volasertib sensitivity on PS translocation subsequent to HS. (A) The histogram represents the apoptotic erythrocytes following six hours of exposure to Ringer's solution (grey area), hypertonic Ringer's solution (black line) and hypertonic Ringer's solution with 2.4 µM of volasertib (dashed line). **(B)** A bar chart representing apoptotic erythrocytes (data represented on arithmetic means ± SD, n = 10) following six hours of treatment with Ringer's solution containing glucose (grey bar), hypertonic Ringer's solution (black bar), and hypertonic Ringer's solution in the presence (white bars) of volasertib (0.8, 1.6 & 2.4 µM). The striped bar indicates the consequence of the solvent (DMSO) with hypertonic Ringer's solution. ***($p<0.001$) points out the statistical significance arising from the control group, ##($p<0.01$) points out the significant difference arising from the absence of volasertib (ANOVA) [from (Al Mamun Bhuyan et al., 2017a)].

HS stimulates eryptosis and causes cell shrinkage (Lang et al., 2012a). This experiment was performed to check the effect of volasertib on the erythrocyte volume subsequent to HS. As illustrated in Figure 39, the FSC of the erythrocytes following six hours of incubation time significantly decrease either in the absence or presence of volasertib (0.8 - 2.4 µM). Hence, volasertib has no inhibitory properties on erythrocyte volume following hyperosmotic shock.

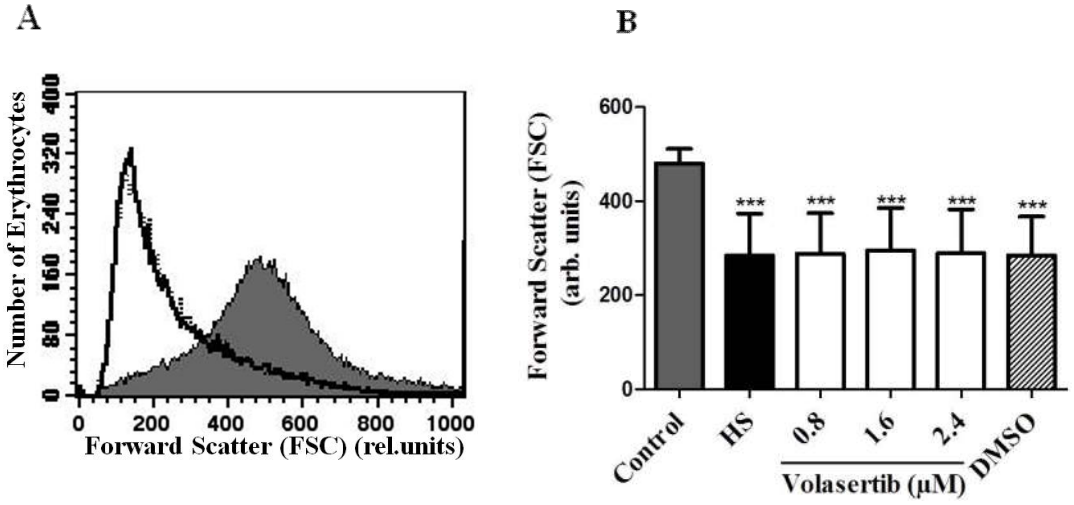

Figure 39: Volasertib sensitivity on erythrocyte volume subsequent to HS. (A) A histogram representing the volume of the erythrocytes following six hours of exposure to Ringer's solution (grey area), hypertonic Ringer's solution (black line), and hypertonic Ringer's solution with 2.4 µM of volasertib (dashed line). **(B)** A bar chart showing the FSC of erythrocytes (data represented on arithmetic means ± SD, n = 10) following six hours of treatment with Ringer's solution (grey bar), hypertonic Ringer's solution (black bar), and hypertonic Ringer's solution in the presence (white bars) of volasertib (0.8, 1.6 & 2.4 µM). the striped bar indicates the effect of the solvent (DMSO) with hypertonic Ringer's solution. ***($p<0.001$) indicates a statistical difference arising from the control group (ANOVA) [from (Al Mamun Bhuyan et al., 2017a)].

Moreover, HS causes a marked increase in the cytosolic calcium level of erythrocytes. Figure 40 demonstrates that volasertib (0.8 - 2.4 µM) blunts Fluo3 fluorescence in the erythrocytes following HS but the effect does not reach a statistically significant level. Hence, volasertib does not change the intracellular calcium level subsequent to hyperosmotic shock.

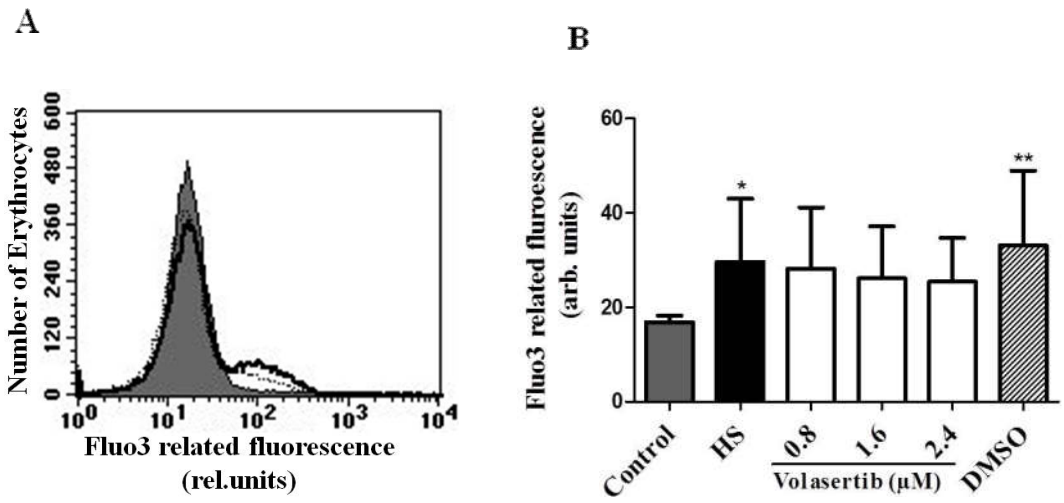

Figure 40: Volasertib sensitivity on cytosolic calcium concentration following HS. **(A)** The histogram represents the cytosolic calcium concentration in erythrocytes following six hours of exposure to Ringer's solution (grey area), hypertonic Ringer's solution (black line), and to hypertonic Ringer's solution in the presence of 2.4 μM of volasertib (dashed line). **(B)** The bar chart indicates the intracellular calcium level in erythrocytes (data represented on arithmetic means ± SD, n = 10) following six hours of treatment with Ringer's solution (grey bar), hypertonic Ringer's solution (black bar), and hypertonic Ringer's solution (white bars) in the presence of volasertib (0.8, 1.6 & 2.4 μM). The striped bar shows the consequence of the solvent (DMSO) with hypertonic Ringer's solution. *($p<0.05$), **($p<0.01$) indicates the statistical difference arising from the control group [from (Al Mamun Bhuyan et al., 2017a)].

Another series of investigations were performed to explore the inhibitory effects of volasertib (0.8 - 2.4 μM) on eryptosis following oxidative stress (OS). The OS-induced environment was created by adding tert-butylhydroperoxide (t-booh) (0.3 mM) in Ringer's solution. Then, healthy erythrocytes were subjected to Ringer's solution and the Ringer's solution with t-booh for 50 minutes in the absence and presence of volasertib (0.8 - 2.4 μM). According to Figure 41, the percentage of PS-translocated erythrocytes significantly increases following OS. The presence of volasertib (0.8 - 2.4 μM) in the OS solution does not interfere in the manoeuvre of PS translocation in erythrocytes. Thus, volasertib has no inhibitory effect on PS-externalisation following oxidative stress.

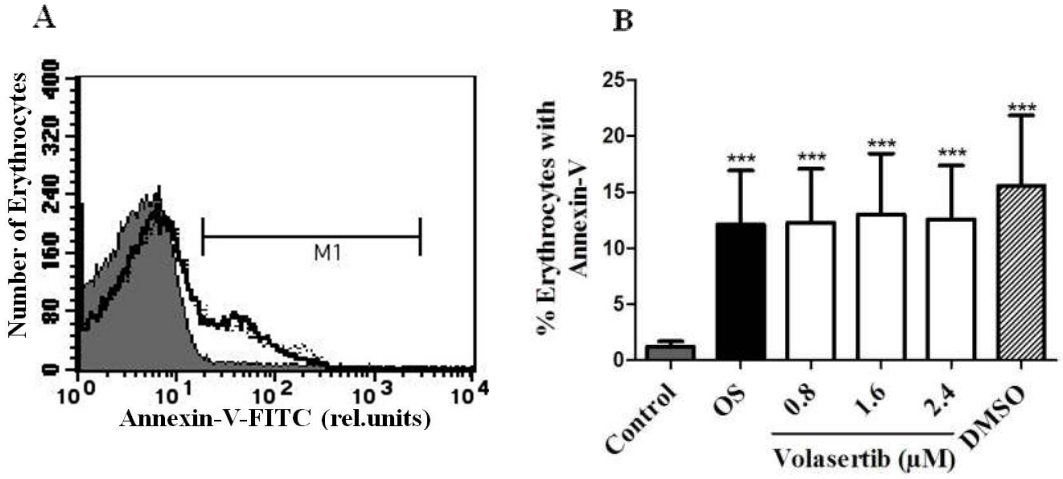

Figure 41: The influence of volasertib on PS externalisation after oxidative stress. **(A)** The histogram represents the PS-translocated erythrocytes following 50 minutes of exposure to Ringer's solution (grey area), Ringer's solution with tert-butylhydroperoxide (t-booh) (0.3 mM) (black line), and Ringer's solution with t-booh in the presence of 2.4 µM of volasertib (dashed line). **(B)** A bar chart representing the apoptotic erythrocytes (data represented on arithmetic means ± SD, n = 15) following 50 minutes of treatment with Ringer's solution (grey bar), Ringer's solution with t-booh (black bar), and Ringer's solution with t-booh (white bars) in the presence of volasertib (0.8, 1.6 & 2.4 µM). The striped bar indicates the consequence of the solvent (DMSO) with t-booh. ***($p<0.001$) indicates the statistical significance arising from the control group (ANOVA) [from (Al Mamun Bhuyan et al., 2017a)].

Again, the influence of volasertib on the FSC of erythrocytes following OS was also explored. According to Figure 42, the erythrocyte volume, subsequent to OS, decreased significantly. However, the volume of the erythrocytes subsequent to OS was identical with and without the presence of volasertib (0.8 - 2.4 µM). Therefore, PLK1 inhibitor volasertib has no statistically significant interference with the size of the erythrocytes following oxidative stress.

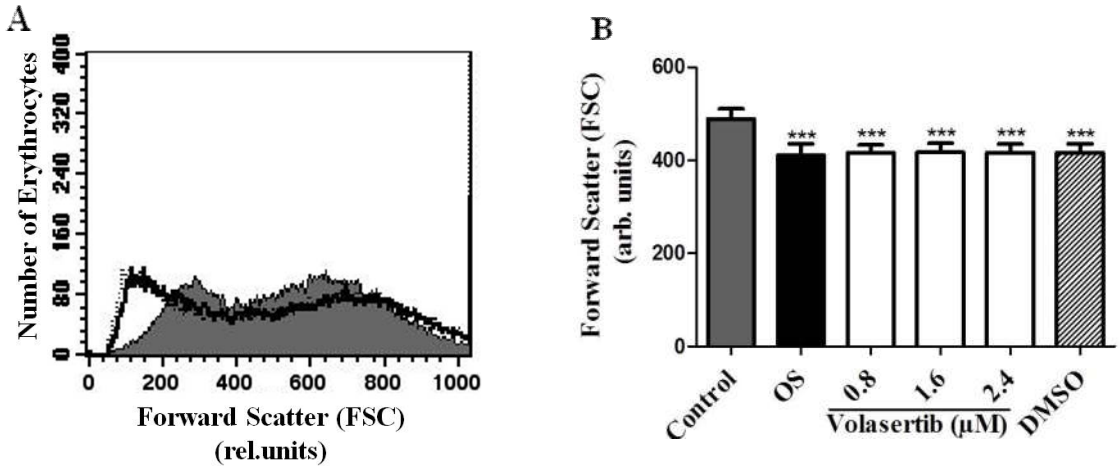

Figure 42: The influence of volasertib on cell volume subsequent to oxidative stress. **(A)** The histogram represents the volume of the erythrocytes following 50 minutes of exposure to Ringer's solution (grey area), Ringer's solution with tert-butylhydroperoxide (t-booh) (0.3 mM) (black line), and Ringer's solution with t-booh in the presence of 2.4 µM of volasertib (dashed line). **(B)** The bar chart indicates the volume of erythrocytes (data represented on arithmetic means ± SD, n = 15) following 50 minutes of treatment in Ringer's solution (grey bar), Ringer's solution with t-booh (black bar), and Ringer's solution with t-booh (white bars) in the presence of volasertib (0.8, 1.6 & 2.4 µM). The striped bar shows the consequence of the solvent (DMSO) with t-booh [from (Al Mamun Bhuyan et al., 2017a)]

Further studies were performed to explore the sensitivity of volasertib following calcium overload in the extracellular space. To achieve a calcium-saturated environment, 1 µM ionophore ionomycin was used in the Ringer's solution and then the healthy erythrocytes were incubated in this solution for 60 minutes. Figure 43 demonstrates a sharp increase in erythrocyte death following ionomycin treatment and the effect of ionomycin is slightly, but not significantly blunted in the presence of volasertib.

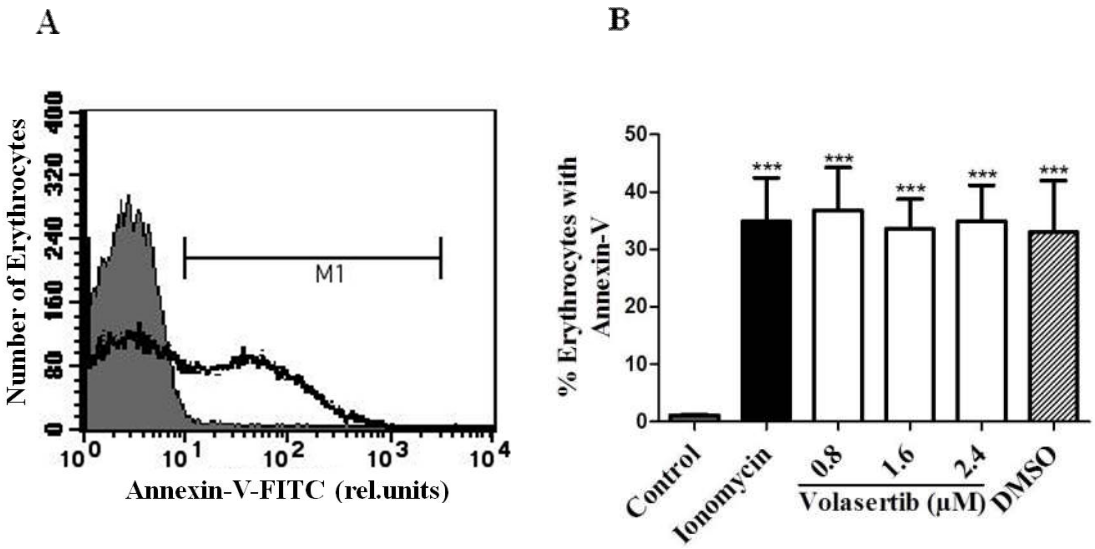

Figure 43: The sensitivity of volasertib on PS translocation following calcium overload. **(A)** The histogram represents the apoptotic erythrocytes following 60 minutes of exposure to Ringer's solution (grey area), Ringer's solution with ionophore ionomycin (1 µM) (black line), and Ringer's solution with ionomycin in the presence of 2.4 µM of volasertib (dashed line). **(B)** The bar chart indicates the erythrocytes with PS-translocation (data represented on arithmetic means ± SD, n = 10) following 60 minutes of exposure to Ringer's solution (grey bar), Ringer's solution with ionomycin (black bar), and Ringer's solution with ionomycin in the presence (white bars) of volasertib (0.8, 1.6 & 2.4 µM). The striped bar indicates the effect of the solvent (DMSO) with ionomycin. ***($p<0.001$) indicates the statistical significance arising from the absence of ionomycin (ANOVA) [from (Al Mamun Bhuyan et al., 2017a)].

The erythrocyte volume significantly decreased when the cytosolic calcium entry was fostered by ionophore ionomycin for 60 minutes. However, Figure 44 reveals that the presence of volasertib (0.8 - 2.4 µM) has no stimulatory or inhibitory action on the volume of erythrocytes following ionomycin treatment.

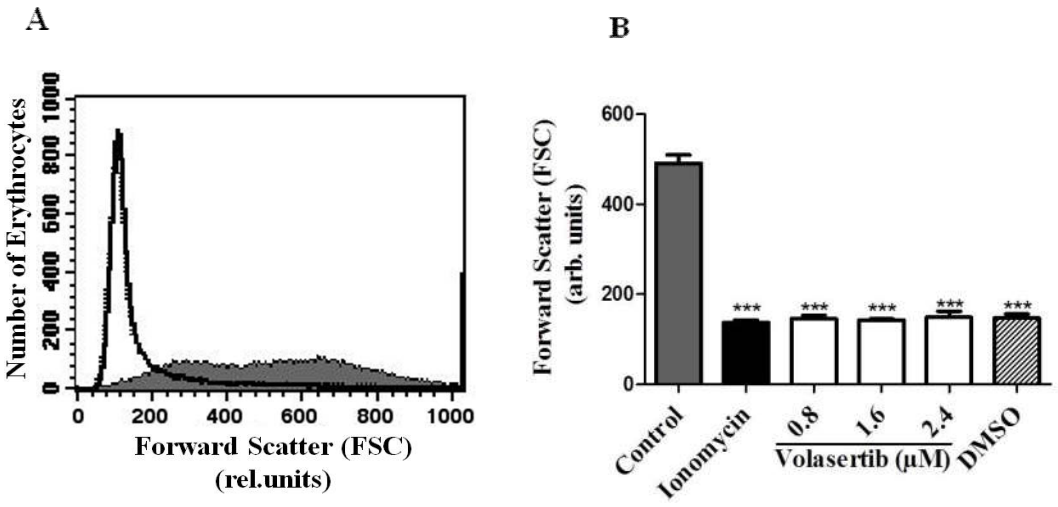

Figure 44: Sensitivity of volasertib on erythrocyte volume following calcium overload. (A) The histogram represents the erythrocyte size following 60 minutes of exposure to Ringer's solution (grey area), Ringer's solution with ionophore ionomycin (1 µM) (black line), and Ringer's solution with ionomycin in the presence of 2.4 µM of volasertib (dashed line). **(B)** The bar chart depicts the erythrocyte volume (data represented on arithmetic means ± SD, n = 10) following 60 minutes of exposure to Ringer's solution (grey bar), Ringer's solution with ionomycin (black bar), and Ringer's solution with ionomycin (white bars) in the presence of volasertib (0.8, 1.6 & 2.4 µM). The striped bar indicates the impact of the solvent (DMSO) with ionomycin. ***($p<0.001$) depicts the statistical difference arising from the absence of ionomycin (ANOVA) [from (Al Mamun Bhuyan et al., 2017a)].

The third investigation revealed that volasertib has an inhibitory action on eryptosis subsequent to energy depletion or hyperosmotic shock but not after oxidative stress or calcium overload. Thus, volasertib shows an anti-eryptotic effect.

4. Discussion

4. 1. The effect of afatinib on eryptosis

The experiments revealed a completely new effect of afatinib. Treatment of fresh, healthy human erythrocytes with afatinib is followed by membrane scrambling with translocation of phosphatidylserine (PS) to the outer erythrocyte surface and shrinkage of the cells. Erythrocyte membrane scrambling and shrinkage is the main feature of eryptosis. The effect of afatinib on PS externalisation reaches statistical significance at 8.2 μM, a concentration several magnitudes higher than the IC_{50} of 14 nM for inhibiting the EGFR tyrosine kinase (Li et al., 2008) and several magnitudes higher than the reported plasma level of afatinib of 78-308 nM in patients (Chu et al., 2014; Gordon et al., 2013; Molife et al., 2013; Wind et al., 2017). The observed effect on eryptosis is thus not likely because of tyrosine kinase inhibition and presumably contributes to developing anaemia only following afatinib intoxication.

The afatinib-triggered PS translocation is paralleled by an increased cytosolic calcium concentration. The raised cytosolic calcium concentration following afatinib treatment could be the result of stimulating calcium entry into erythrocytes from the extracellular space through calcium-permeable non-selective cation channels (NSCC) (Lang et al., 2003a) involving the TRPC6 protein (Föller et al., 2008c). Withdrawal of extracellular calcium significantly blunted the afatinib-induced erythrocyte membrane scrambling, indicating that afatinib influences the calcium entry and subsequent triggering of phosphatidylserine translocation. However, afatinib stimulated erythrocyte death even in the absence of extracellular calcium. Thus, the effect of afatinib on cytosolic calcium entry contributes to but is not fully responsible for eryptosis stimulation, indicating the involvement of additional mechanisms in the afatinib-mediated PS externalisation.

In nucleated cells, afatinib promotes apoptosis through ROS generation (Hu et al., 2017). Again, previous studies proved that oxidative stress activates calcium-permeable non-selective cation channels (NSCC) and stimulates the cell membrane scrambling of eryptosis (Lang et al., 2014; Lang and Qadri, 2012). In the present investigation, afatinib exposure significantly upregulated the ROS in the erythrocytes (Figure 12) and, thus, stimulated eryptosis by an opening of the cation channels. Furthermore, a well-known trigger of eryptosis is ceramide. Ceramide itself can stimulate the membrane scrambling of

erythrocytes or can sensitize the cells for the scrambling effect of calcium (Lang et al., 2004; Lang et al., 2010). Previous studies confirm the ceramide-induced apoptosis in various nucleated cell types (Arana et al., 2010; Nikolova-Karakashian and Rozenova, 2010) including T-lymphocytes (Gulbins et al., 1997), epithelial cells (Teichgraber et al., 2008), hepatocytes (Lang et al., 2007b), and neurons (Jana et al., 2009; Arboleda et al., 2010). In accordance with earlier studies, afatinib significantly increased the ceramide abundance on the surface of erythrocytes in this study (Figure 13).

The afatinib-mediated increased intracellular calcium concentration contributed to the shrinkage of erythrocytes. Erythrocytes express calcium-sensitive potassium channels and activation of these channels causes an efflux of K^+ against its concentration gradient followed by hyperpolarisation of the plasma membrane and exit of Cl^- from the cells. Along with the loss of KCl, water also exits from the erythrocytes as a result of loss of cellular osmolarity resulting in the shrinkage of cells (Lang et al., 2003b; Maher and Kuchel, 2003). Again, removal of extracellular calcium compromises the increase of cytosolic calcium followed by inactivation of the Gardos channels, cell membrane depolarisation resulting in Cl^- entry into the cells, and cell swelling.

Circulating PS-exposing erythrocytes are easily recognised and engulfed by macrophages resulting in rapid clearance from the blood circulation (de Back et al., 2014; Kurosaka et al., 2003; Lang and Qadri, 2012). Thus, even after induction of eryptosis, the number of eryptotic erythrocytes remains low in the circulation. However, the enhanced eryptosis may cause anaemia if the percentage of eryptotic cells that are removed from the bloodstream is higher than the formation of reticulocytes by erythropoiesis (Lang and Lang, 2015). Again, phosphatidylserine-exposing erythrocytes may adhere to the vascular endothelial cells *via* CXCL16/SR-PSO (Borst et al., 2012; Pandolfi et al., 2007) and thus promote the development of thrombosis (Andrews and Low, 1999; Chung et al., 2007; Wood et al., 1996). The thrombus can compromise the microcirculation (Abed et al., 2012; Andrews and Low, 1999; Closse et al., 1999; Gallagher et al., 2003; Pandolfi et al., 2007; Wood et al., 1996) and lead to organ failure.

The present study further discloses that afatinib at 16.4 μM concentration significantly induces haemolysis. The beneficial function of eryptosis is to remove defective

erythrocytes from the blood circulation before haemolysis (Lang and Lang, 2015). Thus, timely removal of defective erythrocytes prevents the release of haemoglobin into the circulation, which may further pass through the renal glomerulus. The acidic lumen of the glomerulus may stimulate the precipitation of the eryptotic erythrocytes followed by occlusion of the nephrons and impaired renal function (Lang et al., 2012a; Harrison et al., 1947).

In conclusion, afatinib stimulates eryptosis, paralleled by calcium entry, oxidative stress, and ceramide formation (Figure 45).

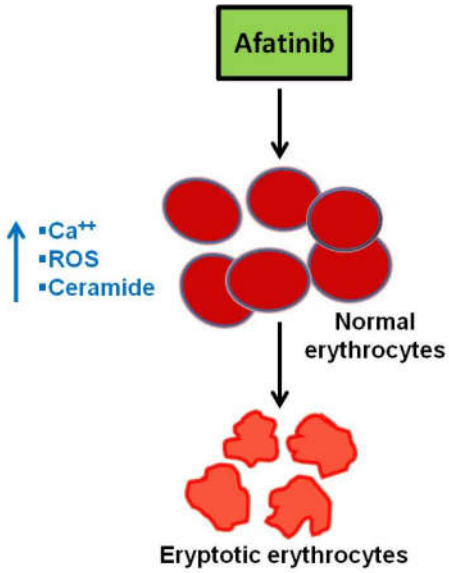

Figure 45: The sensitivity of afatinib on eryptosis. Afatinib-stimulated suicidal erythrocyte death following 48 hours of incubation. The eryptosis is modulated by increased cytosolic calcium concentration, generation of ceramide, and ROS.

4. 2. The effect of ceritinib on eryptosis

The present investigation unveiled a novel effect of ceritinib in relation to eryptosis. Exposure of freshly drawn human erythrocytes to ceritinib resulted in cell shrinkage and membrane scrambling with the externalisation of phosphatidylserine from the inner layer to the erythrocyte surface. Ceritinib-induced PS scrambling reaches statistical significance at 1.25 µM, a concentration by far higher than the IC_{50} of 0.2 nM for inhibition of ALK tyrosine kinase (Marsilje et al., 2013). The recommended dose of ceritinib in patients is 500 mg/day, which leads to a 1.2 µM blood plasma level (Shaw et al., 2014). Values up to 2.5 µM have been observed in the patient plasma (Nishio et al., 2015). However, as 97% of ceritinib bind to blood plasma proteins (Santarpia et al., 2017), the concentration of free ceritinib in blood may be far below the concentration of 1.25 µM required for significant ceritinib-induced erythrocyte death.

Exposure to ceritinib increased the cytosolic calcium concentration, which is a prime regulator of eryptosis (Lang et al., 2012a). The increased cytosolic calcium may result from NSCC stimulation (Lang et al., 2003a) and, thus, the entry of extracellular calcium into the cell, which promotes apoptosis in erythrocytes. It is reported that the TRPC6 cation channel is involved in stimulating calcium entry and amiloride has the potential to block TRPC6 and, thus, inhibit eryptosis (Föller et al., 2008c). In this research, amiloride decreased the ceritinib-triggered annexin-V-binding cells which confirm the involvement of TRPC6 in cytosolic calcium entry and, finally, the translocation of PS. Again, the withdrawal of extracellular calcium significantly decreased, but did not abolish, the PS-externalisation (Figure 19), indicating that additional mechanisms contribute to the membrane scrambling of erythrocytes. The calcium-permeable cation channels could be stimulated by enhanced oxidative stress, leading to eryptosis (Duranton et al., 2002; Lang et al., 2014; Lang et al., 2012b). However, it was observed that ceritinib did not significantly increase the ROS formation (Figure 21). This result supports earlier studies, where ceritinib was not associated with generating oxidative stress in nucleated cells (Novartis, 2015; Marsilje et al., 2013). In addition to oxidative stress, cells could be sensitized for the eryptotic effect of calcium by ceramide or even ceramide itself could trigger cell membrane scrambling (Lang et al., 2004; Lang et al., 2012b; Lang et al., 2010). However, the results showed ceritinib induced erythrocyte death without significant modification of ceramide abundance.

In nucleated cells, ceritinib has been shown to stimulate apoptosis by modifying AKT/PKB (Friboulet et al., 2014). AKT1/2 inhibitor A6330 significantly blunted erythrocyte death following ceritinib exposure.

Protein kinase C (Klarl et al., 2006), p38 kinase (Gatidis et al., 2011), and casein kinase 1α (Zelenak et al., 2012) are well-known inducers of eryptosis. The effect of ceritinib is also sensitive to staurosporine (Figure 24), SB203580 (Figure 25), and D4476 (Figure 26), which are inhibitors of protein kinase C, p38 kinase, and casein kinase 1α, respectively. Further, ceritinib-triggered erythrocyte death was significantly blunted following exposure to pan-caspase inhibitor zVAD (Figure 27). Previous studies also showed the involvement of caspases in triggering suicidal erythrocyte death (Mandal et al., 2005; Mandal et al., 2002). Again, caspases in erythrocytes are stimulated subsequent to oxidative stress (Maellaro et al., 2013; Mandal et al., 2002). Ceritinib, however, did not enhance the oxidative stress in this study. Erythrocytes lack important organelles such as mitochondria and are, thus, unable to stimulate caspases through the mitochondrial pathway. Hence, in this study, it is not clear how caspases are activated in erythrocytes following ceritinib treatment.

In addition to PS translocation, elevated cytosolic calcium may also be responsible for ceritinib-induced cell shrinkage. Erythrocytes express different ion channels and among them, the Gardos channel is the vital regulator of cell shrinkage. Gardos channels are calcium sensitive and are activated by increased intracellular calcium concentration, resulting in the efflux of K^+, hyperpolarisation of the erythrocyte plasma membrane, and subsequent Cl^- release from the cell, finally leading to loss of KCl. Subsequently, water effluxes from the cells as a result of intracellular and extracellular osmotic pressure differences resulting in cell shrinkage (Lang et al., 2003b; Maher and Kuchel, 2003).

Ceritinib significantly increased haemolysis in this study. Eryptotic erythrocytes are engulfed by macrophages (de Back et al., 2014; Kurosaka et al., 2003) and are rapidly cleared from circulation avoiding the release of Hb from the erythrocytes into the bloodstream (Lang et al., 2012b). If released, the Hb can cross the kidney filters and the acidic lumen of the renal tubules may enhance the precipitation followed by occlusion of the renal tubules and, subsequently, kidney failure (Lang and Lang, 2015; Harrison et al., 1947). Crizotinib, another ALK inhibitor, has been found to cause renal

insufficiency (Izzedine et al., 2016) but impaired renal function following ceritinib treatment is largely unexplored.

The free nitric oxide (NO) concentration in the blood plasma is 3 nM -7 μM (Stamler et al., 1992). Erythrocytes possess an NO synthase and thus produce and maintain the circulating NO pool beyond their own store (Kleinbongard et al., 2006). NO is a well-known inhibitor of eryptosis (Nicolay et al., 2008) and low NO levels in the circulation may lead to erythrocyte death (Ghashghaeinia et al., 2017). According to this experiment, the NO donor (nitroprusside) blunted the ceritinib-induced annexin-V-binding (Figure 28) pointing at the inhibitory effect of ceritinib on the NO synthase, leading to a decreased NO production, which is followed by downregulation of S-nitrosylation (Ghashghaeinia et al., 2017).

As there is a rapid clearance of phosphatidylserine translocating erythrocytes from the circulation, increased eryptosis may lead to the development of anaemia if the erythropoiesis is slower than the removal of erythrocytes by eryptosis (Lang et al., 2012b). Anaemia could further result from enhanced haemolysis and/or stimulated apoptosis of progenitor cells. As mentioned previously, phosphatidylserine-exposing erythrocytes tend to adhere to vascular endothelial cells (Closse et al., 1999; Borst et al., 2012; Abed et al., 2012), leading to thrombosis (Andrews and Low, 1999; Chung et al., 2007) and subsequent occlusion of microvessels (Abed et al., 2012; Andrews and Low, 1999; Wood et al., 1996).

In conclusion, ceritinib stimulates eryptosis. Ceritinib-triggered eryptosis is a result of calcium entry, activation of caspases, protein kinase C, p38 kinase, casein kinase 1α, and altered s-nitrosylation (Figure 46).

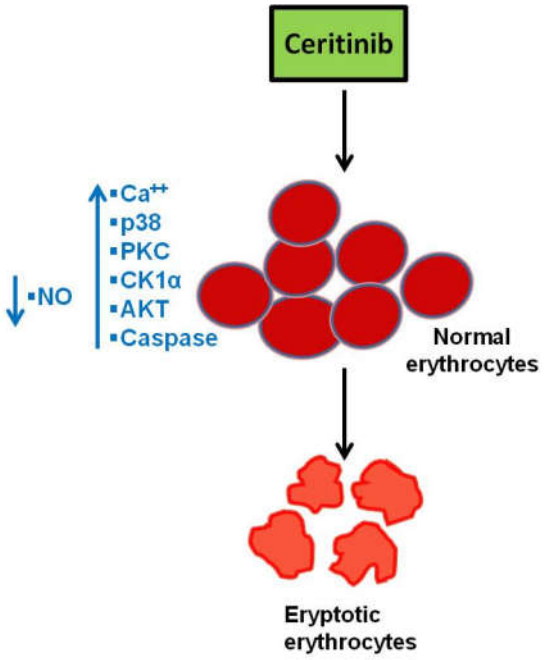

Figure 46: The effect of ceritinib on eryptosis. Ceritinib-triggered suicidal erythrocyte death subsequent to 48 hours of incubation. The erythrocyte death is mediated by increased intracellular calcium, up-regulation of AKT, p38 kinase, protein kinase C (PKC), casein kinase 1α, and down-regulation of NO.

4. 3. The inhibition of suicidal erythrocyte death by volasertib

The present research discloses a novel, unpredicted effect of volasertib on the membrane scrambling of erythrocytes. Erythrocytes obtained from healthy volunteers exposed to volasertib alone in isotonic Ringer's solution did not show any significant changes in the translocation of phosphatidylserine or the shrinkage of the cells. However, volasertib significantly inhibited the PS translocation following exposure to energy-depletion or hyperosmotic shock. The volasertib concentration required to inhibit the eryptosis was 1.6 μM, a concentration several orders of magnitude higher than the IC_{50} of 0.87 nM for inhibition of polo-like kinase 1 (Rudolph et al., 2009). The concentration reported in human blood plasma is 1.2 μM (Schoffski et al., 2012) under the daily volasertib dose of 300 mg/day used in the current clinical trials (Gjertsen and Schoffski, 2015). Volasertib did not cause any significant alteration in the phosphatidylserine externalisation following oxidative stress or calcium overload in the extracellular solution. Again, volasertib did not cause any significant change in the erythrocyte volume following glucose removal, increased osmotic pressure, oxidative stress, or ionomycin exposure.

As volasertib did not significantly increase cytosolic calcium concentration, this could be a possible reason for the inability of volasertib to induce significant cell shrinkage. A previous study revealed that an increased level of intracellular calcium concentration sensitizes the Gardos channel in erythrocytes followed by translocation of K^+ from the intracellular space to the extracellular space resulting in hyperpolarisation of the erythrocyte membrane followed by an efflux of Cl^- and loss of cellular KCl along with the osmotically driven exit of water from the cells (Lang et al., 2003b; Maher and Kuchel, 2003).

Volasertib significantly inhibited the effects on PS translocation following glucose removal and hyperosmotic shock and simultaneously stimulated the apoptosis/PS translocation in nucleated K562 cells, pointing towards its contradictory effect. Although cell membrane scrambling is the common feature observed in both eryptosis and apoptosis, the underlying signalling pathway may be different (Kiraz et al., 2016; Lang and Qadri, 2012). In this sense, apoptosis in nucleated cells *via* inhibition of polo-like kinase1 (PLK1) may be associated with the mitochondrial pathway (Hugle et al., 2015), whereas mature erythrocytes lack this organelle. Considering the apoptotic effect on tumour cells and the

simultaneous protection of mature erythrocytes following energy depletion or hyperosmotic shock, volasertib may be the best choice for reducing cancer-related anaemia (Lang et al., 2017).

The underlying signalling pathways for the inhibitory property of volasertib on cell membrane scrambling following energy depletion or hyperosmotic shock was not disclosed in this study. Enhanced intracellular calcium concentration, ROS formation, or ceramide are well-known triggers of eryptosis that are not significantly altered by volasertib following glucose removal. Hence, further investigation is necessary to explore the mechanisms responsible for volasertib's anti-eryptotic effect following glucose removal and hyperosmotic shock.

Volasertib inhibits eryptosis, irrespective of the underlying mechanisms. Thus, the incidence of anaemia reported in humans following a combination therapy of volasertib may be the outcome of the adverse effects of the combined drugs rather than the use of volasertib alone. However, volasertib stimulates apoptosis in the erythrocyte progenitor cells and may, thus, decrease the generation of new erythrocytes, and lead to anaemia.

Eryptotic erythrocytes are bound to surface receptors of macrophages followed by phagocytosis. Thus, defective erythrocytes are removed from the circulation. Anaemia may, subsequently, develop if the eryptosis rate is higher than the rate of erythropoiesis (Lang et al., 2012b).

The FSC results revealed that volasertib did not interfere with erythrocyte volume, which may be the reason why volasertib does not stimulate haemolysis. During haemolysis, there is a subsequent release of Hb into the blood circulation, which may pass through the renal glomerular filter system and may occlude the kidney nephrons resulting from precipitation in the acidic lumen, finally leading to renal failure (Harrison et al., 1947). As eryptotic erythrocytes tend to adhere to vascular endothelial cells (Borst et al., 2012; Closse et al., 1999), this interaction may stimulate the formation of blood clots/thrombosis (Chung et al., 2007; Andrews and Low, 1999), which may, ultimately, lead to a blockage of the microcirculation (Andrews and Low, 1999; Abed et al., 2012; Wood et al., 1996; Lang et al., 2012b; Gallagher et al., 2003). Hence, eryptosis inhibition may reduce the risk of cardiovascular dysfunction in cancer patients.

In conclusion, volasertib counteracts suicidal erythrocyte death subsequent to energy depletion and hyperosmotic shock but stimulates apoptosis in erythrocyte progenitor cells (Figure 47).

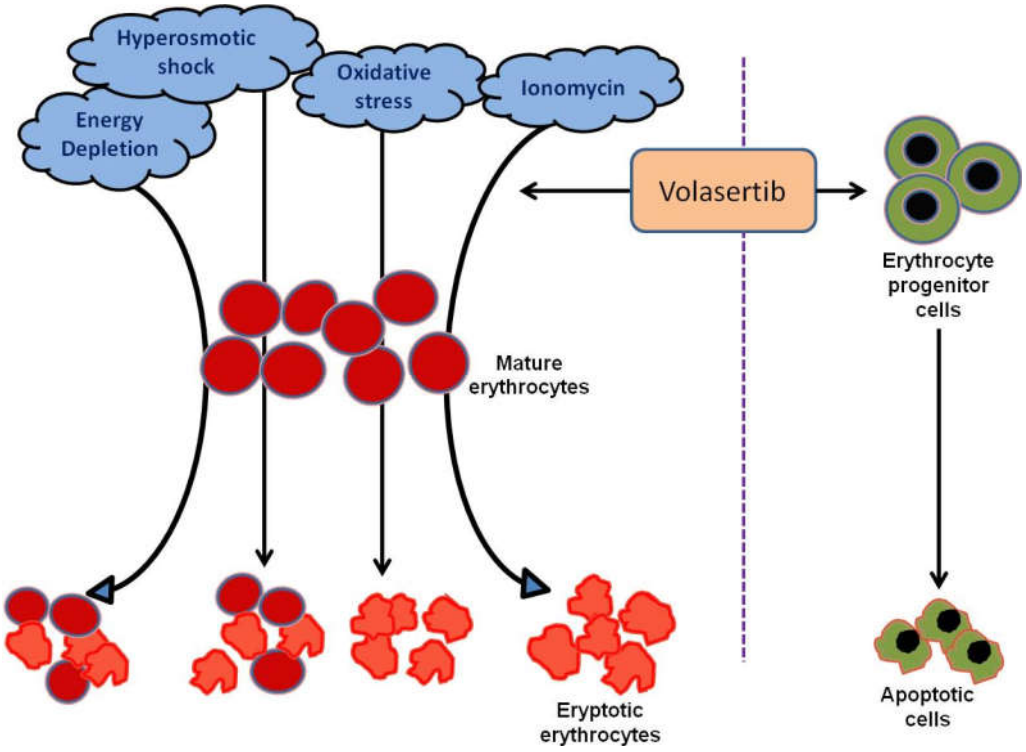

Figure 47: The sensitivity of volasertib on eryptosis. Protective effect of volasertib on eryptosis following energy depletion and hyperosmotic shock (left panel). The right panel indicates the stimulatory properties of volasertib on the apoptosis of erythrocyte progenitor cells.

5. Summary

The thesis explored the effect of the cytostatic molecules afatinib, ceritinib, and volasertib on eryptosis, i.e., the suicidal death of erythrocytes characterised by the breakdown of phosphatidylserine (PS) asymmetry, the shrinkage of the cells, and membrane blebbing. Stimuli of eryptosis include ATP depletion, oxidative stress, hyperosmotic shock, as well as different xenobiotics/diseases. Underlying signalling mechanisms include an excess of intracellular calcium, ceramide, and reactive oxygen species (ROS) generation, as well as the involvement of different kinases and caspases.

Healthy human erythrocytes (0.4% hematocrit) were treated with different concentrations of afatinib, ceritinib, and volasertib at 37°C for 48 hours. Flow cytometry was employed to quantify the PS translocation on the erythrocyte surface from annexin-V-binding, cell shrinkage from forward scatter (FSC), cytosolic calcium from Fluo3-fluorescence, ROS from DCFDA fluorescence, and ceramide using ceramide-specific antibodies.

The first part of the investigation shows that after the respective incubation period, afatinib (≥8.2 μM) significantly enhanced the percentage of eryptotic erythrocytes and significantly decreased the FSC. Afatinib also significantly elevated the intracellular calcium level, ceramide abundance, and ROS production. The effect of afatinib on PS translocation significantly decreased after the removal of extracellular calcium. No significant distinction was observed in PS translocation after application of the inhibitors of caspases or protein kinase C (PKC), p38 kinase, casein kinase 1α (CK1α), and Janus kinase 3 (JAK3). Afatinib (≥16.4 μM) significantly enhanced haemolysis. The afatinib concentration required for induction of eryptosis is by far higher than the plasma concentration of free afatinib in treated patients and, thus, afatinib-triggered eryptosis cannot explain the drug-induced anaemia. Signalling mechanisms of afatinib-triggered eryptosis include the increase of cytosolic calcium, enhanced production of ceramide, and ROS.

The results of the second part of the study indicate that ceritinib (1.8 μM) significantly increased the suicidal erythrocyte death and significantly decreased cell volume. Ceritinib elevated the cytosolic calcium concentration, but not the ROS or ceramide level. The effect of ceritinib on annexin-V-binding was significantly inhibited in the

absence of extracellular calcium, in the presence of the non-selective cation channel inhibitor amiloride (1mM), AKT1/2 inhibitor A6730 (58 nM), PKC blocker staurosporine (1 μM), p38 kinase inhibitor SB203580 (2 μM), CK1α blocker D4476 (10 μM), and caspase inhibitor zVAD (10 μM). Ceritinib also significantly triggered haemolysis. In conclusion, ceritinib stimulates suicidal erythrocyte death. The ceritinib concentration required for inducing eryptosis is by far higher than the plasma concentration of free ceritinib in treated patients and ceritinib-triggered eryptosis cannot explain the drug-induced anaemia. Signalling of ceritinib-induced eryptosis includes calcium entry, activation of AKT1/2 signalling, and the activation of caspases and kinases such as PKC, p38, and CK1α.

Finally, the third part of the study reveals that volasertib did not stimulate suicidal erythrocyte death, but rather showed an anti-eryptotic property following exposure of erythrocyte concentrates to various eryptotic stimuli. Human erythrocytes were exposed to energy-depleted Ringer's solution for 48 hours, hyperosmotic Ringer's solution (550 mM sucrose was added) for six hours, oxidative stress (0.3 mM tert-butylhydroperoxide [t-booh] was added) for 50 minutes, or to calcium ionophore ionomycin (1 μM) for 60 minutes in the absence and presence of volasertib (0.8 - 2.4 μM). For a comparative study of volasertib on nucleated and anucleated cells, the erythrocyte progenitor cell line (K562 cells) with RPMI-1640 medium was exposed to volasertib (0.8 – 2.4 μM) for 48 hours and then PS externalisation and FSC were quantified. Glucose depletion, oxidative stress, hyperosmotic shock, and calcium overload increased the percentage of PS-exposing erythrocytes and decreased FSC. Volasertib significantly blunted the suicidal erythrocyte death following energy depletion or osmotic shock, but not after oxidative stress or ionomycin treatment. Volasertib did not show any influence on FSC or calcium entry following any manoeuvre. The ROS generation or ceramide production following energy depletion was not changed in the presence of volasertib. Volasertib significantly stimulated apoptosis in nucleated K562 cells, as well as considerably decreased the cell volume. Thus, volasertib possesses an anti-eryptotic power following energy depletion or hyperosmotic shock, observations contrasting stimulation of apoptosis in K562 cells.

Finally, collective data from the above investigations show that afatinib and ceritinib stimulate eryptosis whereas volasertib shows a protective effect against mature erythrocyte death but triggered apoptosis in the erythrocyte progenitor K562 cell line.

6. Zusammenfassung

Afatinib, Ceritinib und Volasertib werden zur Behandlung von Malignomen eingesetzt. Eine Nebenwirkung ist Anämie, die das Resultat einer übermäßigen Eryptose sein könnte. Die Eryptose, der suizidale Erythrozytentod, ist durch Zusammenbrechen der Phosphatidylserin (PS) - Asymmetrie in der Zellmembran, Zellschrumpfung und Bildung von Membranbläschen gekennzeichnet. Stimuli wie z.B. Energieentzug, hyperosmotischer Schock, oxidativer Stress sowie verschiedene Xenobiotika/Erkrankungen sind bekannte Stimulatoren der Eryptose. Die Signalmechanismen, die der Eryptose zu Grunde liegen, umfassen einen Überschuss an intrazellulärem Kalzium, Ceramid und reaktiven Sauerstoffspezies (ROS) sowie die Beteiligung verschiedener Kinasen und Caspasen. Um eine Wirkung der Substanzen auf Eryptose aufzudecken, wurden gesunde humane Erythrozyten (0,4% Hämatokrit) verschiedenen Konzentrationen der Substanzen ausgesetzt und für 48 Stunden bei 37°C inkubiert. Die Durchflusszytometrie wurde zur Bestimmung der PS-Translokation auf der Erythrozytenoberfläche anhand der Annexin-V-Bindung, der Zellschrumpfung durch das Vorwärtsstreulicht (FSC), des zytosolischen Kalziumgehalts anhand der Fluo3-Fluoreszenz, der Bildung von ROS anhand der DCFDA-Fluoreszenz sowie der Ceramid-Abundanz anhand von spezifischen Antikörpern eingesetzt.

Die Ergebnisse des ersten Teils der Studie zeigen, dass Afatinib (≥8,2 µM) den Prozentsatz an eryptotischen Erythrozyten nach der jeweiligen Inkubationszeit signifikant erhöht und das FSC signifikant senkt. Afatinib erhöhte zudem den intrazellulären Kalziumspiegel, die Ceramid-Abundanz und die ROS-Produktion signifikant. Die Wirkung von Afatinib auf die PS-Translokation war nach Entfernen von extrazellulärem Kalzium signifikant verringert. Es konnte kein signifikanter Unterschied in der PS-Translokation nach Applikation der Inhibitoren von Caspasen oder Proteinkinase C (PKC), p38-Kinase, casein kinase 1α (CK1α) und Janus-Kinase 3 (JAK3) beobachtet werden. Afatinib löste ab einer Konzentration von 16,4 µM eine signifikant erhöhte Hämolyse aus. Für diese Wirkung sind jedoch Afatinib-Konzentrationen erforderlich, die weit über der Plasmakonzentration an freiem Afanitinib in behandelten Patienten liegen. Das Auftreten Afatinib-assoziierter Anämie ist daher wahrscheinlich nicht Folge einer übermäßigen Eryptose und Hämolyse. Der zugrunde liegende Signalmechanismus der durch Afatinib ausgelösten Eryptose umfasst

die Erhöhung des intrazellulären Kalziums sowie eine erhöhte Produktion von Ceramid und ROS.

Die Ergebnisse des zweiten Teils des Forschungsprojektes zeigen, dass Ceritinib (1,8 μM) den suizidalen Erythrozytentod signifikant erhöht und das Zellvolumen signifikant senkt. Ceritinib steigerte die zytosolische Kalziumkonzentration, nicht jedoch den ROS- oder Ceramid-Spiegel. Die Wirkung von Ceritinib auf die Annexin-V-Bindung wurde in Abwesenheit von extrazellulärem Kalzium sowie in Gegenwart des nicht-selektiven Kationenkanalblockers Amilorid (1mM), AKT1/2-Inhibitor A6730 (58 nM), PKC-Blocker Staurosporin (1 μM), p38-Kinase-Inhibitor SB203580 (2 μM), CK1α-Blocker D4476 (10 μM) und durch den Caspase-Inhibitor zVAD (10 μM) signifikant verringert. Ceritinib erhöhte ebenfalls signifikant die Hämolyse. Zusammenfassend lässt sich festhalten, dass Ceritinib den suizidalen Erythrozytentod stimuliert. Für diese Wirkung sind jedoch Ceritinib-Konzentrationen erforderlich, die weit über der Plasmakonzentration an freiem Ceritinib in behandelten Patienten liegen. Das Auftreten Ceritinib-assoziierter Anämie ist daher wahrscheinlich nicht Folge einer übermäßigen Eryptose. Die Ceritinib-induzierte Eryptose wird durch einen Kalziumanstieg, durch Aktivierung des AKT1/2-Signalwegs sowie Aktivierung von Caspasen und Kinasen wie PKC, p38 oder CK1α begleitet.

Schließlich deckt der dritte Teil der Studie auf, dass Volasertib keinen suizidalen Erythrozytentod stimuliert. Nachdem Erythrozyten verschiedenen eryptotischen Stimuli ausgesetzt wurden, zeigte Volasertib vielmehr eine anti-eryptotische Wirkung. Humane Erythrozyten wurden einem Energiemangel 48 Stunden lang, einer hyperosmotischen Ringer-Lösung (550 mM Saccharose wurde zugegeben) für 6 Stunden, einem Oxidans (0,3 mM tert.-Butylhydroperoxid [Tbooh] für 50 Minuten, sowie dem Calcium-Ionophor Ionomycin (1 uM) für 60 min in Abwesenheit und Anwesenheit von Volasertib (0,8 - 2,4 μM) ausgesetzt. Um einen Vergleich der Wirkung von Volasertib auf kernhaltige und kernlose Zellen zu erhalten, wurde die Erythrozyten-Vorläuferzelllinie (K562-Zellen) mit RPMI-1640-Medium 48 Stunden lang mit Volasertib (0,8 - 2,4 μM) inkubiert. Anschließend wurden die PS-Externalisierung und das FSC quantifiziert. Glukosemangel, oxidativer Stress, hyperosmotischer Schock sowie ein Kalziumüberschuss erhöhten den Prozentsatz an PS-exponierenden Erythrozyten und verringerten das FSC. Volasertib verminderte den suizidalen

Erythrozytentod nach Energieentzug oder osmotischem Schock signifikant, nicht jedoch nach oxidativem Stress oder einer Ionomycin-Behandlung. Volasertib zeigte keinen Einfluss auf das FSC oder den Kalziumeinstrom eines jeglichen Manövers. Die ROS- und Ceramidproduktion wurde nach Energieentzug in Gegenwart von Volasertib nicht verändert. Volasertib stimulierte die Apoptose in kernhaltigen K562-Zellen signifikant und verringerte das Zellvolumen erheblich. So besitzt Volasertib nach Energieentzug oder hyperosmotischem Schock eine anti-eryptotische Wirkung im Gegensatz zur Stimulation der Apoptose in K562-Zellen nach Volasertib-Behandlung.

7. References

ABED, M., FEGER, M., ALZOUBI, K., PAKLADOK, T., FRAUENFELD, L., GEIGER, C., TOWHID, S. T. & LANG, F. 2013a. Sensitization of erythrocytes to suicidal erythrocyte death following water deprivation. *Kidney Blood Press Res,* 37**,** 567-78.

ABED, M., TOWHID, S. T., FEGER, M., SCHMIDT, S., KURO, O. M., GAWAZ, M. & LANG, F. 2013b. Adhesion of klotho-deficient eryptotic erythrocytes to endothelial cells. *Acta Physiol (Oxf),* 207**,** 485-93.

ABED, M., TOWHID, S. T., MIA, S., PAKLADOK, T., ALESUTAN, I., BORST, O., GAWAZ, M., GULBINS, E. & LANG, F. 2012. Sphingomyelinase-induced adhesion of eryptotic erythrocytes to endothelial cells. *Am J Physiol Cell Physiol,* 303**,** C991-9.

ADACHI, Y., ISHIKAWA, Y. & KIYOI, H. 2017. Identification of volasertib-resistant mechanism and evaluation of combination effects with volasertib and other agents on acute myeloid leukemia. *Oncotarget,* 8**,** 78452-78465.

AKEL, A., WAGNER, C. A., KOVACIKOVA, J., KASINATHAN, R. S., KIEDAISCH, V., KOKA, S., ALPER, S. L., BERNHARDT, I., WIEDER, T., HUBER, S. M. & LANG, F. 2007. Enhanced suicidal death of erythrocytes from gene-targeted mice lacking the Cl-/HCO(3)(-) exchanger AE1. *Am J Physiol Cell Physiol,* 292**,** C1759-67.

AL MAMUN BHUYAN, A., ASHIQUL HAQUE, A. K. M., SAHU, I., CAO, H., KORMANN, M. S. D. & LANG, F. 2017a. Inhibition of Suicidal Erythrocyte Death by Volasertib. *Cell Physiol Biochem,* 43**,** 1472-1486.

AL MAMUN BHUYAN, A. & LANG, F. 2018. Stimulation of Eryptosis by Afatinib. *Cell Physiol Biochem,* 47**,** 1259-1273.

AL MAMUN BHUYAN, A., SIGNORETTO, E., BISSINGER, R. & LANG, F. 2016a. Enhanced Eryptosis Following Exposure to Dolutegravir. *Cell Physiol Biochem,* 39**,** 639-50.

AL MAMUN BHUYAN, A., SIGNORETTO, E., BISSINGER, R. & LANG, F. 2016b. Stimulation of Suicidal Erythrocyte Death by Ceritinib-Treatment of Human Erythrocytes. *Cell Physiol Biochem,* 40**,** 1129-1140.

AL MAMUN BHUYAN, A., WAGNER, T., CAO, H. & LANG, F. 2017b. Triggering of Suicidal Erythrocyte Death by Gefitinib. *Cell Physiol Biochem,* 41**,** 1697-1708.

ALLAN, D. & MICHELL, R. H. 1977. Calcium ion-dependent diacylglycerol accumulation in erythrocytes is associated with microvesiculation but not with efflux of potassium ions. *Biochem J,* 166**,** 495-9.

ALVAREZ, J. & GARCIA-SANCHO, J. 1987. An estimate of the number of Ca2+-dependent K+ channels in the human red cell. *Biochim Biophys Acta,* 903**,** 543-6.

AMER, J., GOLDFARB, A. & FIBACH, E. 2003. Flow cytometric measurement of reactive oxygen species production by normal and thalassaemic red blood cells. *Eur J Haematol,* 70**,** 84-90.

ANDREWS, D. A. & LOW, P. S. 1999. Role of red blood cells in thrombosis. *Curr Opin Hematol,* 6**,** 76-82.

ARANA, L., GANGOITI, P., OURO, A., TRUEBA, M. & GOMEZ-MUNOZ, A. 2010. Ceramide and ceramide 1-phosphate in health and disease. *Lipids Health Dis,* 9**,** 15.

ARBOLEDA, G., CARDENAS, Y., RODRIGUEZ, Y., MORALES, L. C., MATHEUS, L. & ARBOLEDA, H. 2010. Differential regulation of AKT, MAPK and GSK3beta during C2-ceramide-induced neuronal death. *Neurotoxicology,* 31**,** 687-93.

ASHRAF, M. Z. & GUPTA, N. 2011. Scavenger receptors: Implications in atherothrombotic disorders. *Int J Biochem Cell Biol,* 43**,** 697-700.

ATTANASIO, P., BISSINGER, R., HAVERKAMP, W., PIESKE, B., WUTZLER, A. & LANG, F. 2015. Enhanced suicidal erythrocyte death in acute cardiac failure. *Eur J Clin Invest,* 45**,** 1316-24.

AW, D. C., TAN, E. H., CHIN, T. M., LIM, H. L., LEE, H. Y. & SOO, R. A. 2017. Management of epidermal growth factor receptor tyrosine kinase inhibitor-related cutaneous and gastrointestinal toxicities. *Asia Pac J Clin Oncol,* 14**,** 23-31.

AWADA, A., DUMEZ, H., AFTIMOS, P. G., COSTERMANS, J., BARTHOLOMEUS, S., FORCEVILLE, K., BERGHMANS, T., MEEUS, M. A., CESCUTTI, J., MUNZERT, G., PILZ, K., LIU, D. & SCHOFFSKI, P. 2015. Phase I trial of volasertib, a Polo-like kinase inhibitor, plus platinum agents in solid tumors: safety, pharmacokinetics and activity. *Invest New Drugs,* 33**,** 611-20.

AWASTHI, S., GAYATHIRI, S. K., RAMYA, R., DURAICHELVAN, R., DHASON, A. & SARASWATHI, N. T. 2015. Advanced Glycation-Modified Human Serum Albumin Evokes Alterations in Membrane and Eryptosis in Erythrocytes. *Appl Biochem Biotechnol,* 177**,** 1013-24.

BAUMGARTH, N. & ROEDERER, M. 2000. A practical approach to multicolor flow cytometry for immunophenotyping. *J Immunol Methods,* 243**,** 77-97.

BERG, C. P., ENGELS, I. H., ROTHBART, A., LAUBER, K., RENZ, A., SCHLOSSER, S. F., SCHULZE-OSTHOFF, K. & WESSELBORG, S. 2001. Human mature red blood cells express caspase-3 and caspase-8, but are devoid of mitochondrial regulators of apoptosis. *Cell Death Differ,* 8**,** 1197-206.

BESSIS, M. & DELPECH, G. 1981. Discovery of the red blood cell with notes on priorities and credits of discoveries, past, present and future. *Blood Cells,* 7**,** 447-80.

BESTER, J. & PRETORIUS, E. 2016. Effects of IL-1beta, IL-6 and IL-8 on erythrocytes, platelets and clot viscoelasticity. *Sci Rep,* 6**,** 32188.

BHAVSAR, S. K., GU, S., BOBBALA, D. & LANG, F. 2011. Janus kinase 3 is expressed in erythrocytes, phosphorylated upon energy depletion and involved in the regulation of suicidal erythrocyte death. *Cell Physiol Biochem,* 27**,** 547-56.

BILMEN, S., AKSU, T. A., GUMUSLU, S., KORGUN, D. K. & CANATAN, D. 2001. Antioxidant capacity of G-6-PD-deficient erythrocytes. *Clin Chim Acta,* 303**,** 83-6.

BISSINGER, R., AL MAMUN BHUYAN, A., SIGNORETTO, E. & LANG, F. 2016a. Stimulating Effect of Elvitegravir on Suicidal Erythrocyte Death. *Cell Physiol Biochem,* 38**,** 1111-20.

BISSINGER, R., ARTUNC, F., QADRI, S. M. & LANG, F. 2016b. Reduced Erythrocyte Survival in Uremic Patients Under Hemodialysis or Peritoneal Dialysis. *Kidney Blood Press Res,* 41**,** 966-977.

BISSINGER, R., BHUYAN, A. A. M., QADRI, S. M. & LANG, F. 2018. Oxidative stress, eryptosis and anemia: a pivotal mechanistic nexus in systemic diseases. *FEBS J*.

BISSINGER, R., BOUGUERRA, G., AL MAMUN BHUYAN, A., WAIBEL, S., ABBES, S. & LANG, F. 2015. Efavirenz Induced Suicidal Death of Human Erythrocytes. *Cell Physiol Biochem,* 37**,** 2496-507.

BISSINGER, R., KEMPE-TEUFEL, D. S., HONISCH, S., QADRI, S. M., RANDRIANARISOA, E., HARING, H. U., HENES, J. & LANG, F. 2016c. Stimulated Suicidal Erythrocyte Death in Arteritis. *Cell Physiol Biochem,* 39**,** 1068-77.

BISSINGER, R., LANG, E., GHASHGHAEINIA, M., SINGH, Y., ZELENAK, C., FEHRENBACHER, B., HONISCH, S., CHEN, H., FAKHRI, H., UMBACH, A. T., LIU, G., REXHEPAJ, R., SCHALLER, M., MACK, A. F., LUPESCU, A., BIRNBAUMER, L., LANG, F. & QADRI, S. M. 2016d. Blunted apoptosis of erythrocytes in mice deficient in the heterotrimeric G-protein subunit Galphai2. *Sci Rep,* 6**,** 30925.

BISSINGER, R., MALIK, A., JILANI, K. & LANG, F. 2014. Triggering of erythrocyte cell membrane scrambling by salinomycin. *Basic Clin Pharmacol Toxicol,* 115**,** 396-402.

BISSINGER, R., SCHUMACHER, C., QADRI, S. M., HONISCH, S., MALIK, A., GOTZ, F., KOPP, H. G. & LANG, F. 2016e. Enhanced eryptosis contributes to anemia in lung cancer patients. *Oncotarget,* 7**,** 14002-14.

BONAN, N. B., STEINER, T. M., KUNTSEVICH, V., VIRZI, G. M., AZEVEDO, M., NAKAO, L. S., BARRETO, F. C., RONCO, C., THIJSSEN, S., KOTANKO, P., PECOITS-FILHO, R. & MORENO-AMARAL, A. N. 2016. Uremic Toxicity-Induced Eryptosis and Monocyte Modulation: The Erythrophagocytosis as a Novel Pathway to Renal Anemia. *Blood Purif,* 41**,** 317-23.

BORST, O., ABED, M., ALESUTAN, I., TOWHID, S. T., QADRI, S. M., FOLLER, M., GAWAZ, M. & LANG, F. 2012. Dynamic adhesion of eryptotic erythrocytes to endothelial cells via CXCL16/SR-PSOX. *Am J Physiol Cell Physiol,* 302**,** C644-51.

BRATOSIN, D., ESTAQUIER, J., PETIT, F., ARNOULT, D., QUATANNENS, B., TISSIER, J. P., SLOMIANNY, C., SARTIAUX, C., ALONSO, C., HUART, J. J., MONTREUIL, J. & AMEISEN, J. C. 2001. Programmed cell death in mature erythrocytes: a model for investigating death effector pathways operating in the absence of mitochondria. *Cell Death Differ,* 8**,** 1143-56.

CHA, M. Y., LEE, K. O., KIM, M., SONG, J. Y., LEE, K. H., PARK, J., CHAE, Y. J., KIM, Y. H., SUH, K. H., LEE, G. S., PARK, S. B. & KIM, M. S. 2012. Antitumor activity of HM781-36B, a highly effective pan-HER inhibitor in erlotinib-resistant NSCLC and other EGFR-dependent cancer models. *Int J Cancer,* 130**,** 2445-54.

CHAKRABARTI, A., HALDER, S. & KARMAKAR, S. 2016. Erythrocyte and platelet proteomics in hematological disorders. *Proteomics Clin Appl,* 10**,** 403-14.

CHAN, W. Y., LAU, P. M., YEUNG, K. W. & KONG, S. K. 2018. The second generation tyrosine kinase inhibitor dasatinib induced eryptosis in human erythrocytes-An in vitro study. *Toxicol Lett,* 295**,** 10-21.

CHIA, P. L., MITCHELL, P., DOBROVIC, A. & JOHN, T. 2014. Prevalence and natural history of ALK positive non-small-cell lung cancer and the clinical impact of targeted therapy with ALK inhibitors. *Clin Epidemiol,* 6**,** 423-32.

CHOLEWA, B. D., PELLITTERI-HAHN, M. C., SCARLETT, C. O. & AHMAD, N. 2014. Large-scale label-free comparative proteomics analysis of polo-like kinase 1 inhibition via the small-molecule inhibitor BI 6727 (Volasertib) in BRAF(V600E) mutant melanoma cells. *J Proteome Res,* 13**,** 5041-50.

CHU, Q. S., SANGHA, R., HOTTE, S. J., SERGENSON, G., SCHNELL, D., CHAND, V. K. & HIRTE, H. W. 2014. A phase I, dose-escalation trial of continuous- and pulsed-dose afatinib combined with pemetrexed in patients with advanced solid tumors. *Invest New Drugs,* 32**,** 1226-35.

CHUNG, S. M., BAE, O. N., LIM, K. M., NOH, J. Y., LEE, M. Y., JUNG, Y. S. & CHUNG, J. H. 2007. Lysophosphatidic acid induces thrombogenic activity through phosphatidylserine exposure and procoagulant microvesicle generation in human erythrocytes. *Arterioscler Thromb Vasc Biol,* 27**,** 414-21.

CLOSSE, C., DACHARY-PRIGENT, J. & BOISSEAU, M. R. 1999. Phosphatidylserine-related adhesion of human erythrocytes to vascular endothelium. *Br J Haematol,* 107**,** 300-2.

CONNOR, J., PAK, C. C. & SCHROIT, A. J. 1994. Exposure of phosphatidylserine in the outer leaflet of human red blood cells. Relationship to cell density, cell age, and clearance by mononuclear cells. *J Biol Chem,* 269**,** 2399-404.

COOPER, M. R., CHIM, H., CHAN, H. & DURAND, C. 2015. Ceritinib: a new tyrosine kinase inhibitor for non-small-cell lung cancer. *Ann Pharmacother,* 49**,** 107-12.

CRINO, L., AHN, M. J., DE MARINIS, F., GROEN, H. J., WAKELEE, H., HIDA, T., MOK, T., SPIGEL, D., FELIP, E., NISHIO, M., SCAGLIOTTI, G., BRANLE, F., EMEREMNI, C., QUADRIGLI, M., ZHANG, J. & SHAW, A. T. 2016. Multicenter Phase II Study of Whole-Body and Intracranial Activity With Ceritinib in Patients With ALK-Rearranged Non-Small-Cell Lung Cancer Previously Treated With Chemotherapy and Crizotinib: Results From ASCEND-2. *J Clin Oncol,* 34**,** 2866-73.

CRISP, R. L., VOTA, D. M., DONATO, H., GARCIA, E., RAPETTI, M. C., MALTANERI, R. E., VITTORI, D. C. & NESSE, A. B. 2016. Eryptosis is induced by hyperthermia in hereditary spherocytosis red blood cells. *Clin Chem Lab Med,* 54**,** e165-8.

DAMONTE, G., GUIDA, L., SDRAFFA, A., BENATTI, U., MELLONI, E., FORTELEONI, G., MELONI, T., CARAFOLI, E. & DE FLORA, A. 1992. Mechanisms of perturbation of erythrocyte calcium homeostasis in favism. *Cell Calcium,* 13**,** 649-58.

DAUGAS, E., CANDE, C. & KROEMER, G. 2001. Erythrocytes: death of a mummy. *Cell Death Differ,* 8**,** 1131-3.

DE BACK, D. Z., KOSTOVA, E. B., VAN KRAAIJ, M., VAN DEN BERG, T. K. & VAN BRUGGEN, R. 2014. Of macrophages and red blood cells; a complex love story. *Front Physiol,* 5**,** 9.

DEEKS, E. D. 2016. Ceritinib: a Review in ALK-Positive Advanced NSCLC. *Target Oncol,* 11**,** 693-700.

DHILLON, S. & CLARK, M. 2014. Ceritinib: first global approval. *Drugs,* 74**,** 1285-91.

DONG, M., LIU, B. & ZHU, R. 2016. Targeting ROS for Cancer Therapy

Chemotherapy:Open Access, 5**,** 2-7.

DURANTON, C., HUBER, S. M. & LANG, F. 2002. Oxidation induces a Cl(-)-dependent cation conductance in human red blood cells. *J Physiol,* 539**,** 847-55.

EBERL, M., KLINGLER, S., MANGELBERGER, D., LOIPETZBERGER, A., DAMHOFER, H., ZOIDL, K., SCHNIDAR, H., HACHE, H., BAUER, H. C., SOLCA, F., HAUSER-KRONBERGER, C., ERMILOV, A. N., VERHAEGEN, M. E., BICHAKJIAN, C. K., DLUGOSZ, A. A., NIETFELD, W., SIBILIA, M., LEHRACH, H., WIERLING, C. & ABERGER, F. 2012. Hedgehog-EGFR cooperation response genes determine the oncogenic phenotype of basal cell carcinoma and tumour-initiating pancreatic cancer cells. *EMBO Mol Med,* 4**,** 218-33.

EL-OSTA, H. & SHACKELFORD, R. 2015. Personalized treatment options for ALK-positive metastatic non-small-cell lung cancer: potential role for Ceritinib. *Pharmgenomics Pers Med,* 8**,** 145-54.

ESKENS, F. A., MOM, C. H., PLANTING, A. S., GIETEMA, J. A., AMELSBERG, A., HUISMAN, H., VAN DOORN, L., BURGER, H., STOPFER, P., VERWEIJ, J. & DE VRIES, E. G. 2008. A phase I dose escalation study of BIBW 2992, an irreversible dual inhibitor of epidermal growth factor receptor 1 (EGFR) and 2 (HER2) tyrosine kinase in a 2-week on, 2-week off schedule in patients with advanced solid tumours. *Br J Cancer,* 98**,** 80-5.

FÖLLER, M., BOBBALA, D., KOKA, S., HUBER, S. M., GULBINS, E. & LANG, F. 2009a. Suicide for survival--death of infected erythrocytes as a host mechanism to survive malaria. *Cell Physiol Biochem,* 24**,** 133-40.

FÖLLER, M., FEIL, S., GHORESCHI, K., KOKA, S., GERLING, A., THUNEMANN, M., HOFMANN, F., SCHULER, B., VOGEL, J., PICHLER, B., KASINATHAN, R. S., NICOLAY, J. P., HUBER, S. M., LANG, F. & FEIL, R. 2008a. Anemia and splenomegaly in cGKI-deficient mice. *Proc Natl Acad Sci U S A,* 105**,** 6771-6.

FOLLER, M., HARRIS, I. S., ELIA, A., JOHN, R., LANG, F., KAVANAGH, T. J. & MAK, T. W. 2013. Functional significance of glutamate-cysteine ligase modifier for erythrocyte survival in vitro and in vivo. *Cell Death Differ,* 20**,** 1350-8.

FÖLLER, M., HUBER, S. M. & LANG, F. 2008b. Erythrocyte programmed cell death. *IUBMB Life,* 60**,** 661-8.

FÖLLER, M., KASINATHAN, R. S., KOKA, S., HUBER, S. M., SCHULER, B., VOGEL, J., GASSMANN, M. & LANG, F. 2007. Enhanced susceptibility to suicidal death of erythrocytes from transgenic mice overexpressing erythropoietin. *Am J Physiol Regul Integr Comp Physiol,* 293**,** R1127-34.

FÖLLER, M., KASINATHAN, R. S., KOKA, S., LANG, C., SHUMILINA, E., BIRNBAUMER, L., LANG, F. & HUBER, S. M. 2008c. TRPC6 contributes to the Ca(2+) leak of human erythrocytes. *Cell Physiol Biochem,* 21**,** 183-92.

FÖLLER, M., MAHMUD, H., KOKA, S. & LANG, F. 2008d. *Reduced Ca2+ entry and suicidal death of erythrocytes in PDK1 hypomorphic mice.* 455.

FÖLLER, M., MAHMUD, H., QADRI, S. M., GU, S., BRAUN, M., BOBBALA, D., HOCHER, B. & LANG, F. 2010. Endothelin B receptor stimulation inhibits suicidal erythrocyte death. *FASEB J,* 24**,** 3351-9.

FÖLLER, M., SOPJANI, M., KOKA, S., GU, S., MAHMUD, H., WANG, K., FLORIDE, E., SCHLEICHER, E., SCHULZ, E., MUNZEL, T. & LANG, F. 2009b. Regulation of erythrocyte survival by AMP-activated protein kinase. *FASEB J,* 23**,** 1072-80.

FRIBOULET, L., LI, N., KATAYAMA, R., LEE, C. C., GAINOR, J. F., CRYSTAL, A. S., MICHELLYS, P. Y., AWAD, M. M., YANAGITANI, N., KIM, S., PFERDEKAMPER, A. C., LI, J., KASIBHATLA, S., SUN, F., SUN, X., HUA, S., MCNAMARA, P., MAHMOOD, S., LOCKERMAN, E. L., FUJITA, N., NISHIO, M., HARRIS, J. L., SHAW, A. T. & ENGELMAN, J. A. 2014. The ALK inhibitor ceritinib overcomes crizotinib resistance in non-small cell lung cancer. *Cancer Discov,* 4**,** 662-673.

GALLAGHER, P. G., CHANG, S. H., RETTIG, M. P., NEELY, J. E., HILLERY, C. A., SMITH, B. D. & LOW, P. S. 2003. Altered erythrocyte endothelial adherence and membrane phospholipid asymmetry in hereditary hydrocytosis. *Blood,* 101**,** 4625-7.

GAO, C., JI, S., DONG, W., QI, Y., SONG, W., CUI, D. & SHI, J. 2015. Indolic uremic solutes enhance procoagulant activity of red blood cells through phosphatidylserine exposure and microparticle release. *Toxins (Basel),* 7**,** 4390-403.

GATIDIS, S., ZELENAK, C., FAJOL, A., LANG, E., JILANI, K., MICHAEL, D., QADRI, S. M. & LANG, F. 2011. p38 MAPK activation and function following osmotic shock of erythrocytes. *Cell Physiol Biochem,* 28**,** 1279-86.

GAUDREAULT, V., WIRBEL, J., JARDIM, A., ROHRBACH, P. & SCORZA, T. 2015. Red Blood Cells Preconditioned with Hemin Are Less Permissive to Plasmodium Invasion In Vivo and In Vitro. *PLoS One,* 10**,** e0140805.

GHASHGHAEINIA, M., CLUITMANS, J. C., AKEL, A., DREISCHER, P., TOULANY, M., KOBERLE, M., SKABYTSKA, Y., SAKI, M., BIEDERMANN, T., DUSZENKO, M., LANG, F., WIEDER, T. & BOSMAN, G. J. 2012. The impact of erythrocyte age on eryptosis. *Br J Haematol,* 157**,** 606-14.

GHASHGHAEINIA, M., GIUSTARINI, D., KORALKOVA, P., KOBERLE, M., ALZOUBI, K., BISSINGER, R., HOSSEINZADEH, Z., DREISCHER, P., BERNHARDT, I., LANG, F., TOULANY, M., WIEDER, T., MOJZIKOVA, R., ROSSI, R. & MROWIETZ, U. 2016. Pharmacological targeting of glucose-6-phosphate dehydrogenase in human erythrocytes by Bay 11-7082, parthenolide and dimethyl fumarate. *Sci Rep,* 6**,** 28754.

GHASHGHAEINIA, M., WESSELING, M. C., RAMOS, E., PETKOVA-KIROVA, P., WAIBEL, S., LANG, E., BISSINGER, R., ALZOUBI, K., EDELMANN, B., HOSSEINZADEH, Z., DREISCHER, P., SHAHVAROUGHI-FARAHANI, A., MROWIETZ, U., KOBERLE, M., KAESTNER, L., BERNHARDT, I., MARTINEZ-RUIZ, A., WIEDER, T. & LANG, F. 2017. Trifluoperazine-Induced Suicidal Erythrocyte Death and S-Nitrosylation Inhibition, Reversed by the Nitric Oxide Donor Sodium Nitroprusside. *Cell Physiol Biochem,* 42**,** 1985-1998.

GJERTSEN, B. T. & SCHOFFSKI, P. 2015. Discovery and development of the Polo-like kinase inhibitor volasertib in cancer therapy. *Leukemia,* 29**,** 11-9.

GOODMAN, S. R., KURDIA, A., AMMANN, L., KAKHNIASHVILI, D. & DAESCU, O. 2007. The human red blood cell proteome and interactome. *Exp Biol Med (Maywood),* 232**,** 1391-408.

GORDON, M. S., MENDELSON, D. S., GROSS, M., UTTENREUTHER-FISCHER, M., OULD-KACI, M., ZHAO, Y., STOPFER, P. & AGUS, D. B. 2013. A Phase I, open-label, dose-escalation study of continuous once-daily oral treatment with afatinib in patients with advanced solid tumors. *Invest New Drugs,* 31**,** 409-16.

GOROSHCHUK, O., KOLOSENKO, I., VIDARSDOTTIR, L., AZIMI, A. & PALM-APERGI, C. 2019. Polo-like kinases and acute leukemia. *Oncogene,* 38**,** 1-16.

GREULICH, H., KAPLAN, B., MERTINS, P., CHEN, T. H., TANAKA, K. E., YUN, C. H., ZHANG, X., LEE, S. H., CHO, J., AMBROGIO, L., LIAO, R., IMIELINSKI, M., BANERJI, S., BERGER, A. H., LAWRENCE, M. S., ZHANG, J., PHO, N. H., WALKER, S. R., WINCKLER, W., GETZ, G., FRANK, D., HAHN, W. C., ECK, M. J., MANI, D. R., JAFFE, J. D., CARR, S. A., WONG, K. K. & MEYERSON, M. 2012. Functional analysis of receptor tyrosine kinase mutations in lung cancer identifies oncogenic extracellular domain mutations of ERBB2. *Proc Natl Acad Sci U S A,* 109**,** 14476-81.

GULBINS, E., SZABO, I., BALTZER, K. & LANG, F. 1997. Ceramide-induced inhibition of T lymphocyte voltage-gated potassium channel is mediated by tyrosine kinases. *Proc Natl Acad Sci U S A,* 94**,** 7661-6.

HALEY, K. 2017. Congenital Hemolytic Anemia. *Med Clin North Am,* 101**,** 361-374.

HALL, A. C. & ELLORY, J. C. 1986. Evidence for the presence of volume-sensitive KCl transport in 'young' human red cells. *Biochim Biophys Acta,* 858**,** 317-20.

HARRISON, H. E., BUNTING, H., ORDWAY, N. K. & ALBRINK, W. S. 1947. The Pathogenesis of the Renal Injury Produced in the Dog by Hemoglobin or Methemoglobin. *J Exp Med,* 86**,** 339-56.

HILLMAN, S, R., AULT, A, K., RINDER & M., E. (eds.) 2005. *Hematology in Clinical Practice: A Guide to Diagnosis and Management (4 ed.). McGraw-Hill Professional. p. 1. ISBN 978-0-07-144035-6.*

HU, X., SHI, S., WANG, H., YU, X., WANG, Q., JIANG, S., JU, D., YE, L. & FENG, M. 2017. Blocking autophagy improves the anti-tumor activity of afatinib in lung adenocarcinoma with activating EGFR mutations in vitro and in vivo. *Sci Rep,* 7**,** 4559.

HUBER, S. M., GAMPER, N. & LANG, F. 2001. Chloride conductance and volume-regulatory nonselective cation conductance in human red blood cell ghosts. *Pflugers Arch,* 441**,** 551-8.

HUBER, S. M., UHLEMANN, A. C., GAMPER, N. L., DURANTON, C., KREMSNER, P. G. & LANG, F. 2002. Plasmodium falciparum activates endogenous Cl(-) channels of human erythrocytes by membrane oxidation. *EMBO J,* 21**,** 22-30.

HUGLE, M., BELZ, K. & FULDA, S. 2015. Identification of synthetic lethality of PLK1 inhibition and microtubule-destabilizing drugs. *Cell Death Differ,* 22**,** 1946-56.

INGELHEIM, B. 2020. Results of Phase III study of volasertib for the treatment of acute myeloid leukemia presented at European Hematology Association Annual Meeting [Online]. Available: https://www.boehringer-ingelheim.us/press-

release/results-phase-iii-study-volasertib-treatment-acute-myeloid-leukemia-presented-european [Accessed 29 January 2020].

IOANNOU, N., DALGLEISH, A. G., SEDDON, A. M., MACKINTOSH, D., GUERTLER, U., SOLCA, F. & MODJTAHEDI, H. 2011. Anti-tumour activity of afatinib, an irreversible ErbB family blocker, in human pancreatic tumour cells. *Br J Cancer,* 105**,** 1554-62.

IZZEDINE, H., EL-FEKIH, R. K. & PERAZELLA, M. A. 2016. Invest New Drugs. 2016 The renal effects of ALK inhibitors. 34**,** 643-9.

JANA, A., HOGAN, E. L. & PAHAN, K. 2009. Ceramide and neurodegeneration: susceptibility of neurons and oligodendrocytes to cell damage and death. *J Neurol Sci,* 278**,** 5-15.

JEMAA, M., FEZAI, M., BISSINGER, R. & LANG, F. 2017. Methods Employed in Cytofluorometric Assessment of Eryptosis, the Suicidal Erythrocyte Death. *Cell Physiol Biochem,* 43**,** 431-444.

JIANG, P., BIAN, M., MA, W., LIU, C., YANG, P., ZHU, B., XU, Y., ZHENG, M., QIAO, J., SHUAI, Z., ZHOU, X. & HUANG, D. 2016. Eryptosis as an Underlying Mechanism in Systemic Lupus Erythematosus-Related Anemia. *Cell Physiol Biochem,* 40**,** 1391-1400.

KATAYAMA, R., FRIBOULET, L., KOIKE, S., LOCKERMAN, E. L., KHAN, T. M., GAINOR, J. F., IAFRATE, A. J., TAKEUCHI, K., TAIJI, M., OKUNO, Y., FUJITA, N., ENGELMAN, J. A. & SHAW, A. T. 2014. Two novel ALK mutations mediate acquired resistance to the next-generation ALK inhibitor alectinib. *Clin Cancer Res,* 20**,** 5686-96.

KEATING, G. M. 2014. Afatinib: a review of its use in the treatment of advanced non-small cell lung cancer. *Drugs,* 74**,** 207-21.

KEMPE, D. S., AKEL, A., LANG, P. A., HERMLE, T., BISWAS, R., MURESANU, J., FRIEDRICH, B., DREISCHER, P., WOLZ, C., SCHUMACHER, U., PESCHEL, A., GOTZ, F., DORING, G., WIEDER, T., GULBINS, E. & LANG, F. 2007. Suicidal erythrocyte death in sepsis. *J Mol Med (Berl),* 85**,** 273-81.

KHOZIN, S., BLUMENTHAL, G. M., ZHANG, L., TANG, S., BROWER, M., FOX, E., HELMS, W., LEONG, R., SONG, P., PAN, Y., LIU, Q., ZHAO, P., ZHAO, H., LU, D., TANG, Z., AL HAKIM, A., BOYD, K., KEEGAN, P., JUSTICE, R. & PAZDUR, R. 2015. FDA approval: ceritinib for the treatment of metastatic anaplastic lymphoma kinase-positive non-small cell lung cancer. *Clin Cancer Res,* 21**,** 2436-9.

KIM, D. W., MEHRA, R., TAN, D. S. W., FELIP, E., CHOW, L. Q. M., CAMIDGE, D. R., VANSTEENKISTE, J., SHARMA, S., DE PAS, T., RIELY, G. J., SOLOMON, B. J., WOLF, J., THOMAS, M., SCHULER, M., LIU, G., SANTORO, A., SUTRADHAR, S., LI, S., SZCZUDLO, T., YOVINE, A. & SHAW, A. T. 2016. Activity and safety of ceritinib in patients with ALK-rearranged non-small-cell lung cancer (ASCEND-1): updated results from the multicentre, open-label, phase 1 trial. *Lancet Oncol,* 17**,** 452-463.

KIRAZ, Y., ADAN, A., KARTAL YANDIM, M. & BARAN, Y. 2016. Major apoptotic mechanisms and genes involved in apoptosis. *Tumour Biol,* 37**,** 8471-86.

KLARL, B. A., LANG, P. A., KEMPE, D. S., NIEMOELLER, O. M., AKEL, A., SOBIESIAK, M., EISELE, K., PODOLSKI, M., HUBER, S. M., WIEDER, T. & LANG, F. 2006. Protein kinase C mediates erythrocyte "programmed cell death" following glucose depletion. *Am J Physiol Cell Physiol,* 290**,** C244-53.

KLEINBONGARD, P., SCHULZ, R., RASSAF, T., LAUER, T., DEJAM, A., JAX, T., KUMARA, I., GHARINI, P., KABANOVA, S., OZUYAMAN, B., SCHNURCH, H. G., GODECKE, A., WEBER, A. A., ROBENEK, M., ROBENEK, H., BLOCH, W., ROSEN, P. & KELM, M. 2006. Red blood cells express a functional endothelial nitric oxide synthase. *Blood,* 107**,** 2943-51.

KUROSAKA, K., TAKAHASHI, M., WATANABE, N. & KOBAYASHI, Y. 2003. Silent cleanup of very early apoptotic cells by macrophages. *J Immunol,* 171**,** 4672-9.

LANG, E., BISSINGER, R., FAJOL, A., SALKER, M. S., SINGH, Y., ZELENAK, C., GHASHGHAEINIA, M., GU, S., JILANI, K., LUPESCU, A., REYSKENS, K. M., ACKERMANN, T. F., FOLLER, M., SCHLEICHER, E., SHEFFIELD, W. P., ARTHUR, J. S., LANG, F. & QADRI, S. M. 2015a. Accelerated apoptotic death and in vivo turnover of erythrocytes in mice lacking functional mitogen- and stress-activated kinase MSK1/2. *Sci Rep,* 5**,** 17316.

LANG, E., BISSINGER, R., QADRI, S. M. & LANG, F. 2017. Suicidal death of erythrocytes in cancer and its chemotherapy: A potential target in the treatment of tumor-associated anemia. *Int J Cancer,* 141**,** 1522-1528.

LANG, E., JILANI, K., BISSINGER, R., REXHEPAJ, R., ZELENAK, C., LUPESCU, A., LANG, F. & QADRI, S. M. 2015b. Vitamin D-Rich Diet in Mice Modulates Erythrocyte Survival. *Kidney Blood Press Res,* 40**,** 403-12.

LANG, E. & LANG, F. 2015. Mechanisms and pathophysiological significance of eryptosis, the suicidal erythrocyte death. *Semin Cell Dev Biol,* 39**,** 35-42.

LANG, E., QADRI, S. M. & LANG, F. 2012a. Killing me softly - suicidal erythrocyte death. *Int J Biochem Cell Biol,* 44**,** 1236-43.

LANG, E., ZELENAK, C., EBERHARD, M., BISSINGER, R., ROTTE, A., GHASHGHAEINIA, M., LUPESCU, A., LANG, F. & QADRI, S. M. 2015c. Impact of cyclin-dependent kinase CDK4 inhibition on eryptosis. *Cell Physiol Biochem,* 37**,** 1178-86.

LANG, F., ABED, M., LANG, E. & FOLLER, M. 2014. Oxidative stress and suicidal erythrocyte death. *Antioxid Redox Signal,* 21**,** 138-53.

LANG, F., GULBINS, E., LANG, P. A., ZAPPULLA, D. & FOLLER, M. 2010. Ceramide in suicidal death of erythrocytes. *Cell Physiol Biochem,* 26**,** 21-8.

LANG, F., HUBER, S. M., SZABO, I. & GULBINS, E. 2007a. Plasma membrane ion channels in suicidal cell death. *Arch Biochem Biophys,* 462**,** 189-94.

LANG, F., LANG, E. & FOLLER, M. 2012b. Physiology and pathophysiology of eryptosis. *Transfus Med Hemother,* 39**,** 308-14.

LANG, F. & QADRI, S. M. 2012. Mechanisms and significance of eryptosis, the suicidal death of erythrocytes. *Blood Purif,* 33**,** 125-30.

LANG, K. S., DURANTON, C., POEHLMANN, H., MYSSINA, S., BAUER, C., LANG, F., WIEDER, T. & HUBER, S. M. 2003a. Cation channels trigger apoptotic death of erythrocytes. *Cell Death Differ,* 10**,** 249-56.

LANG, K. S., MYSSINA, S., BRAND, V., SANDU, C., LANG, P. A., BERCHTOLD, S., HUBER, S. M., LANG, F. & WIEDER, T. 2004. Involvement of ceramide in hyperosmotic shock-induced death of erythrocytes. *Cell Death Differ,* 11**,** 231-43.

LANG, P. A., KAISER, S., MYSSINA, S., WIEDER, T., LANG, F. & HUBER, S. M. 2003b. Role of Ca2+-activated K+ channels in human erythrocyte apoptosis. *Am J Physiol Cell Physiol,* 285**,** C1553-60.

LANG, P. A., KEMPE, D. S., MYSSINA, S., TANNEUR, V., BIRKA, C., LAUFER, S., LANG, F., WIEDER, T. & HUBER, S. M. 2005a. PGE(2) in the regulation of programmed erythrocyte death. *Cell Death Differ,* 12**,** 415-28.

LANG, P. A., KEMPE, D. S., TANNEUR, V., EISELE, K., KLARL, B. A., MYSSINA, S., JENDROSSEK, V., ISHII, S., SHIMIZU, T., WAIDMANN, M., HESSLER, G., HUBER, S. M., LANG, F. & WIEDER, T. 2005b. Stimulation of erythrocyte ceramide formation by platelet-activating factor. *J Cell Sci,* 118**,** 1233-43.

LANG, P. A., SCHENCK, M., NICOLAY, J. P., BECKER, J. U., KEMPE, D. S., LUPESCU, A., KOKA, S., EISELE, K., KLARL, B. A., RUBBEN, H., SCHMID, K. W., MANN, K., HILDENBRAND, S., HEFTER, H., HUBER, S. M., WIEDER, T., ERHARDT, A., HAUSSINGER, D., GULBINS, E. & LANG, F. 2007b. Liver cell death and anemia in Wilson disease involve acid sphingomyelinase and ceramide. *Nat Med,* 13**,** 164-70.

LEE, H. J., SCHAEFER, G., HEFFRON, T. P., SHAO, L., YE, X., SIDERIS, S., MALEK, S., CHAN, E., MERCHANT, M., LA, H., UBHAYAKAR, S., YAUCH, R. L., PIRAZZOLI, V., POLITI, K. & SETTLEMAN, J. 2013. Noncovalent wild-type-sparing inhibitors of EGFR T790M. *Cancer Discov,* 3**,** 168-81.

LEW, V. L. & BOOKCHIN, R. M. 2005. Ion transport pathology in the mechanism of sickle cell dehydration. *Physiol Rev,* 85**,** 179-200.

LEW, V. L., MUALLEM, S. & SEYMOUR, C. A. 1982. Properties of the Ca2+-activated K+ channel in one-step inside-out vesicles from human red cell membranes. *Nature,* 296**,** 742-4.

LI, D., AMBROGIO, L., SHIMAMURA, T., KUBO, S., TAKAHASHI, M., CHIRIEAC, L. R., PADERA, R. F., SHAPIRO, G. I., BAUM, A., HIMMELSBACH, F., RETTIG, W. J., MEYERSON, M., SOLCA, F., GREULICH, H. & WONG, K. K. 2008. BIBW2992, an irreversible EGFR/HER2 inhibitor highly effective in preclinical lung cancer models. *Oncogene,* 27**,** 4702-11.

LIAO, B. C., LIN, C. C. & YANG, J. C. 2013. First-line management of EGFR-mutated advanced lung adenocarcinoma: recent developments. *Drugs,* 73**,** 357-69.

LUPESCU, A., SHAIK, N., JILANI, K., ZELENAK, C., LANG, E., PASHAM, V., ZBIDAH, M., PLATE, A., BITZER, M., FOLLER, M., QADRI, S. M. & LANG, F. 2012. Enhanced erythrocyte membrane exposure of phosphatidylserine following sorafenib treatment: an in vivo and in vitro study. *Cell Physiol Biochem,* 30**,** 876-88.

MAELLARO, E., LEONCINI, S., MORETTI, D., DEL BELLO, B., TANGANELLI, I., DE FELICE, C. & CICCOLI, L. 2013. Erythrocyte caspase-3 activation and oxidative imbalance in erythrocytes and in plasma of type 2 diabetic patients. *Acta Diabetol,* 50**,** 489-95.

MAHER, A. D. & KUCHEL, P. W. 2003. The Gardos channel: a review of the Ca2+-activated K+ channel in human erythrocytes. *Int J Biochem Cell Biol,* 35**,** 1182-97.

MANDAL, D., MAZUMDER, A., DAS, P., KUNDU, M. & BASU, J. 2005. Fas-, caspase 8-, and caspase 3-dependent signaling regulates the activity of the aminophospholipid translocase and phosphatidylserine externalization in human erythrocytes. *J Biol Chem,* 280**,** 39460-7.

MANDAL, D., MOITRA, P. K., SAHA, S. & BASU, J. 2002. Caspase 3 regulates phosphatidylserine externalization and phagocytosis of oxidatively stressed erythrocytes. *FEBS Lett,* 513**,** 184-8.

MARSHALL, J., HWANG, J., ESKENS, F. A., BURGER, H., MALIK, S., UTTENREUTHER-FISCHER, M., STOPFER, P., OULD-KACI, M., COHEN, R. B. & LEWIS, N. L. 2013. A Phase I, open-label, dose escalation study of afatinib, in a 3-week-on/1-week-off schedule in patients with advanced solid tumors. *Invest New Drugs,* 31**,** 399-408.

MARSILJE, T. H., PEI, W., CHEN, B., LU, W., UNO, T., JIN, Y., JIANG, T., KIM, S., LI, N., WARMUTH, M., SARKISOVA, Y., SUN, F., STEFFY, A., PFERDEKAMPER, A. C., LI, A. G., JOSEPH, S. B., KIM, Y., LIU, B., TUNTLAND, T., CUI, X., GRAY, N. S., STEENSMA, R., WAN, Y., JIANG, J., CHOPIUK, G., LI, J., GORDON, W. P., RICHMOND, W., JOHNSON, K., CHANG, J., GROESSL, T., HE, Y. Q., PHIMISTER, A., AYCINENA, A., LEE, C. C., BURSULAYA, B., KARANEWSKY, D. S., SEIDEL, H. M., HARRIS, J. L. & MICHELLYS, P. Y. 2013. Synthesis, structure-activity relationships, and in vivo efficacy of the novel potent and selective anaplastic lymphoma kinase (ALK) inhibitor 5-chloro-N2-(2-isopropoxy-5-methyl-4-(piperidin-4-yl)phenyl)-N4-(2-(isopropylsulf onyl)phenyl)pyrimidine-2,4-diamine (LDK378) currently in phase 1 and phase 2 clinical trials. *J Med Chem,* 56**,** 5675-90.

MAVELLI, I., CIRIOLO, M. R., ROSSI, L., MELONI, T., FORTELEONI, G., DE FLORA, A., BENATTI, U., MORELLI, A. & ROTILIO, G. 1984. Favism: a hemolytic disease associated with increased superoxide dismutase and decreased glutathione peroxidase activities in red blood cells. *Eur J Biochem,* 139**,** 13-8.

MCCORMICK, C. J., CRAIG, A., ROBERTS, D., NEWBOLD, C. I. & BERENDT, A. R. 1997. Intercellular adhesion molecule-1 and CD36 synergize to mediate adherence of Plasmodium falciparum-infected erythrocytes to cultured human microvascular endothelial cells. *J Clin Invest,* 100**,** 2521-9.

METRO, G. & CRINO, L. 2011. The LUX-Lung clinical trial program of afatinib for non-small-cell lung cancer. *Expert Rev Anticancer Ther,* 11**,** 673-82.

MODJTAHEDI, H., CHO, B. C., MICHEL, M. C. & SOLCA, F. 2014. A comprehensive review of the preclinical efficacy profile of the ErbB family blocker afatinib in cancer. *Naunyn Schmiedebergs Arch Pharmacol,* 387**,** 505-21.

MOHANDAS, N. & GALLAGHER, P. G. 2008. Red cell membrane: past, present, and future. *Blood,* 112**,** 3939-48.

MOLIFE, L. R., RUDMAN, S. M., ALAM, S., TAN, D. S., KRISTELEIT, H., MIDDLETON, G., PROPPER, D., BENT, L., STOPFER, P., UTTENREUTHER-FISCHER, M., WALLENSTEIN, G., DE BONO, J. & SPICER, J. 2013. Phase II, open-label trial to assess QTcF effects, pharmacokinetics and antitumor activity of afatinib in patients with relapsed or refractory solid tumors. *Cancer Chemother Pharmacol,* 72**,** 1213-22.

MUKAI, H., MASUDA, N., ISHIGURO, H., MITSUMA, A., SHIBATA, T., YAMAMURA, J., TOI, M., WATABE, A., SARASHINA, A., UTTENREUTHER-FISCHER, M. & ANDO, Y. 2015. Phase I trial of afatinib plus vinorelbine in Japanese patients with advanced solid tumors, including breast cancer. *Cancer Chemother Pharmacol,* 76**,** 739-50.

MUKHERJEE, A., BARNETT, M. A., VENKATESH, V., VERMA, S. & SADLER, P. J. 2015. Human serum transferrin fibrils: nanomineralisation in bacteria and destruction of red blood cells. *Chembiochem,* 16**,** 149-55.

NAM, H. J., KIM, H. P., YOON, Y. K., SONG, S. H., MIN, A. R., HAN, S. W., IM, S. A., KIM, T. Y., OH, D. Y. & BANG, Y. J. 2012b. The irreversible pan-HER inhibitor PF00299804 alone or combined with gemcitabine has an antitumor effect in biliary tract cancer cell lines. *Invest New Drugs,* 30**,** 2148-60.

NELSON, V., ZIEHR, J., AGULNIK, M. & JOHNSON, M. 2013. Afatinib: emerging next-generation tyrosine kinase inhibitor for NSCLC. *Onco Targets Ther,* 6**,** 135-43.

NICOLAY, J. P., LIEBIG, G., NIEMOELLER, O. M., KOKA, S., GHASHGHAEINIA, M., WIEDER, T., HAENDELER, J., BUSSE, R. & LANG, F. 2008. Inhibition of suicidal erythrocyte death by nitric oxide. *Pflugers Arch,* 456**,** 293-305.

NIKOLOVA-KARAKASHIAN, M. N. & ROZENOVA, K. A. 2010. Ceramide in stress response. *Adv Exp Med Biol,* 688**,** 86-108.

NISHIO, M., MURAKAMI, H., HORIIKE, A., TAKAHASHI, T., HIRAI, F., SUENAGA, N., TAJIMA, T., TOKUSHIGE, K., ISHII, M., BORAL, A., ROBSON, M. & SETO, T. 2015. Phase I Study of Ceritinib (LDK378) in Japanese Patients with Advanced, Anaplastic Lymphoma Kinase-Rearranged Non-Small-Cell Lung Cancer or Other Tumors. *J Thorac Oncol,* 10**,** 1058-66.

NOVARTIS 2015. Novartis Pharmaceuticals Corporation. Zykadia™ (ceritinib) capsules, for oral use: US prescribing information.2015. http://www. fda.gov. 19 Sep 2016.

PANDOLFI, A., DI PIETRO, N., SIROLLI, V., GIARDINELLI, A., DI SILVESTRE, S., AMOROSO, L., DI TOMO, P., CAPANI, F., CONSOLI, A. & BONOMINI, M. 2007. Mechanisms of uremic erythrocyte-induced adhesion of human monocytes to cultured endothelial cells. *J Cell Physiol,* 213**,** 699-709.

PATRAS DE CAMPAIGNO, E., BONDON-GUITTON, E., LAURENT, G., MONTASTRUC, F., MONTASTRUC, J. L., LAPEYRE-MESTRE, M. & DESPAS, F. 2017. Identification of cellular targets involved in cardiac failure caused by PKI in oncology: an approach combining pharmacovigilance and pharmacodynamics. *Br J Clin Pharmacol,* 83**,** 1544-1555.

PETERS, L. L., SHIVDASANI, R. A., LIU, S. C., HANSPAL, M., JOHN, K. M., GONZALEZ, J. M., BRUGNARA, C., GWYNN, B., MOHANDAS, N., ALPER, S. L., ORKIN, S. H. & LUX, S. E. 1996. Anion exchanger 1 (band 3) is required to prevent erythrocyte membrane surface loss but not to form the membrane skeleton. *Cell,* 86**,** 917-27.

PIERIGE, F., SERAFINI, S., ROSSI, L. & MAGNANI, M. 2008. Cell-based drug delivery. *Adv Drug Deliv Rev,* 60**,** 286-95.

POMPEO, G., GIRASOLE, M., CRICENTI, A., BOUMIS, G., BELLELLI, A. & AMICONI, S. 2010. Erythrocyte death in vitro induced by starvation in the absence of Ca(2+). *Biochim Biophys Acta,* 1798**,** 1047-55.

PRETORIUS, E., BESTER, J. & KELL, D. B. 2016a. A Bacterial Component to Alzheimer's-Type Dementia Seen via a Systems Biology Approach that Links Iron Dysregulation and Inflammagen Shedding to Disease. *J Alzheimers Dis,* 53**,** 1237-56.

PRETORIUS, E., DU PLOOY, J. N. & BESTER, J. 2016b. A Comprehensive Review on Eryptosis. *Cell Physiol Biochem,* 39**,** 1977-2000.

PRETORIUS, E., SWANEPOEL, A. C., BUYS, A. V., VERMEULEN, N., DUIM, W. & KELL, D. B. 2014. Eryptosis as a marker of Parkinson's disease. *Aging (Albany NY),* 6**,** 788-819.

QADRI, S. M., BISSINGER, R., SOLH, Z. & OLDENBORG, P. A. 2017. Eryptosis in health and disease: A paradigm shift towards understanding the (patho)physiological implications of programmed cell death of erythrocytes. *Blood Rev,* 31**,** 349-361.

QADRI, S. M., MAHMUD, H., LANG, E., GU, S., BOBBALA, D., ZELENAK, C., JILANI, K., SIEGFRIED, A., FOLLER, M. & LANG, F. 2012. Enhanced suicidal erythrocyte death in mice carrying a loss-of-function mutation of the adenomatous polyposis coli gene. *J Cell Mol Med,* 16**,** 1085-93.

QUESNELLE, K. M. & GRANDIS, J. R. 2011. Dual kinase inhibition of EGFR and HER2 overcomes resistance to cetuximab in a novel in vivo model of acquired cetuximab resistance. *Clin Cancer Res,* 17**,** 5935-44.

RIXE, O. & FOJO, T. 2007. Is cell death a critical end point for anticancer therapies or is cytostasis sufficient? *Clin Cancer Res,* 13**,** 7280-7.

RUDOLPH, D., STEEGMAIER, M., HOFFMANN, M., GRAUERT, M., BAUM, A., QUANT, J., HASLINGER, C., GARIN-CHESA, P. & ADOLF, G. R. 2009. BI 6727, a Polo-like kinase inhibitor with improved pharmacokinetic profile and broad antitumor activity. *Clin Cancer Res,* 15**,** 3094-102.

SANTARPIA, M., DAFFINA, M. G., D'AVENI, A., MARABELLO, G., LIGUORI, A., GIOVANNETTI, E., KARACHALIOU, N., GONZALEZ CAO, M., ROSELL, R. & ALTAVILLA, G. 2017. Spotlight on ceritinib in the treatment of ALK+ NSCLC: design, development and place in therapy. *Drug Des Devel Ther,* 11**,** 2047-2063.

SCHOFFSKI, P. 2009. Polo-like kinase (PLK) inhibitors in preclinical and early clinical development in oncology. *Oncologist,* 14**,** 559-70.

SCHOFFSKI, P., AWADA, A., DUMEZ, H., GIL, T., BARTHOLOMEUS, S., WOLTER, P., TATON, M., FRITSCH, H., GLOMB, P. & MUNZERT, G. 2012. A phase I, dose-escalation study of the novel Polo-like kinase inhibitor volasertib (BI 6727) in patients with advanced solid tumours. *Eur J Cancer,* 48**,** 179-86.

SCHWAB, C. L., BELLONE, S., ENGLISH, D. P., ROQUE, D. M., LOPEZ, S., COCCO, E., NICOLETTI, R., BORTOLOMAI, I., BONAZZOLI, E., RATNER, E., SILASI, D. A., AZODI, M., SCHWARTZ, P. E., RUTHERFORD, T. J. & SANTIN, A. D. 2014. Afatinib demonstrates remarkable activity against HER2-amplified uterine serous endometrial cancer in vitro and in vivo. *Br J Cancer,* 111**,** 1750-6.

SEQUIST, L. V., YANG, J. C., YAMAMOTO, N., O'BYRNE, K., HIRSH, V., MOK, T., GEATER, S. L., ORLOV, S., TSAI, C. M., BOYER, M., SU, W. C., BENNOUNA, J., KATO, T., GORBUNOVA, V., LEE, K. H., SHAH, R., MASSEY, D., ZAZULINA, V., SHAHIDI, M. & SCHULER, M. 2013. Phase III study of afatinib or cisplatin plus pemetrexed in patients with metastatic lung adenocarcinoma with EGFR mutations. *J Clin Oncol,* 31**,** 3327-34.

SHAIK, N., LUPESCU, A. & LANG, F. 2012. Sunitinib-sensitive suicidal erythrocyte death. *Cell Physiol Biochem,* 30**,** 512-22.

SHARMA, N. & GRAZIANO, S. 2018. Overview of the LUX-Lung clinical trial program of afatinib for non-small cell lung cancer. *Cancer Treat Rev,* 69**,** 143-151.

SHAW, A. T., KIM, D. W., MEHRA, R., TAN, D. S., FELIP, E., CHOW, L. Q., CAMIDGE, D. R., VANSTEENKISTE, J., SHARMA, S., DE PAS, T., RIELY, G. J., SOLOMON, B. J., WOLF, J., THOMAS, M., SCHULER, M., LIU, G., SANTORO, A., LAU, Y. Y., GOLDWASSER, M., BORAL, A. L. & ENGELMAN, J. A. 2014. Ceritinib in ALK-rearranged non-small-cell lung cancer. *N Engl J Med,* 370**,** 1189-97.

SIGNORETTO, E., ZIERLE, J., BISSINGER, R., CASTAGNA, M., BOSSI, E. & LANG, F. 2016. Triggering of Suicidal Erythrocyte Death by Pazopanib. *Cell Physiol Biochem,* 38**,** 926-38.

SOLCA, F., DAHL, G., ZOEPHEL, A., BADER, G., SANDERSON, M., KLEIN, C., KRAEMER, O., HIMMELSBACH, F., HAAKSMA, E. & ADOLF, G. R. 2012. Target binding properties and cellular activity of afatinib (BIBW 2992), an irreversible ErbB family blocker. *J Pharmacol Exp Ther,* 343**,** 342-50.

SPARTA, A. M., BRESSANIN, D., CHIARINI, F., LONETTI, A., CAPPELLINI, A., EVANGELISTI, C., MELCHIONDA, F., PESSION, A., BERTAINA, A., LOCATELLI, F., MCCUBREY, J. A. & MARTELLI, A. M. 2014. Therapeutic targeting of Polo-like kinase-1 and Aurora kinases in T-cell acute lymphoblastic leukemia. *Cell Cycle,* 13**,** 2237-47.

STADLER, W. M., VAUGHN, D. J., SONPAVDE, G., VOGELZANG, N. J., TAGAWA, S. T., PETRYLAK, D. P., ROSEN, P., LIN, C. C., MAHONEY, J., MODI, S., LEE, P., ERNSTOFF, M. S., SU, W. C., SPIRA, A., PILZ, K., VINISKO, R., SCHLOSS, C., FRITSCH, H., ZHAO, C. & CARDUCCI, M. A. 2014. An open-label, single-arm, phase 2 trial of the Polo-like kinase inhibitor volasertib (BI 6727) in patients with locally advanced or metastatic urothelial cancer. *Cancer,* 120**,** 976-82.

STAMLER, J. S., JARAKI, O., OSBORNE, J., SIMON, D. I., KEANEY, J., VITA, J., SINGEL, D., VALERI, C. R. & LOSCALZO, J. 1992. Nitric oxide circulates in mammalian plasma primarily as an S-nitroso adduct of serum albumin. *Proc Natl Acad Sci U S A,* 89**,** 7674-7.

SUZUKI-KARASAKI, M., OCHIAI, T. & SUZUKI-KARASAKI, Y. 2014. Crosstalk between mitochondrial ROS and depolarization in the potentiation of TRAIL-induced apoptosis in human tumor cells. *Int J Oncol,* 44**,** 616-28.

TAGAMI, T., YANAI, H., TERADA, Y. & OZEKI, T. 2016. Evaluation of Phosphatidylserine-Specific Peptide-Conjugated Liposomes Using a Model System of Malaria-Infected Erythrocytes. *Biol Pharm Bull,* 38**,** 1649-51.

TANAKA, H., ICHIKAWA, Y., NISHIDA, K., KONDO, E. & NAKANISHI, H. 2012. Antitumor and anti-metastatic effect of an irreversible TKI (afatinib) against HER2- positive gastric cancer cell lines. *71th Ann Meeting of the Japanese Cancer Association (JCA).* Sapporo

TEICHGRABER, V., ULRICH, M., ENDLICH, N., RIETHMULLER, J., WILKER, B., DE OLIVEIRA-MUNDING, C. C., VAN HEECKEREN, A. M., BARR, M. L., VON KURTHY, G., SCHMID, K. W., WELLER, M., TUMMLER, B., LANG, F., GRASSME, H., DORING, G. & GULBINS, E. 2008. Ceramide accumulation mediates inflammation, cell death and infection susceptibility in cystic fibrosis. *Nat Med,* 14**,** 382-91.

TONE, S., SUGIMOTO, K., TANDA, K., SUDA, T., UEHIRA, K., KANOUCHI, H., SAMEJIMA, K., MINATOGAWA, Y. & EARNSHAW, W. C. 2007. Three distinct stages of apoptotic nuclear condensation revealed by time-lapse imaging, biochemical and electron microscopy analysis of cell-free apoptosis. *Exp Cell Res,* 313**,** 3635-44.

VAN WIJK, R. & VAN SOLINGE, W. W. 2005. The energy-less red blood cell is lost: erythrocyte enzyme abnormalities of glycolysis. *Blood,* 106**,** 4034-42.

VISKUPICOVA, J., BLASKOVIC, D., GALINIAK, S., SOSZYNSKI, M., BARTOSZ, G., HORAKOVA, L. & SADOWSKA-BARTOSZ, I. 2015. Effect of high glucose concentrations on human erythrocytes in vitro. *Redox Biol,* 5**,** 381-7.

WALKER, B., TOWHID, S. T., SCHMID, E., HOFFMANN, S. M., ABED, M., MUNZER, P., VOGEL, S., NEIS, F., BRUCKER, S., GAWAZ, M., BORST, O. & LANG, F. 2014. Dynamic adhesion of eryptotic erythrocytes to immobilized platelets via platelet phosphatidylserine receptors. *Am J Physiol Cell Physiol,* 306**,** C291-7.

WANDERSEE, N. J., OLSON, S. C., HOLZHAUER, S. L., HOFFMANN, R. G., BARKER, J. E. & HILLERY, C. A. 2004. Increased erythrocyte adhesion in mice and humans with hereditary spherocytosis and hereditary elliptocytosis. *Blood,* 103**,** 710-6.

WIKIPEDIA. 2019a. *Afatinib* [Online]. Available: https://en.wikipedia.org/wiki/Afatinib [Accessed Accessed on 12 January 2019].

WIKIPEDIA. 2019b. *Volasertib* [Online]. Available: https://en.wikipedia.org/wiki/Volasertib [Accessed Accessed on 12 January 2019].

WIND, S., SCHNELL, D., EBNER, T., FREIWALD, M. & STOPFER, P. 2017. Clinical Pharmacokinetics and Pharmacodynamics of Afatinib. *Clin Pharmacokinet,* 56**,** 235-250.

WISSING, M. D., MENDONCA, J., KORTENHORST, M. S., KAELBER, N. S., GONZALEZ, M., KIM, E., HAMMERS, H., VAN DIEST, P. J., CARDUCCI, M. A. & KACHHAP, S. K. 2010. Targeting prostate cancer cell lines with polo-like kinase 1 inhibitors as a single agent and in combination with histone deacetylase inhibitors. *FASEB J,* 27**,** 4279-93.

WOOD, B. L., GIBSON, D. F. & TAIT, J. F. 1996. Increased erythrocyte phosphatidylserine exposure in sickle cell disease: flow-cytometric measurement and clinical associations. *Blood,* 88**,** 1873-80.

WU, X., YAO, Z., ZHAO, L., ZHANG, Y., CAO, M., LI, T., DING, W., LIU, Y., DENG, R., DONG, Z., CHEN, H., NOVAKOVIC, V. A., BI, Y., KOU, J., TIAN, Y., ZHOU, J. & SHI, J. 2016. Phosphatidylserine on blood cells and endothelial cells contributes to the hypercoagulable state in cirrhosis. *Liver Int,* 36**,** 1800-1810.

YANG, J., SEQUIST, L. & O'BYRNE, K. 2013. Epidermal growth factor receptor (EGFR)-mediated adverse events in patients with EGFR mutation-positive non-small cell lung cancer (NSCLC) treated with afatinib. *European Cancer Congress.* Amsterdam.

YANG, J. C., SHIH, J. Y., SU, W. C., HSIA, T. C., TSAI, C. M., OU, S. H., YU, C. J., CHANG, G. C., HO, C. L., SEQUIST, L. V., DUDEK, A. Z., SHAHIDI, M., CONG, X. J., LORENCE, R. M., YANG, P. C. & MILLER, V. A. 2012.

Afatinib for patients with lung adenocarcinoma and epidermal growth factor receptor mutations (LUX-Lung 2): a phase 2 trial. *Lancet Oncol,* 13**,** 539-48.

YANG, K., DU, C., WANG, X., LI, F., XU, Y., WANG, S., CHEN, S., CHEN, F., SHEN, M., CHEN, M., HU, M., HE, T., SU, Y., WANG, J. & ZHAO, J. 2017. Indoxyl sulfate induces platelet hyperactivity and contributes to chronic kidney disease-associated thrombosis in mice. *Blood,* 129**,** 2667-2679.

YAP, T. A., VIDAL, L., ADAM, J., STEPHENS, P., SPICER, J., SHAW, H., ANG, J., TEMPLE, G., BELL, S., SHAHIDI, M., UTTENREUTHER-FISCHER, M., STOPFER, P., FUTREAL, A., CALVERT, H., DE BONO, J. S. & PLUMMER, R. 2010. Phase I trial of the irreversible EGFR and HER2 kinase inhibitor BIBW 2992 in patients with advanced solid tumors. *J Clin Oncol,* 28**,** 3965-72.

ZELENAK, C., EBERHARD, M., JILANI, K., QADRI, S. M., MACEK, B. & LANG, F. 2012. Protein kinase CK1alpha regulates erythrocyte survival. *Cell Physiol Biochem,* 29**,** 171-80.

ZELENAK, C., FOLLER, M., VELIC, A., KRUG, K., QADRI, S. M., VIOLLET, B., LANG, F. & MACEK, B. 2011. Proteome analysis of erythrocytes lacking AMP-activated protein kinase reveals a role of PAK2 kinase in eryptosis. *J Proteome Res,* 10**,** 1690-7.

ZIERLE, J., BISSINGER, R., EGLER, J. & LANG, F. 2015. Lapatinib Induced Suicidal Death of Human Erythrocytes. *Cell Physiol Biochem,* 37**,** 2275-87.

8. Declaration of contributions

I am declaring that the submitted dissertation is my original doctoral project. I also like to ensure this thesis or any part of this thesis is not submitted directly or indirectly, anywhere in Germany or other parts of the world as a separate doctoral thesis or for funding purposes. To the best of my knowledge, this dissertation does not possess any data from other researchers without acknowledging them through proper citation or references or without taking written consent.

All of the biological samples were obtained after taking written consent from the volunteers. The entire experimental work was conducted at the Institute of Physiology1, Eberhard Karls University of Tübingen, Germany.

This dissertation was made using data from the following three published articles:

1. **Al Mamun Bhuyan A**, Lang F: Stimulation of Eryptosis by Afatinib. Cell Physiol Biochem. 2016;40(5):1129-1140.
2. **Al Mamun Bhuyan A**, Signoretto E, Bissinger R, Lang F: Stimulation of Suicidal Erythrocyte Death by Ceritinib-Treatment of Human Erythrocytes. Cell Physiol Biochem. 2016;40(5):1129-1140.
3. **Al Mamun Bhuyan A**, Ashiqul Haque AKM, Sahu I, Cao H, Kormann MSD, Lang F. Inhibition of Suicidal Erythrocyte Death by Volasertib. Cell Physiol Biochem. 2017;43(4):1472-1486.

I designed the entire three research projects and conducted most of the experiments, data analysis, as well as made the figures. Prof. Lang wrote the first draft of articles no 1 and 2 whereas Prof. Lang and Prof. Korman jointly wrote manuscript 3. Rosi Bissinger, Elena Signoretto, and Hang Cao helped me with their valuable suggestions and comments to accomplish the studies. AKM Ashiqul Haque and Itishri Sahu were responsible for the K562 cell culture and provided the data for Figure 34 and Figure 35. The final manuscript was checked by all authors and approved for publication after receiving written consent. Again, I would like to affirm that this thesis is solely my work and all of the efforts related to the articles were fully acknowledged.

Abdulla Al Mamun Bhuyan

9. Original Publications

1. **Al Mamun Bhuyan A**, Lang F. Inhibition of Erythrocyte Cell Membrane Scrambling Following Energy Depletion and Hyperosmotic Shock by Alectinib. Cell Physiol Biochem. 2018;51(5):1996-2009.
2. **Al Mamun Bhuyan A**, Sahu I, Cao H, Lang F. Sonidegib, a Novel Inhibitor of Suicidal Erythrocyte Death. Cell Physiol Biochem. 2018;47(4):1352-1364.
3. **Al Mamun Bhuyan A,** Lang F. Stimulation of Eryptosis by Afatinib. Cell Physiol Biochem. 2018;47(3):1259-1273.
4. **Al Mamun Bhuyan A**, Ashiqul Haque AKM, Sahu I, Cao H, Kormann MSD, Lang F. Inhibition of Suicidal Erythrocyte Death by Volasertib. Cell Physiol Biochem. 2017;43(4):1472-1486.
5. **Al Mamun Bhuyan A**, Nüßle S, Cao H, Zhang S, Lang F. Simvastatin, a Novel Stimulator of Eryptosis, the Suicidal Erythrocyte Death. Cell Physiol Biochem. 2017;43(2):492-506.
6. **Al Mamun Bhuyan A**, Bissinger R, Cao H, Lang F. Inhibition of Erythrocyte Cell Membrane Scrambling by ASP3026. Cell Physiol Biochem. 2017;43(2):507-517
7. **Al Mamun Bhuyan A**, Cao H, Lang F. Triggering of Eryptosis, the Suicidal Erythrocyte Death by Mammalian Target of Rapamycin (mTOR) inhibitor Temsirolimus. Cell Physiol Biochem. 2017;42(4):1575-1591.
8. **Al Mamun Bhuyan A**, Bissinger R, Cao H, Lang F. Triggering of Suicidal Erythrocyte Death by Exemestane. Cell Physiol Biochem. 2017;42(1):1-12
9. **Al Mamun Bhuyan A**, Wagner T, Cao H, Lang F: Triggering of Suicidal Erythrocyte Death by Gefitinib. Cell Physiol Biochem. 2017 Mar 29;41(4):1697-1708.
10. **Al Mamun Bhuyan A**, Nguyen MT, Bissinger R, Götz F, Lang F: Lipopeptide-Induced Suicidal Erythrocyte Death Correlates with the Degree of Acylation. Cell Physiol Biochem. 2017 Jan 24;41(1):296-309.
11. **Al Mamun Bhuyan A**, Bissinger R, Cao H, Lang F: Triggering of Suicidal Erythrocyte Death by Bexarotene. Cell Physiol Biochem. 2016;40(5):1239-1251.
12. **Al Mamun Bhuyan A**, Signoretto E, Bissinger R, Lang F: Stimulation of Suicidal Erythrocyte Death by Ceritinib-Treatment of Human Erythrocytes. Cell Physiol Biochem. 2016;40(5):1129-1140.
13. **Al Mamun Bhuyan A**, Bissinger R, Stockinger K, Lang F: Stimulation of Suicidal Erythrocyte Death by Tafenoquine. Cell Physiol Biochem. 2016;39(6):2464-2476.
14. **Al Mamun Bhuyan A**, Signoretto E, Lang F: Triggering of Suicidal Erythrocyte Death by Psammaplin A. Cell Physiol Biochem. 2016;39(3):908-18.
15. **Al Mamun Bhuyan A**, Signoretto E, Bissinger R, Lang F: Enhanced **Eryptosis** Following Exposure to Dolutegravir. Cell Physiol Biochem. 2016;39(2):639-50.
16. Fink M, **Al Mamun Bhuyan A**, Zacharopoulou N, Lang F. Taurolidine Sensitivity of Eryptosis, the Suicidal Erythrocyte Death. Cell Physiol Biochem. 2018;51(2):501-512.
17. Fink M, **Al Mamun Bhuyan A**, Zacharopoulou N, Lang F. Stimulation of Eryptosis, the Suicidal Erythrocyte Death, by Costunolide. Cell Physiol Biochem. 2018;50(6):2283-2295.

18. Bissinger R, Lang E, Gonzalez-Menendez I, Quintanilla-Martinez L, Ghashghaeinia M, Pelzl L, Sukkar B, **Bhuyan AAM**, Salker MS, Singh Y, Fehrenbacher B, Fakhri H, Umbach AT, Schaller M, Qadri SM, Lang F. Genetic deficiency of the tumor suppressor protein p53 influences erythrocyte survival. Apoptosis. 2018 Dec;23(11-12):641-650.
19. Bissinger R, **Bhuyan AAM**, Qadri SM, Lang F. Oxidative stress, eryptosis and anemia: a pivotal mechanistic nexus in systemic diseases. FEBS J. 2018 Jul
20. Saising J, Nguyen MT, Härtner T, Ebner P, **Al Mamun Bhuyan A**, Berscheid A, Muehlenkamp M, Schäkermann S, Kumari N, Maier ME, Voravuthikunchai SP, Bandow J, Lang F, Brötz-Oesterhelt H, Götz F. Rhodomyrtone (Rom) is a membrane-active compound. Biochim Biophys Acta. 2018 Jan 6;1860(5):1114-1124.
21. Abed M, Alzoubi K, **Al Mamun Bhuayn A**, Lang F: Stimulation of Phospholipid Scrambling of the Erythrocyte Membrane by 9-Cis-Retinoic Acid. Cell Physiol Biochem. 2017 Jan 31;41(2):543-554.
22. Signoretto E, Zierle J, **Bhuyan AA**, Castagna M, Lang F: Ceranib-2-induced suicidal erythrocyte death. Cell Biochem Funct. 2016 Jul;34(5):359-66.
23. Signoretto E, Castagna M, **Al Mamun Bhuyan A**, Lang F: Stimulating Effect of Terfenadine on Erythrocyte Cell Membrane Scrambling. Cell Physiol Biochem. 2016;38(4):1425-34.
24. Bissinger R, **Bhuyan AA**, Signoretto E, Lang F: Stimulating Effect of Elvitegravir on Suicidal Erythrocyte Death. Cell Physiol Biochem. 2016;38(3):1111-20.
25. Bissinger R, Bouguerra G, **Al Mamun Bhuyan A**, Waibel S, Abbès S, Lang F: Efavirenz Induced Suicidal Death of Human Erythrocytes. Cell Physiol Biochem. 2015;37(6):2496-507.
26. Bissinger R, Waibel S, Bouguerra G, **Al Mamun Bhuyan A**, Abbès S, Lang F: Enhanced Eryptosis Following Exposure to Lopinavir. Cell Physiol Biochem. 2015;37(6):2486-95.

10. Acknowledgements

It's my immense pleasure to express my indebtedness, deepest sense of gratitude, candid appreciation, and profound regards to my supervisor, Prof. Florian Lang, who gave me a chance to study under his scholastic supervision. His scientific wisdom, guidance, constructive criticism, patience, and encouragement in the research were a great help. It is my strong belief that without his cordial support, it would never have been possible to submit my doctoral thesis. I also wish to express my gratefulness and sincere appreciation to Prof. Meinrad Gawaz and my co-supervisor Prof. Dr med. Dr rer. nat. Bernd Nürnberg for their relevant suggestions and cooperation during my research tenure.

I am ever grateful and want to give special thanks to Rosi Bissinger and Mehrdad Ghashghaeinia for sharing their scientific knowledge related to eryptosis. I am also thankful to Hang Cao for her help in arranging the biological specimens for my research.

I am thankful to Lejla Subasic, Uwe Schuler, and Tanja Loch for their technical and administrative assistance.

I am highly grateful to the University of Rajshahi, Rajshahi, Bangladesh, for allowing me to conduct my PhD by providing all kinds of administrative support.

Besides this, I would like to express my gratitude to my well-wishers Madhuri Salker, Yogesh Singh, Itishri Sahu, Ashiqul Haque Rudro, Anjali Ralhan Singh, Anurag Singh, Basma Sukkar, Lisann Pelzl, Khalid Elnady, Anja Umbach, Myriam Fezai, Elena Signoretto, Anubah Seth, and Carlos Eduardo Calderon Castro for their valuable advice and in-depth discussions around my work, as well as for their lovely support and wishes for my family.

Last but not least, I am grateful to my beloved parents and my family, especially to Pinky and Mikhaeel for their sacrifices, blessings, and encouragement. Without their support, it was unrealistic to finish my research and stay here in Germany!

The author

March, 2020